Cell Journal (Yakhteh)

Guide for Authors

Aims and Scope: The "Cell Journal (Yakhteh)" is a peer review and monthly English publication of Royan Institute of Iran. The aim of the journal is to disseminate information through publishing the most recent scientific research studies on exclusively Cellular, Molecular and other related topics. **Cell J**, has been certified by the Ministry of Culture and Islamic Guidance since 1999 and also accredited as a scientific and research journal by HBI (Health and Biomedical Information) Journal Accreditation Commission since 2000 which is an open access journal. **This journal holds the membership of the Committee on Publication Ethics (COPE).**

1. Types of articles

The articles in the field of Cellular and Molecular can be considered for publications in **Cell J.** These articles are as below:

A. Original articles

Original articles are scientific reports of the original research studies. The article consists of English Abstract (structured), Introduction, Materials and Methods, Results, Discussion, Conclusion, Acknowledgements, Author's Contributions, and References **(Up to 40).**

B. Review articles

Review articles are the articles written by well experienced authors and those who have excellence in the related fields. The corresponding author of the review article must be one of the authors of at least three published articles appearing in the references. The review article consists of English Abstract (unstructured), Introduction, Conclusion, Author's Contributions, and References **(Up to 70).**

C. Systematic Reviews

Systematic reviews are a type of literature review that collect and critically analyzes multiple research studies or papers. The Systematic reviews consist of English Abstract (unstructured), Introduction, Materials and Methods, Results, Discussion, Conclusion, Acknowledgements, Author's Contributions, and References **(Up to 70).**

D. Short communications

Short communications are articles containing new findings. Submissions should be brief reports of ongoing researches. The short communication consists of English Abstract (unstructured), the body of the manuscript (should not hold heading or subheading), Acknowledgements, Author's Contributions, and References **(Up to 30).**

E. Case reports

Case reports are short discussions of a case or case series with unique features not previously described which make an important teaching point or scientific observation. They may describe novel techniques or use equipment, or new information on diseases of importance. It consists of English Abstracts (Unstructured), Introduction, Case Report, Discussion, Acknowledgements, Author's Contributions, and References **(Up to 30).**

F. Editorial

Editorials are articles should be written in relevant and new data of journals' filed by either the editor in chief or the editorial board.

G. Imaging in biology

Images in biology should focus on a single case with an interesting illustration such as a photograph, histological specimen or investigation. Color images are welcomed. The text should be brief and informative.

H. Letter to the editors

Letter to the editors are in response to previously published **Cell J** articles, and may also include interesting cases that do not meet the requirement of being truly exceptional, as well as other brief technical or clinical notes of general interest.

I. Debate

Debates are articles which show a discussion of the positive and negative view of the author concerning all aspect of the issue relevant to scientific research.

2. Submission process

It is recommended to see the guidelines for reporting different kinds of manuscripts. This guide explains how to prepare the

manuscript for submission. Before submitting, we suggest authors to familiarize themselves with **Cell J** format and content by reading the journal via the website (www.celljournal.com). The corresponding author ensures that all authors are included in the author list and agree with its order, and they must be aware of the manuscript submission.

A. Author contributions statements

It is essential for authors to include a statement of responsibility in the manuscript that specifies the contribution of every one of them. This participation must include conception and design of the manuscript, data acquisition or data analysis and interpretation, drafting of the manuscript and/or revising it for critically important intellectual content, revision and final approval of the manuscript and statistical analysis, obtaining funding, administrative, technical, or material support, or supervision. Authors who do not meet the above criteria should be acknowledged in the **Acknowledgments section.**

B. Cover letter and copyright

Each manuscript should be accompanied by a cover letter, signed by all authors specifying the following statement: "The manuscript has been seen and approved by all authors and is not under active consideration for publication. It has neither been accepted for publication nor published in another journal fully or partially (except in abstract form). **Also, no manuscript would be accepted in case it has been pre-printed or submitted to other websites.** I hereby assign the copyright of the enclosed manuscript to **Cell J.**" Corresponding author must confirm the proof of the manuscript before online publishing. Also, it is needed to suggest three peer reviewers in the field of their manuscript.

C. Manuscript preparation

Authors whose first language is not English encouraged to consult a native English speaker in order to confirm his manuscripts to American or British (not a mixture) English usage and grammar. It is necessary to mention that we will check the plagiarism of your manuscript by iThenticate Software. The manuscript should be prepared in accordance with the "International Committee of Medical Journal Editors (ICMJE)". Please send your manuscript in two formats word and PDF (including: title, name of all the authors with their degree, abstract, full text, references, tables and figures) and also send tables and figures separately in the site. The abstract and text pages should have consecutive line numbers in the left margin beginning with the title page and continuing through the last page of the written text. Each abbreviation must be defined in the abstract and text when they are mentioned for the first time. Avoid using abbreviation in the title. Please use the international and standard abbreviations and symbols

It should be added that an essential step toward the integration and linking of scientific information reported in published literature is using standardized nomenclature in all fields of science and medicine. Species names must be italicized (*e.g., Homo sapiens*) and also the full genus and species written out in full, both in the title of the manuscript and at the first mention of an organism in a paper.

It is necessary to mention that genes, mutations, genotypes, and alleles must be indicated in italics. Please use the recommended name by consulting the appropriate genetic nomenclature database, e.g., HUGO for human genes. In another words; if it is a human gene, you must write all the letters in capital and italic (*e.g., OCT4, c-MYC*). If not, only write the first letter in capital and italic (*e.g., Oct4, c-Myc*). **In addition, protein designations are the same as the gene symbol but are not italicized.**

Of note, Cell J will only consider publishing genetic association study papers that are novel and statistically robust. Authors are advised to adhere to the recommendations outlined in the STREGA statement (http://www.strega-statement.org). The following criteria must be met for all submissions:

1. Hardy-Weinberg Equilibrium (HWE) calculations must be carried out and reported along with the P-values if applicable [see Namipashaki et al. 2015 (Cell J, Vol 17, N 2, Pages: 187-192) for a discussion].

2. Linkage disequilibrium (LD) structure between SNPs (if multiple SNPs are reported) must be presented.

3. Appropriate multiple testing correction (if multiple independent SNPs are reported) must be included.

Submissions that fail to meet the above criteria will be rejected before being sent out for review.

Each of the following manuscript components should begin in the following sequence:

Authors' names and order of them must be carefully considered (full name(s), highest awarded academic degree(s), email(s), and institutional affiliation(s) of all the authors in English. Also, you must send mobile number and full postal address of the corresponding author).

Changes to Authorship such as addition, deletion or rearrangement of author names must be made only before the manuscript has been accepted in the case of approving by the journal editor. In this case, the corresponding author must explain the reason of changing and confirm them (which has been signed by all authors of the manuscript). If the manuscript has already been published in an online issue, an erratum is needed.

Title is providing the full title of the research (do not use abbreviations in title).

Running title is providing a maximum of 7 words (no more than 50 characters).

Abstract must include Objective, Materials and Methods, Results, and Conclusion (no more than 300 words).

Keywords, three to five, must be supplied by the authors at the foot of the abstract chosen from the Medical Subject Heading (MeSH). Therefore; they must be specific and relevant to the paper.

The following components should be identified after the abstract:

Introduction: The Introduction should provide a brief background to the subject of the paper, explain the importance of the study, and state a precise study question or purpose.

Materials and Methods: It includes the exact methods or observations of experiments. If an apparatus is used, its manufacturer's name and address should be stipulated in parenthesis. If the method is established, give reference but if the method is new, give enough information so that another author can perform it. If a drug is used, its generic name, dose, and route of administration must be given. Standard units of measurements and chemical symbols of elements do not need to be defined.

Statistical analysis: Type of study and statistical methods should be mentioned and specified by any general computer program used.

Ethical considerations*:* Please state that informed consent was obtained from all human adult participants and from the parents or legal guardians of minors and include the name of the appropriate institutional review board that approved the project. It is necessary to indicate in the text that the maintenance and care of experimental animals complies with National Institutes of Health guidelines for the humane use of laboratory animals, or those of your Institute or agency.

Clinical trial registration: All of the Clinical Trials performing in Iran must be registered in Iranian Registry of Clinical Trials (www.irct.ir). The clinical trials performed abroad, could be considered for publication if they register in a registration site approved by WHO or www.clinicaltrials.gov. If you are reporting phase II or phase III randomized controlled trials, you must refer to the CONSORT Statement for recommendations to facilitate the complete and transparent reporting of trial findings. Reports that do not conform to the CONSORT guidelines may need to be revised before peer-reviewing.

Results: They must be presented in the form of text, tables, and figures. Take care that the text does not repeat data that are presented in tables and/or figures. Only emphasize and summarize the essential features of the main results. Tables and figures must be numbered consecutively as appeared in the text and should be organized in separate pages at the end of the manuscript while their location should be mentioned in the main text.

Tables and figures: If the result of your manuscript is too short, it is better to use the text instead of tables & figures. Tables should have a short descriptive heading above them and also any footnotes. Figure's caption should contain a brief title for the whole figure and continue with a short explanation of each part and also the symbols used (no more than 100 words). All figures must be prepared based on cell journal's guideline in color (no more than 6 Figures and Tables) and also in TIF format with 300 DPI resolution.

Of Note: Please put the tables & figures of the result in the results section not any other section of the manuscript.

Supplementary materials would be published on the online version of the journal. This material is important to the understanding and interpretation of the report and should not repeat material within the print article. The amount of supplementary material should be limited. Supplementary material should be original and not previously published and will undergo editorial and peer review with the main manuscript. Also, they must be cited in the manuscript text in parentheses, in a similar way as when citing a figure or a table. Provide a caption for each supplementary material submitted.

Discussion: It should emphasize the present findings and the variations or similarities with other researches done by other researchers. The detailed results should not be repeated in the discussion again. It must emphasize the new and important aspects of the study.

Conclusion: It emphasizes the new and important aspects of the study. All conclusions are justified by the results of the study.

Acknowledgements: This part includes a statement thanking those who contributed substantially with work relevant to the study but does not have authorship criteria. It includes those who provided technical help, writing assistance and name of departments that provided only general support. You must mention financial support in the study. Otherwise; write this sentence "There is no financial support in this study".

Conflict of interest: Any conflict of interest (financial or otherwise) and sources of financial support must be listed in the Acknowledgements. It includes providers of supplies and services from a commercial organization. Any commercial affiliation must be disclosed, regardless of providing the funding or not.

Of Note: If you have already any patent related to the subject of your manuscript, or you are going to apply for such a patent, it must be mentioned in this part.

References: The references must be written based on the Vancouver style. Thus the references are cited numerically in the text and listed in the bibliography by the order of their appearance. The titles of journals must be abbreviated according to the style used in the list of Journals Indexed in PubMed. Write surname and initials of all authors when there are six or less. In the case of seven or more authors, the names of the first six authors followed by "et al." must be listed. You can download Endnote file for Journal references style: endnote file

The reference of information must be based on the following order:

Article:

Surname(s) and first letter of name &middle name(s) of author(s) .Manuscript title. Journal title (abbr).publication date (year); Volume & Issue: Page number.

Example: Manicardi GC, Bianchi PG, Pantano S, Azzoni P, Bizzaro D, Bianchi U, et al. Presence of endogenous nicks in DNA of ejaculated human spermatozoa and its relationship to chromomycin A3 accessibility. Biol Reprod. 1995; 52(4): 864-867.

Book:

Surname(s) and first letter of name & middle name(s) of author(s).Book title. Edition. Publication place: publisher name; publication date (year); Page number.

Example: Edelman CL, Mandle CL. Health promotion throughout the lifespan. 2nd ed. ST Louis: Mosby; 1998; 145-163.

Chapter of book:

Surname(s) and first letter of name & middle name(s) of author(s).Chapter title. In: Surname(s) and first letter of name & middle name(s) of editor(s), editors. Book title. Edition. Publication place: publisher name; publication date (year); Page number.

Example: Phillips SJ, Whisnant JP. Hypertension and stroke. In: Laragh JH, Brenner BM, editors. Hypertension: pathophysiology, diagnosis, and management. 2nd ed. New York: Raven Press; 1995; 465-478.

Abstract book:

Example: Amini rad O.The antioxidant effect of pomegranate juice on sperm parameters and fertility potential in mice. Cell J. 2008;10 Suppl 1:38.

Thesis:

Name of author. Thesis title. Degree. City name. University. Publication date (year).

Example: Eftekhari Yazdi P. Comparison of fragment removal and co-culture with Vero cell monolayers on development of human fragmented embryos. Presented for the Ph.D., Tehran. Tarbiyat Modarres University. 2004.

Internet references

Article:

Example: Jahanshahi A, Mirnajafi-Zadeh J, Javan M, Mohammad-Zadeh M, Rohani M. Effect of low-frequency stimulation on adenosineA1 and A2A receptors gene expression in dentate gyrus of perforant path kindled rats. Cell J. 2008; 10 (2): 87-92. Available from: http://www.celljournal.org. (20 Oct 2008).

Book:

Example: Anderson SC, Poulsen KB. Anderson's electronic atlas of hematology.[CD-ROM]. Philadelphia: Lippincott Williams & Wilkins; 2002.

D. Proofs are sent by email as PDF files and should be checked and returned within 72 hours of receipt. It is the authors' responsibility to check that all the text and data as contained in the page proofs are correct and suitable for publication. **We are requested to pay particular attention to author's names and affiliations as it is essential that these details be accurate when the article is published.**

E. Pay for publication: Publishing an article in **Cell J** requires Article Processing Charges (APC) that will be billed to the submitting author following the acceptance of an article for publication. For more information please see www.celljournal.org.

F. Ethics of scientific publication: Manuscripts that have been published elsewhere with the same intellectual material will refer to duplicate publication. If authors have used their own previously published work or work that is currently under review, as the basis for a submitted manuscript, they are required to cite the previous work and indicate how their submitted manuscript offers novel contributions beyond those of the previous work. Research and publication misconduct is considered a serious breach of ethics.

The Journal systematically employs iThenticate, plagiarism detection and prevention software designed to ensure the originality of written work before publication. Plagiarism of text from a previously published manuscript by the same or another author is a serious publication offence. Some parts of text may be used, only where the source of the quoted material is clearly acknowledged.

3. General information

A. You can send your manuscript via online submission system which is available on our website. If the manuscript is not prepared according to the format of **Cell J**, it will be returned to authors.

B. The order of article appearance in the Journal is not demonstrating the scientific characters of the authors.

C. Cell J has authority to accept or reject the manuscript.

D. The received manuscript will be evaluated by associate editor. **Cell J** uses a single-blind peer review system and if the manuscript suits the journal criteria, we select the reviewers. If three reviewers pass their judgments on the manuscript, it will be presented to the editorial board of **Cell J.** If the editorial board has a positive judgment about the manuscript, reviewers' comments will be presented to the corresponding author (the identification of the reviewers will not be revealed). The executive member of journal will contact the corresponding author directly within 3-4 weeks by email. If authors do not receive any reply from journal office after the specified time, they can contact journal office. Finally, executive manager will respond promptly to authors' request.

The Final Checklist

The authors must ensure that before submitting the manuscript for publication, they have to consider the following parts:

1. The first page of manuscript should contain title, name of the author/coauthors, their academic qualifications, designation & institutions they are affiliated with, mailing address for future correspondence, email address, phone, and fax number.

2. Text of manuscript and References prepared as stated in the "guide for authors" section.

3. Tables should be on a separate page. Figures must be sent in color and also in JPEG (Jpg) format.

4. Cover Letter should be uploaded with the signature of all authors.

5. An ethical committee letter should be inserted at the end of the cover letter.

The Editor-in-Chief: Ahmad Hosseini, Ph.D.

Cell Journal *(Yakhteh)*

P.O. Box: 16635-148, Iran

Tel/Fax: + 98-21-22510895

Emails: Celljournal@royaninstitute.org

info@celljournal.org

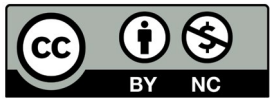

Dr. Saeed Kazemi Ashtiani

IN THE NAME OF GOD

Gone But not Forgotten

In the memory of the late Director of Royan Institute, Founder of Stem Cells Research in Iran and Chairman of ***Cell Journal*** *(Yakhteh)*. May he rest in peace.

PUBLISHED & SPONSORED BY:
Publication of Royan Institute (ACECR)

Indexed in:
1. Thomson Reuters (ISI)
2. PubMed
3. PubMed Central (PMC)
4. National Library Medicine (NLM)
5. Biosis Preview
6. Index Medicus for the Eastern Mediterranean Region (IMEMR)
7. Regional Information Center for Sciences and Technology (RICeST)
8. Index Copernicus International
9. Cambridge Scientific Abstract (CSA)
10. EMBASE
11. Scopus
12. Cinahl Database
13. Google Scholar
14. Chemical Abstract Service (CAS)
15. Proquest
16. Directory of Open Access Journals (DOAJ)
17. Open Academic Journals Index (OAJI)
18. Directory of Research Journals Indexing (DRJI)
19. Scientific Information Database (SID)
20. Iranmedex
21. Islamic World Science Citation Center (ISC)
22. Magiran
23. Science Library Index
24. Biological Abstracts
25. Essential Science Indicators
26. EuroPub

Editorial Office Address (Dr. Ahmad Hosseini):
Royan Institute, P.O.Box: 16635-148,
Tehran, Iran
Tel & Fax: (+9821)22510895
Website: www.celljournal.org
Emails: info@celljournal.org
celljournal@royaninstitute.org

Printing Company:
Naghshe e Johar Co.
No. 103, Fajr alley, Tehranpars Street,
Tehran, Iran.

Cell Journal(Yakhteh), Vol 24, No 4, April 2022, Serial Number: 99, Pages: 163-214

CONTENTS

Original Articles

Short Communication

Original Article

Methylation and Expression Status of The CpG-Island of *SMG1* Promoter in Acute Myeloid Leukemia: A Follow-Up Study in Patients

Neda Karami, M.Sc.[1], Mohammad Hossein Ahmadi, Ph.D.[2] , Saeed Mohammadi, Ph.D.[3], Amirhosein Maali, M.Sc.[1, 4], Ahad Alizadeh, Ph.D.[5], Shaghayegh Pishkhan Dibazar, M.Sc.[6], Mehdi Azad, Ph.D.[2]*

1. Department of Medicine Biotechnology, Faculty of Allied Medicine, Qazvin University of Medical Science, Qazvin, Iran
2. Department of Medical Laboratory Sciences, Faculty of Allied Medicine, Qazvin University of Medical Sciences, Qazvin, Iran
3. Hematology-Oncology and Stem Cell Transplantation Research Center, Shariati Hospital of Tehran, Tehran, Iran
4. Department of Immunology, Pasteur Institute of Iran, Tehran, Iran
5. Metabolic Diseases Research Center, Research Institute for Prevention of Non-Communicable Diseases, Qazvin University of Medical Sciences, Qazvin, Iran
6. Department of Immunology, Tarbiat Modares University, Tehran, Iran

**Corresponding Address: P.O.Box: 34197-59811, Department of Medical Laboratory Sciences, Faculty of Allied Medicine, Qazvin University of Medical Sciences, Qazvin, Iran*
Email: haematologicca@gmail.com

Received: 01/October/2020, Accepted: 23/February/2021

Abstract

Objective: Aberrant alterations in DNA methylation are known as one of the hallmarks of oncogenesis and play a vital role in the progression of acute myeloid leukemia (AML). *SMG1* is a member of the Phosphoinositide 3-kinases family, acting as a tumor suppressor gene. The aim of this study was the evaluation of the expression level and methylation status of *SMG1* in AML.

Materials and Methods: In this follow-up study on AML patients admitted to Shariati Hospital, Tehran, Iran, the methylation status of *SMG1* [performed by methylation-specific polymerase chain reaction (PCR)] and its expression level (performed by qRT-PCR) were evaluated in three phases: newly diagnosed, under treatment and complete remission. The correlation of the methylation status of *SMG1*, its expression level, and clinical/paraclinical data was analyzed by SPSS ver.25.

Results: This study on 18 patients and five control individuals showed that the CpG-islands of the *SMG1* promoter in newly diagnosed cases is hypomethylated compared to the normal group (P=0.002) The fold change of *SMG1* expression levels in new cases is 0.464 ± 0.468, while the fold change of *SMG1* expression levels in under-treatment and in-remission patients is 0.973 ± 1.159 and 0.685 ± 0.885, respectively. In under-treatment patients, white blood cell (WBC) count decreases 114176.36 cell/μl with each unit of increase in fold change of SMG1 (P<0.0001), and Hb unit increases 2.062 g/dl with each unit of increase in fold change (P<0.0001) Also, in the remission phase, the Hb unit increases 1.395 g/dl with each unit increase in fold change (P=0.019).

Conclusion: The robust results of our study suggest that the methylation and expression of SMG1 have a high impact on the pathogenesis of AML. Also, the methylation and expression of *SMG1* can play a prognostic role in AML.

Keywords: Acute Myeloid Leukemia, DNA Methylation, Follow-Up Studies, SMG1

Cell Journal(Yakhteh), Vol 24, No 4, April 2022, Pages: 163-169

Citation: Karami N, Ahmadi MH, Mohammadi S, Maali AH, Alizadeh A, Pishkhan Dibazar Sh, Azad M. Methylation and expression status of the CpG-Island of SMG1 promoter in acute myeloid leukemia: a follow-up study in patients. Cell J. 2022; 24(4): 163-169. doi: 10.22074/cellj.2022.7798.

Introduction

Acute myeloid leukemia (AML), as a hematopoietic malignancy, is the most common form of acute leukemia in adults and involves abnormal proliferation and differentiation of hematopoietic stem cell colonies (1). AML presents with more than 20,000 new cases per year in the United States alone. The prevalence of AML is three to five individuals per 100,000. The distinct cellular feature in AML is abnormal myeloid cell development and neoplastic proliferation in the bone marrow (2). Also, some cytogenetic abnormalities lead to complications in diagnosis, prognosis, and treatment (3), making necessary to investigate novel approaches for this type of leukemia.

DNA methylation is a gene expression regulatory mechanism occurring in GC-rich sites of the genome. Hypermethylation of the CpG-islands of tumor suppressor genes leads to tumorigenesis. Also, hypomethylation in the CpG-islands of proto-oncogenes is one of the events causing cancer. Aberrant DNA methylation alterations are known as one of the hallmarks of oncogenesis and play a vital role in the progression of AML (4, 5).

SMG1 (Suppressor with morphogenetic effect on genitalia family member 1) is considered a tumor suppressor gene. Dysregulation of *SMG1* leads to tumorigenesis. *SMG1* is a member of the Phosphoinositide 3-kinases family, involved in nonsense-mediated decay (NMD) (6). Also, *SMG1* participates in initiating DNA damage responses, telomere retention, oxidative/hypoxic stress responses, and stress granule formation. *SMG1* is required for the G1/S checkpoint site maximum activity for ionizing radiation exposure or during oxidative stress. Complete absence of *Smg1* expression during the early stages of mouse fetal development causes the fetus to die.

Also, the absence of a single allele of *SMG1* increases the risk of cancer, especially lung adenocarcinoma and lymphoma. *SMG1* deficiency causes high levels of basal inflammation and oxidative damage of tissue in the pre-cancerous stage, which may indicate the role of this cascade in carcinogenesis (7, 8)

Regarding the lack of theoretical and experimental knowledge about AML and the impact of methylation in this leukemia, we investigated the *SMG1* CpG-island methylation patterns in AML patients and its correlation with the *SMG1* expression level to introduce a potential hallmark in hematopoietic malignancy. We also investigated the effect of *SMG1* expression on paraclinical indexes as the therapeutic outcome.

Material and Methods

Sampling

In this follow-up study, 18 patients with AML who had been admitted to Shariati Hospital, Tehran, Iran, were studied, whose AML had been confirmed based on laboratory tests. The patients were separated into three groups: new cases, receiving medications, and in remission. Also, five healthy individuals were considered as control. The signed informed consent was obtained from all participants. This study was approved by the ethics committee of Qazvin University of Medical Sciences (IR.QUMS.REC.1397.198). All samples were collected in heparin-lithium CBC tubes. All patients received a regular therapeutic regime for AML based on FDA protocol (Cytarabine for seven days and Anthracycline drugs such as Daunorubicin (Daunomycin) or Idarubicin three days).

DNA extraction and bisulfite treatment

The DNA was extracted using GeneAll kit (GeneAll, South Korea), as per the manufacturer's protocol. The bisulfite treatment was performed to replace unmethylated cytosine residues with uracil, using EpiTect Fast DNA Bisulfite Kit (Qiagen, USA), following the manufacturer's protocol.

Methylation-specific PCR for the *SMG1* CpG-island

Methylation-specific PCR (MSP) was conducted for the amplification of bisulfite-treated DNA. For this aim, 10 µl of TEMPase Hot Start 2x Master Mix BLUE (Ampliqon, Denmark), 1 µl of each set of reverse and forward primers of methylated and unmethylated sets (Table 1), 1 µl of bisulfite-treated DNA template were used and adjusted to the final volume of 20 µl using ddH_2O. The thermal cycling of MSP was performed using ABI Applied Biosystems™ (Thermofisher, USA) as follows: 10 minutes in 95˚C for pre-denaturation, and 30 cycles including 15 seconds at 94˚C for denaturation, 30 seconds at 53˚C for denaturation, and 15 seconds at 72˚C for the extension, per cycle. Also, the amplicons were incubated for 10 minutes at 72˚C for a final extension. For detection of the methylation status of the *SMG1* promoter in AML patients and healthy individuals, the MSP products were loaded on 1% agarose electrophoresis gel. Positive and negative controls for methylation were used to verify the accuracy of the MSP. EpiTect Control DNA Bisulfite converted (Qiagen, USA) was used for MSP control ([Methylated control (lot No: 157047896) and unmethylated control (lot No: 157045952)].

RNA extraction and cDNA synthesis

The total RNA of samples was extracted using the GeneAll RNA extraction kit (GeneAll, South Korea), as per the manufacturer's protocol. The reverse transcription of extracted RNA samples was performed using Thermo Scientific RevertAid First Strand cDNA Synthesis kit (Thermo Scientific, USA), following the manufacturer's protocol.

SMG1 expression level

Real-time PCR was used to evaluate *SMG1* expression level in patients and healthy individuals, using 7.5 µl of RealQ Plus 2x Master Mix Green Without ROX™ (Ampliqon, Denmark), 0.5 µl of each primer (forward and reverse), and 1 µl of cDNA, which was adjusted using ddH_2O. Real-time PCR stages were conducted using ABI Applied Biosystems™ (Thermofisher, USA) as bellow: 15 minutes at 95˚C for pre-denaturation, and 19 seconds at 95˚C for denaturation, 19 seconds at 61.5˚C for denaturation and extension, per cycle. The Rotor-Gene device (Qiagen, USA) was used to perform thermal processes. Also, the *GAPDH* gene was used as the internal control gene. The sequences of forward and reverse primers of *SMG1* and *GAPDH* genes are given in Table 1.

Hematopoietic laboratory indexes

White blood cells (WBC, cells/µl), red blood cells (RBC, cells/µl), platelets (Plt, cells/µl), and hemoglobin (Hb, g/dl) were measured using Sysmex cell counter (Sysmex Corporation, Japan). All parameters were evaluated in control individuals and all studied phases in patients.

Statistical analysis

The multiple linear model and ordinal logistic regression were used to identify the correlations. All statistical analysis was performed by SPSS software, version 25 (IBM, USA). The significant level was considered as 5%. Also, Ct values of real-time PCR results were calculated using the REST software.

Results

Sampling characteristics

Out of a total of 18 patients (seven males and 11 females, aged 15 to 67) admitted to Shariati Hospital, Tehran, Iran, nine patients were monitored for methylation status of the *SMG1* promoter in three phases of the disease (newly

diagnosed/under treatment/remission). Four patients participated in two phases (under treatment/ remission), and five patients were involved in only one phase (newly diagnosed cases).

Methylation status of the CpG-island of the *SMG1* promoter in patients in different phases of AML

While all control individuals show the hemi-methylated status in their CpG-islands of *SMG1*, the results of Ordinal Logistic Regression analysis show that the methylation status of the CpG-islands of the *SMG1* in newly diagnosed cases is significantly hypomethylated compared to the control group (P=0.002). Also, there was no significant difference in the methylation status of the CpG-islands of *SMG1* between the patients in the under-treatment phase and remission phase with the control group (P=0.236 and P=1.000, respectively, Fig.1). The demographic data of the methylation pattern frequency in participants are reported in Table 2.

SMG1 expression level in different phases of acute myeloid leukemia

The *Pfaffl* statistics showed that the fold change of *SMG1* expression levels in new cases is 0.464 ± 0.468, while *SMG1* expression levels in the under-treatment and in-remission patients are 0.973 ± 1.159 and 0.685 ± 0.885, respectively. Therefore, the expression level of *SMG1* in new cases and in-remission patients are reduced compared to the control group.

Multiple linear models showed that in the remission phase, the fold changes are significantly different between patients with methylated and unmethylated Promoters (P=0.001). Also, in the remission phase, the fold changes are significantly different between hemi-methylated and unmethylated patients (P=0.002, Table 3).

Table 1: Methylated and un-methylated primers for MSP of SMG1 CpG-islands and the primer sequences of *SMG1* and *GADPH* (internal control) for evaluating the expression level of *SMG1* by real time polymerase chain reaction

Methylation state of primers	Length (bp)	Primer sequence (5′-3′)
Methylated primer	22	F: GCGTACGTGAATTTAAGGGTAC
	25	R: AACAAAAAATCTCCACTACTACGAC
UnMethylated primer	25	F: GGTGTATGTGAATTTAAGGGTATGT
	25	R: AACAAAAAATCTCCACTACTACAAC
SMG1	20	F: GTGGAGAGTTACGCAGTCTT
	23	R: CGCATAATGTGTAAAACCTGCTC
GAPDH	20	F: CAATGACCCCTTCATTGACC
	20	R: TGGAAGATGGTGATGGGATT

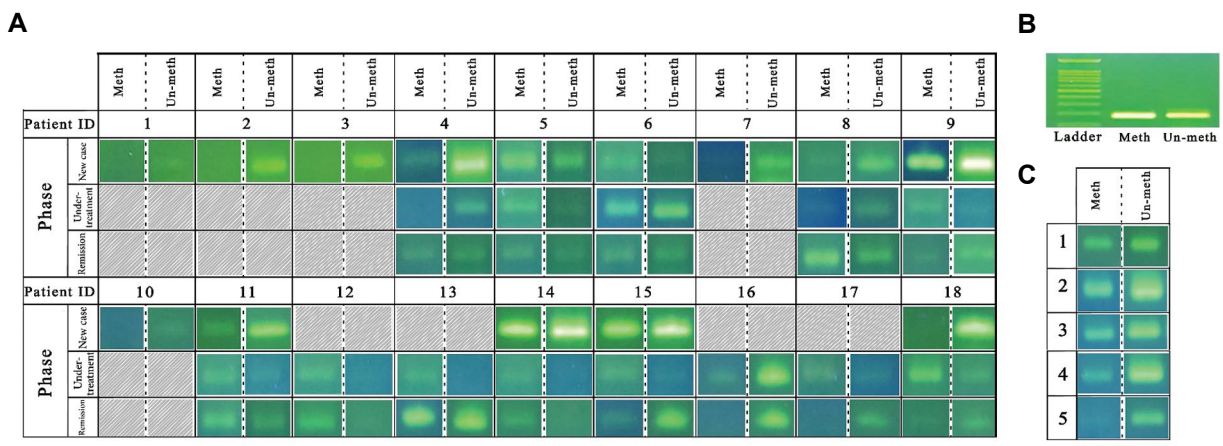

Fig.1: Methylation status of *SMG1* gene promoter in acute myeloid leukemia (AML) patients. **A.** AML patients were classified into three phases: new cases, under-treatments, and in-remissions. The methylation status of *SMG1* was evaluated by MSP, using methylated (Meth) and unmethylated (Un-meth) specific primers. The results were shown on 1.5% agar gel electrophoresis. **B.** Positive and negative control of MSP. **C.** MSP of the *SMG1* promoter in healthy individuals (control group). Most healthy individuals show hemimethylated status in the *SMG1* promoter.

Table 2: Demographic data of methylation status in different phases of AML

Methylation status		Phase			Total
		New cases	Under treatment	Remission	
Un-methylated	Count (% within phase)	6 (42.9)	1 (7.7)	2 (15.4)	9 (22.5)
Hemi-methylated	Count (% within phase)	8 (57.1)	9 (69.2)	9 (69.2)	26 (65.0)
Methylated	Count (% within phase)	0 (0.0)	3 (23.1)	2 (15.4)	5 (12.5)
Total		14 (100)	13 (100)	13 (100)	30 (100)

Data are presented as n (%). AML; Acute myeloid leukemia.

Table 3: Correlation of fold changes in different phases and methylation statuses

Phase	Methylation status		Mean difference (95% Wald confidence interval for difference)	P value
Remission	Methylated	Hemi-methylated	-.0778 (-0.2465, 0.0910)	0.366
		Un-methylated	-2.1500[a] (-3.4739, -0.8261)	0.001
	Hemi-methylated	Un-methylated	-2.0722[a] (-3.9323, -0.7521)	0.002
Under- treatment	Methylated	Hemi-methylated	-.0750 (1.2334, 1.0834)	0.899
		Un-methylated	0.3500 (-0.4122, 1.1122)	0.368
	Hemi-methylated	Un-methylated	0.4250 (-0.4472, 1.2972)	0.340
New cases	Hemi-methylated	Un-methylated	0.1125 (-0.3256, 0.5506)	0.615

Correlation of *SMG1* expression and paraclinical indexes

The analysis of the interaction of phase and methylation status shows that no one of the paraclinical indexes is significantly different (Table 4). Also, WBC, RBC, Plt, and Hb are all significantly different in different phases (P<0.001, for all) While WBC and Plt counts are significantly different in different methylation statuses (P=0.018 and P=0.029, respectively), Hb and RBC are not different in patients with different methylation status.

The results of the generalized estimating equation (GEE) statistical test in patients who participated in three phases of this trial show that in under-treatment patients, WBC count decreases 114176.36 cell/µl on overage with each unit of increase in fold change [P<0.001, 95% confidence interval (CI): (-177285.38, -51067.34)]. Also, in the remission phase, WBC count averagely decreases 115229.26 cell/µl with each unit of increase in fold change [P<0.001, 95% CI: (-178497.21, -51961.31)].

In under-treatment patients, Hb unit increases 2.062 g/dl with each unit of increase in fold change [P<0.001, 95% CI: (0.930, 3.195)]. Also, in the in-remission phase, Hb unit increases 1.395 g/dl with each unit of increase in fold change [P=0.019, 95% CI: (0.233, 2.558)].

Regarding the Plt count in under-treatment patients, the Plt count increases 36637.75 cell/µl with each unit of increase in fold change [P=0.012, 95% CI: (7999.16, 65276.36)]. There were no significant correlations between other indexes/phases and fold change of the *SMG1* gene (Table 5).

Table 4: Correlation of laboratory indexes in different phases and methylation status

Laboratory indexes	Phase		Methylation status		Interaction of phase and methylation status	
	Wald chi-square (df=2)	P value	Wald chi-square (df=2)	P value	Wald chi-square (df=3)	P value
WBC (/µL)	25.961	<0.001	8.042	0.018	2.509	0.474
RBC (10^6/µL)	15.223	<0.001	0.474	0.789	0.904	0.824
Hemoglobin (g/dl)	15.898	<0.001	0.941	0.625	1.049	0.789
Platelet (/µL)	26.491	<0.001	7.051	0.029	2.807	0.422
Fold change	15.478	<0.001	4.718	0.095	4.718	<0.001

WBC; White blood cell, RBC; Red blood cell, and df; Degree of freedom.

Table 5: Correlation of *SMG1* fold change and paraclinical indexes

Indexes		Under-treatment	Remission
WBC (cell/µl)	B (95% CI)	-114176.356 (-177285.376, -51067.337)*	-115229.26 (-178497.29, -51961.31)
	P value	<0.0001	<0.0001
RBC (10^6 cell/µl)	B (95% CI)	0.552 (-0.061, 1.166)	0.356 (-0.248, 0.960)
	P value	0.078	0.248
Hemoglobin (cell/µl)	B (95% CI)	2.062 (0.930, 3.195)	1.395 (0.233, 2.558)
	P value	<0.0001	0.019
Platelet (cell/µl)	B (95% CI)	36637.750 (7999.164, 65276.335)	-28148.811 (-73289.437, 16991.816)
	P value	0.012	0.222

WBC; White blood cells, RBC; Red blood cells, and *; Change in amount of paraclinical indexes with each unit of increase in fold change compared with new cases.

Discussion

Aberrant DNA methylation is a critical etiology in leukemia. The relative methylation of the CpG-islands of the SMG1 promoter, as a tumor suppressor gene, is involved in the progression of various types of cancers. Our results showed that methylation of the CpG-islands of the SMG1 promoter changed through the phases (from diagnosis to complete remission). In this study, it was demonstrated that the hemimethylated status of *SMG1* is dominant in all groups (control and cases), but in new cases (patients who have not received medication), the methylation status of *SMG1* is hypomethylated compared to the control, under-treatment and remission groups. Also, the distribution of the unmethylated alleles of *SMG1* is detected more frequently in new cases than control, medication-receiving, and in-remission groups. These finding show two facts: first, in AML, the epigenomic anti-cancer mechanisms lead to less methylation in the *SMG1* promoter, which leads to stronger tumor-suppressive effects of this gene, and two, the methylation status will return to a normal state following remission. The second finding can be due to the medications or the physiologic response of the body.

Different studies established that the *SMG1* gene acts as a tumor suppressor gene involved in various cancers, especially hematopoietic malignancies. On the other hand, CpG-island methylation patterns play a critical role in enhancing or inducing gene expression. Different studies established the role of epigenetics, especially DNA methylation, in the progression of hematopoietic malignancies (4). In order to correct the aberrant DNA methylation pattern, there are some methylation-targeting drugs. i.e., hypomethylating agents (HMAs), which have been developed for leukemia, lymphoma, and myeloma. Following the last studies on the impact of aberrant DNA methylation in cancer, various technologies are developed for gene-specific methylation modifications, i.e., CRISPR-Cas9-mediated methylome modifiers (9, 10). Alongside

the progression in methylation modifier technologies, the investigations are held on finding more methylation-based therapeutic, diagnostic, and prognostic biomarkers (11). In this study, we tried to investigate the role of the CpG-islands methylation patterns of *SMG1* in AML progression and its status during follow-up of patients

Our results showed that in new cases, the fold change of *SMG1* expression levels is 0.464 ± 0.468, while the CpG-islands of *SMG1* were in hypomethylated status, compared to the control group. Therefore, in new cases, the regulation of *SMG1* expression is not affected by promoter methylation. Also, *SMG1* expression levels in under-treatment and in-remission patients are 0.973 ± 1.159 and 0.685 ± 0.885, respectively, and the CpG-islands of *SMG1* are partially methylated compared to the control group. Therefore, the *SMG1* expression level is regulated by methylation of its promoter when patients receive medications (under-treatment and in-remission patients). Also, the regulation of *SMG1* expression in not affected by promoter methylation in new cases, but in under-treatment and remission phases, the *SMG1* expression level and promoter methylation is close to the control group.

Regarding the role of *SMG1* methylation status in cancer, Gholipour et al. (12) utilized that the CpG-islands methylation pattern of *SMG1* is in hemimethylated status in multiple myeloma patients. Gubanova et al. (13) showed that the CpG-islands methylation pattern of *SMG1* is in the hypermethylated state in head and neck cancer patients, compared to healthy individuals. Pourkarim et al. (7) showed that the CpG-islands methylation pattern of *SMG1* is hypermethylated in acute lymphoblastic leukemia (ALL) patients. A study was conducted in 2019 by Ho et al. (14) to investigate the effect of *SMG1* and *ATM* on mice. In mice, complete loss of fetal *Smg1* is fatal, and loss of a single allele increases the growth rate of cancers, especially hematopoietic cancers and lung cancer. The data showed that the simultaneous decrease in *ATM* and *SMG1* expression increased the progression of hematopoietic cancer. The results of this study confirm the importance of our study on the potential effects of *SMG1* on the incidence of AML. In a 2019 study by Mai et al. (15), they showed that miR-18a expression is upregulated in nasopharyngeal carcinoma tissues and is positively correlated with tumor size and tumor-nodes-metastases stage. *SMG1* was identified as the target of miR-18a. The results confirmed that miR-18a plays its carcinogenic role by suppressing *SMG1*, reducing its expression and activating the mTOR pathway in nasopharyngeal carcinoma cells. The results of this study, which indicate the importance of *SMG1* in the incidence of cancer, validate our results to show *SMG1* as a vital factor in the development of AML. A 2014 study by Du et al. (16) was conducted to evaluate the function of *SMG1* in AML. The results showed that *SMG1* was hypermethylated in the promoter. It should be noted that in this study, the relationship between *SMG1* gene expression and patients' clinical symptoms was not discussed. On the other hand, expression and methylation in different phases of the disease (at diagnosis, under treatment, and remission) were not studied.

In this study, we showed that the expression of *SMG1* is correlated to the *SMG1* methylation pattern. In the under-treatment group, the unmethylated allele of *SMG1* is most prevalent, while the expression level of *SMG1* is lower compared to other studied groups. In the remission group, the methylated allele of *SMG1* is more prevalent than in new cases and control, but not the under-treatment group. Furthermore, the expression level of *SMG1* is lower compared to new cases and control groups, while *SMG1* is more highly expressed in the remission group compared to the under-treatment group. These patterns are also the same in the control and new cases group. Regarding our findings, different studies established that the expression of *SMG1* is under the control of the CpG-islands methylation patterns of this gene.

The investigation of the correlation of *SMG1* expression and laboratory indexes showed that in under-treatment and in-remission patients, WBC count was reduced with each unit of increase in the fold change of *SMG1*. Also, the increase in fold change is responsible for the rise in Plt and Hb of patients in the under-treatment phase. Therefore, high expression of *SMG1*, as a tumor suppressor gene, leads to a better outcome in the remission phase of AML patients, regarding the induction of Plt generation and hematopoiesis and WBC reduction count.

Based on our results, the expression level and methylation status of *SMG1* is varied in different phases of AML and control individuals. Also, the expression level of *SMG1* is correlated with outcome-related laboratory hallmarks. Therefore, *SMG1* can be a potential prognostic biomarker for AML patients, requiring more studies.

Conclusion

This study followed-up the methylation status and gene expression of *SMG1* in AML. In new cases, the CpG-island of *SMG1* is hypomethylated compared to the control group. Also, there are different expression levels in different phases and methylation statuses, but the expression level of *SMG1* is not regulated by promoter DNA methylation in new cases. Finally, due to the correlation of the expression level of *SMG1* and laboratory indexes, it can be suggested that *SMG1* expression and methylation status can predict the outcome of chemotherapy. The low number of participants, the mortality of involved patients in the follow-up process, and trouble in accessing patients were limitations of our study.

Acknowledgments

There is no financial support and conflict of interest in this study.

Authors' Contributions

N.K.; Has participated in study design, data collection and assessments, and conducting the molecular experiments. M.H.A., Sh.P.D.; Advised the molecular experiments and qRT-PCR analysis. S.M.; Contributed to data collection and assessments. A.M.; Contributed to data collection and drafting the manuscript. A.A.; Contributed to the advanced statistical analysis and data assessments. M.A.; Contributed to the conception, design, and all experimental works, and supervised this study. All authors read and approved the final manuscript.

References

1. Azad M, Bakhshi Biniaz R, Goudarzi M, Mobarra N, Alizadeh S, Nasiri H, et al. Short view of leukemia diagnosis and treatment in iran. Int J Hematol Oncol Stem Cell Res. 2015; 9(2): 88-94.
2. Rowe JM. Will new agents impact survival in AML? Best Pract Res Clin Haematol. 2019; 32(4): 101094.
3. Goudarzi M, Heidary M, Azad M, Fazeli M, Goudarzi H. Evaluation of antimicrobial susceptibility and integron carriage in Helicobacter pylori isolates from patients. Gastroenterol Hepatol Bed Bench. 2016; 9 Suppl1: S47-S52.
4. Meng H, Cao Y, Qin J, Song X, Zhang Q, Shi Y, et al. DNA methylation, its mediators and genome integrity. Int J Biol Sci. 2015; 11(5): 604-617.
5. Azad M, Kaviani S, Soleimani M, Nourouzinia M, Hajfathali A. Common polymorphism's analysis of thiopurine S-methyltransferase (TPMT) in Iranian population. Cell J. 2009; 11(3): 263-347.
6. Alipour S, Sakhinia E, Khabbazi A, Samadi N, Babaloo Z, Azad M, et al. Methylation status of interleukin-6 gene promoter in patients with Behçet's disease. Reumatol Clin (Engl Ed). 2020; 16(3): 229-234.
7. Pourkarim H, Azad M, Haghi Ashtiani MT, Keshavarz S, Nadali F. The correlation between SMG1 promoter methylation and its expression in acute lymphoblastic leukemia patient. Arch Med Lab Sci. 2016; 2(4): 111-116.
8. Ghorban K, Shanaki M, Mobarra N, Azad M, Asadi J, Pakzad R, et al. Apolipoproteins A1, B, and other prognostic biochemical cardiovascular risk factors in patients with beta-thalassemia major. Hematology. 2016; 21(2): 113-120.
9. Vinyard ME, Su C, Siegenfeld AP, Waterbury AL, Freedy AM, Gosavi PM, et al. CRISPR-suppressor scanning reveals a nonenzymatic role of LSD1 in AML. Nat Chem Biol. 2019; 15(5): 529-539.
10. Vojta A, Dobrinić P, Tadić V, Bočkor L, Korać P, Julg B, et al. Repurposing the CRISPR-Cas9 system for targeted DNA methylation. Nucleic Acids Res. 2016; 44(12): 5615-5628.
11. Cai SF, Levine RL. Genetic and epigenetic determinants of AML pathogenesis. Semin Hematol. 2019; 56(2): 84-89.
12. Gholipour H, Abroun S, Noruzinia M, Ghaffari S, Maali A, Azad M. Methylation status of smg1 gene promoter in multiple myeloma. J Blood Cancer. 2018; 10(4): 114-116.
13. Gubanova E, Brown B, Ivanov SV, Helleday T, Mills GB, Yarbrough WG, et al. Downregulation of SMG-1 in HPV-positive head and neck squamous cell carcinoma due to promoter hypermethylation correlates with improved survival. Clin Cancer Res. 2012; 18(5): 1257-1267.
14. Ho U, Luff J, James A, Lee CS, Quek H, Lai HC, et al. SMG1 heterozygosity exacerbates haematopoietic cancer development in Atm null mice by increasing persistent DNA damage and oxidative stress. J Cell Mol Med. 2019; 23(12): 8151-8160.
15. Mai S, Xiao R, Shi L, Zhou X, Yang T, Zhang M, et al. MicroRNA-18a promotes cancer progression through SMG1 suppression and mTOR pathway activation in nasopharyngeal carcinoma. Cell Death Dis. 2019; 10(11): 819.
16. Du Y, Lu F, Li P, Ye J, Ji M, Ma D, et al. SMG1 acts as a novel potential tumor suppressor with epigenetic inactivation in acute myeloid leukemia. Int J Mol Sci. 2014; 15(9): 17065-17076.

Original Article

CYP19A1 Promoters Activity in Human Granulosa Cells: A Comparison between PCOS and Normal Subjects

Zohreh Hashemain, M.Sc.[1, 2, 3], Amir Amiri-Yekta, Ph.D.[1], Mona Khosravifar, M.Sc.[1], Faezeh Alvandian, M.Sc.[1], Maryam Shahhosseini, Ph.D.[1, 3], Saman Hosseinkhani, Ph.D.[4*], Parvaneh Afsharian, Ph.D.[1, 3*]

1. Department of Genetics, Reproductive Biomedicine Research Center, Royan Institute for Reproductive Biomedicine, ACECR, Tehran, Iran
2. Human and Animal Cell Bank, Iranian Biological Resource Center (IBRC), ACECR, Tehran, Iran
3. Faculty of Sciences and Advanced Technologies in Biology, University of Science and Culture, Tehran, Iran
4. Department of Biochemistry, Faculty of Biological Sciences, Tarbiat Modares University, Tehran, Iran

Corresponding Addresses: P.O.Box: 14115-175, Department of Biochemistry, Faculty of Biological Sciences, Tarbiat Modares University, Tehran, Iran
P.O.Box: 16635-148, Department of Genetics, Reproductive Biomedicine Research Center, Royan Institute for Reproductive Biomedicine, ACECR, Tehran, Iran
Emails: saman_h@modares.ac.ir, pafshar@royaninstitute.org

Received: 16/September/2020, Accepted: 01/March/2021

Abstract

Objective: Estrogen, a female hormone maintaining several critical functions in women's physiology, e.g., folliculogenesis and fertility, is predominantly produced by ovarian granulosa cells where aromatase enzyme converts androgen to estrogen. The principal enzyme responsible for this catalytic reaction is encoded by the *CYP19A1* gene, with a long regulatory region. Abnormalities in this process cause metabolic disorders in women, one of the most common of which is polycystic ovary syndrome (PCOS). The main purpose of this research was to determine the effect of the promoters on aromatase expression in cells with normal and PCOS characteristics.

Materials and Methods: In this experimental study, four promoters of the *CYP19A1* gene, including PII, I.3, I.4, and PII/ I .3 promoter fragments, were cloned upstream of the luciferase gene and transfected into normal and PCOS granulosa cells. Subsequently, the effect of follicle-stimulating hormone (FSH) on the activity of these regulatory regions was examined in the presence and absence of FSH. Western blotting was used to confirm aromatase expression in all groups. Data analysis was performed using ANOVA and paired sample t test, compared by post-hoc least significant difference (LSD) test.

Results: Luciferase results confirmed the intense activity of PII promoter in the presence of FSH. Moreover, the study demonstrated reduced activity of PII promoter in normal granulosa cells, possibly due to the regulatory region of I.3 next to PII.

Conclusion: FSH stimulates transcription of aromatase enzyme by affecting PII promoter, a process regulated by the inhibitory role of the I.3 region in PII activity in granulosa cells. Given the distinct role of these promoters in normal and PCOS granulosa cells, the importance of nuclear factors residing in these regions can be discerned.

Keywords: Aromatase, Granulosa, Luciferase, Polycystic Ovary Syndrome, Promoter

Cell Journal(Yakhteh), Vol 24, No 4, April 2022, Pages: 170-175

Citation: Hashemain Z, Amiri-Yekta A, Khosravifar M, Alvandian F, Shahhosseini M, Hosseinkhani S, Afsharian P. CYP19A1 promoters activity in human granulosa cells: a comparison between PCOS and normal subjects. Cell J. 2022; 24(4): 170-175. doi: 10.22074/cellj.2022.7787.

Introduction

Women's reproductive system is complex machinery comprised of components such as hormones and ovarian factors working in perfect harmony. The normal reproduction process requires timely adequate secretion of hormones to regulate the input of a hormone from the central nervous system, the pituitary gland, and the ovary. Any disturbances in this process lead to reproductive system disorders and subsequent infertility. Hormones are the main actors in the process of folliculogenesis and ovulation, and imbalances in the secretion of hormones disturb the folliculogenesis process (1-3). Polycystic ovary syndrome (PCOS) is a common endocrinopathy disorder accompanied by an increase in androgen levels, disturbed follicular maturation process, and absent ovulation (4).

Generally, hormones are the main actors in folliculogenesis and ovulation. Estrogen, one of these major hormones, is essential for regulating hemostasis and pathological pathways, especially infertility (2). Follicles are the primary source of local and circulatory estrogen in mammals. Synthesis of follicular estradiol depends on the effective reaction between pituitary gonadotropin hormone, follicle-stimulating hormone (FSH), luteinizing effective hormone (LH), cytokines, and growth hormones, among which FSH is the leading causative agent governing estrogen synthesis. Regulation of *CYP19A1* gene transcription is conducted via binding of FSH to the relevant receptor on granulosa cells and subsequent production of cAMP, NR5A1, and sequential signals. This gene encodes the aromatase enzyme, which plays a crucial role in the irreversible conversion of androstenedione to estrogen (5-7). In a PCOS woman; however, decreased level of the aromatase enzyme leads to the reduction of estrogens hormone, which finally caused the increase in androgen hormone. Production of androgens blocks the feedback between the ovaries and the pituitary gland. Therefore, the pituitary generates high levels of LH, which further produce more androgens from

Theca cells of the follicle. High levels of androgens inhibit follicular growth, and the egg cannot grow. Therefore, ovulation will not occur, and the premature oocyte becomes a small cyst with a thin wall instead of being released from the ovary. This leads to the production of androgens and prevention from follicular growth in the following months. In other words, acceleration of primary follicular growth is mainly due to an excessive increase in androgens, which results in excessive growth of small follicles (8).

The enzyme aromatase is expressed periodically and specifically in the granulosa cells of the ovary and is essential for regulating folliculogenesis autocrine, endocrine control of reproduction in females, and coordination during gonadotropin secretion (7, 9). The wide regulatory area of the *CYP19A1* gene is about 93 kb and contains 11 discovered promoters. These promoters have been determined to regulate aromatase expression in various tissues in a tissue-specific manner (9-13). Various regulatory sequences of DNA, transcription factors, cytokines, and hormones bind to the aromatase promoter's regulatory regions in each cell type, resulting in the induction of aromatase expression in those cells (13). Among multiple promoters of *CYP19A1*, promoter II (PII) is actively involved in aromatase expression in granulosa cells (14-17). Besides, some studies indicated the presence of promoters I.3 and I.4 and promoter II for aromatase expression in ovarian cells (18, 19).

As mentioned, there are still ambiguities about the function of aromatase regulatory regions in granulosa cells and our aim was to clarify the most effective promoter of the *CYP19A1* gene in granulosa cells. In the present study, we examined the activity of PII, I.3, PII/I.3, and I.4 promoters in normal and PCOS granulosa cells via measurement of luciferase activity as a biosensor in the presence and absence of FSH. Moreover, we investigated aromatase expression in different groups of normal and PCOS granulosa cells.

Materials and Methods

Cell culture and morphological observation

Granulosa cells were obtained from samples of women with normal folliculogenesis and PCOS who had undergone assisted reproductive technology (ART) process. It should be noted that the specimens were approved by the Embryology Department and Ethics Committee of Royan Institute (IR.ACECR.ROYAN.REC.1394.87). Primary culture and immortalization of normal granulosa cells (GCN) and PCOS granulosa cells (GCP) were performed in collaboration with the Iranian biological resource center and the Genetics Department of Royan Institute. GCN-01 and GCP-01 cell lines were banked at the Iranian biological resource center. GCP-01cells were cultured in DMEM/Ham's F-12 medium supplemented with 17.5% fetal bovine serum (FBS, Gibco, US), 2.5% horse Serum, 4mM L-Glutamine (Gibco, US), 2 mM non-essential amino acids (Sigma, US), 100 IU/mL penicillin, 100 mg/mL streptomycin (Gibco, US), 100 ng/mL recombinant FSH (rFSH, Gonal-F, Merck, France), 100 ng/mL bFGF (Royan, Iran), 25 ng/mL epidermal growth factor (EGF, Royan, Iran), 0.5 µg/mL hydrocortisone (Merck, France), 50 µg/mL ascorbic acid (Sigma, US), 100 ng/mL cholera toxin (Sigma, US), and 1X insulin-transferrin-selenium (Gibco, US). In addition, GCN-01 cells were cultured in a DMEM/Ham's F-12 medium Supplemented as mentioned above but lacked horse Serum and rFSH (20).

GCP-01 and GCN01 were seeded in 6-well plates and treated with or without 100 ng/mL rFSH. Subsequently, the morphological features of GCP-01 and GCN-01 were examined under an optical microscope.

Promoter constructs

PII, I.3, PII/I.3, and I.4 promoters of CYP19 were amplified by polymerase chain reaction (PCR) from human genomic DNA in a reaction mixture of 120 µL containing 100 ng genomic DNA, Mastermix (Ampliqon, Denmark), and primers. Primers are listed in Table 1. After amplification, PCR products were purified by High Pure PCR Product Purification Kit (Roche). Next, fragments were digested using SacI and XhoI restriction enzymes (Fermentas) and subcloned into a pGL4-26 vector (Promega, Madison, WI, USA), which carries firefly luciferase as its reporter gene. In the first step, the presence of each promoter fragment in the vector was confirmed using colony PCR and double digestion by SacI and XhoI enzymes. In the end, the inserts were sequenced to ensure fidelity of the amplified sequences.

Table 1: Primers used for promoter constructs in the present study

Insert	Primer sequence (5′-3′)	Annealing temperature (˚C)	PCR product (bp)
I.3	F: ACTG**GAGCTC**TCAACGATGCCCAAG 3′	57	390
	R: ATCG**CTCGAG**AACAAGGAAGCCCAAG 3′		
PII	F: ACTG**GAGCTC**CCTTGTTTTGACTTG 3′	57	490
	R: ATCG**CTCGAG**GACATAGTCTTCAGAG 3′		
I.4	F: ACTG**GAGCTC**GAGAATGGGAATGTTG 3′	58	925
	R: ATCG**CTCGAG**TACCTGGTTTGATGG 3′		
PII/I.3	F: ACTG**GAGCTC**TCAACGATGCCCAAG 3′	57	835
	R: ATCG**CTCGAG**GACATAGTCTTCAGAG 3′		

F; Forward Primer (SacI restriction site: 5′-**GAGCTC**-3′), R; Reverser Primer (XhoI restriction site: 5′-**CTCGAG**-3′), and PCR; Polymerase chain reaction.

Transfection

GCN and GCP were grown in 12-well plates at 60-80% confluency, and transient transfection was carried out using the Lipofectamine 3000 kit (Invitrogen, US) according to the manufacturer's instructions. Cells were transfected with 1 mg of each pGL4-26/CYP19 promoter. The transfection experiments were performed in triplicate for each construct. After transfection, GCN and GCP were incubated in DMEM without FBS for 8 hours, and subsequently, the medium was replaced with complete media, with or without 100 ng/mL r-FSH (Gonal-f). After treatments, cells were incubated for 48 hours and observed for the firefly luciferase activities in the cell lysates.

Luciferase assay

Cells were washed with PBS and lyzed in 30 µL Cell Lysis Reagent (Promega, UK, Southampton, United Kingdom). Cell lysates were harvested, and spun for 15 minutes. The cell lysates (20 µL) were added to 20 µL of luciferin complex (Promega, UK, Southampton, United Kingdom). Luciferase bioluminescence measurements were performed at room temperature using a luminometer (Sirius tube Luminometer, Berthold Detection System, Germany). The activity was expressed as relative light units (RLU) emitted from total assays versus background activity. In addition, protein concentrations were measured by the Bradford method, and firefly luciferase activities were normalized against the total protein.

Western blot analysis

Total protein was extracted from all groups of transfected GCN and GCP. Protein concentration was determined using the Bradford assay. Here, 30 µg of each sample protein was separated by SDS-PAGE and electroblotted onto Polyvinylidene fluoride (PVDF) membranes. The membranes were blocked using 5% non-fat skim milk in Tris-buffered saline containing Tween 20 and subsequently incubated overnight at 4˚C with anti-aromatase (MCA2077S, Bio-Rad, US), anti-β actin (sc-47778, Santa Cruz, US). The membranes were then incubated for 60 minutes at room temperature with mouse secondary antibodies conjugated to horseradish peroxidase (STAR133, Bio-Rad, and DB9571, Kalazist, Iran). After washing with TBST for 15 minutes once and 5 minutes thrice, ECL reagent (BIO-RAD, Hercules, CA) was added, and the membranes were exposed to X-ray film (GE Healthcare, Cambridge, UK).

Statistical analysis

Statistical analyses were performed using the IBM SPSS statistic 21 software (IBM Corp., Armonk, NY). The ANOVA test determined significant differences between groups, while paired sample t test was used to compare the normal and PCOS subgroups. Also, significant differences between the subgroups were measured by the LSD test. A $P<0.05$ was considered significant.

Results

Medium changes indicative of changes in cellular secretion after FSH treatment

Both GCN and GCP (normal and PCOS granulosa cells, respectively) were cultured in two groups for 6 hours at a density of 5×10^5 cells per well. One group of each normal or PCOS cells was treated with FSH. After 48 hours, without changing the medium, cellular morphology and alterations in the culture medium were precisely monitored by light microscopy. Steroids secretion by normal cells was significantly higher in the presence of FSH. These secretory changes were observed after treatment with FSH in the presence of secretory vacuoles in cells and lipid-like droplets suspended in cell culture medium. Also, secretion of the PCOS cells increased after FSH treatment, but this elevation was lower than that observed for normal cells (Fig.1).

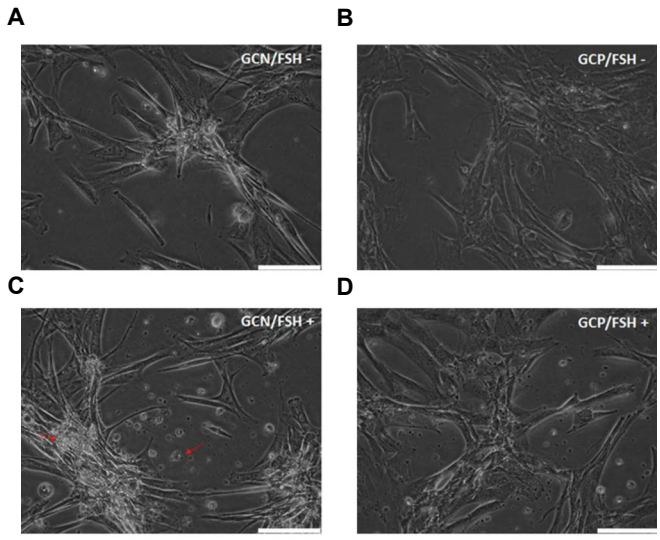

Fig.1: FSH affects the morphology and culture medium of GCN and GCP. **A.** GCN was grown without FSH and **B.** With FSH. **C.** GCP was grown without FSH and **D.** With FSH (scale bar: 100 µm). Red arrows indicate the lipid-like droplets. GCN; Normal granulosa cells, GCP; PCOS granulosa cells, PCOS; Polycystic ovary syndrome, and FSH; Follicle-stimulating hormone.

Functional analysis of the promoter regions in normal and PCOS cells

The mentioned promoters were cloned upstream of the luciferase reporter gene of the pGL4-26 plasmid. These were transiently transferred to the normal and PCOS granulosa cells in different groups. The four designed promoter constructs included PII, I.3, PII-I.3, and PI.4. Luciferase assays were performed on cultures maintained with or without FSH. The luciferase assay results after normalization against total protein showed that in both cells, the promoter PII had a significant role in luciferase expression as a 2.3-fold increase was observed in normal cells and a 2.2-fold increase in PCOS cells. However, the PII-I.3 promoter fragment has a different pattern in luciferase expression in normal and PCOS cells. A 1.7-fold increase compared to the control and a 0.3-fold

decrease compared to the promoter PII alone were observed in normal cells. In addition, a 0.5-fold decrease compared to the control and a 0.8-fold decrease compared to the promoter PII alone were detected in PCOS cells. Increasedactivity of the promoter I.3 in the normal cell was not significant. In contrast, the reduction in its activity in the PCOS group was significantly larger than that in the normal group and the control subgroup. Also, FSH removal in this subgroup did not show any significant changes in promotor activity . Promoter I.4 activity decreased in both normal and PCOS groups; however, this decrease reached a significant level only in the normal group. Promoter I.4 exhibited similar behavior in the presence or absence of FSH (Fig.2).

Evaluation of aromatase and β actin gene expression

Cell preparation protocol for protein extraction was similar to that described for luciferase assay. Total proteins were extracted from all cell groups. Expression of β actin protein as internal control and aromatase were determined to assess changes in expression induced by vector transfection and FSH treatment using western blotting. Subsequently, the density of the western blot bands was evaluated by ImageJ software. The aromatase expression and luciferase assay were normalized against β actin expression in each group. After analysis of the results, it was found that transfection with the promoter fragments caused no significant change in protein expression. However, FSH treatment increased by 2.3-fold in normal cells and 2.1-fold in PCOS cells. It should be noted that comparing between before- and after-FSH-treatment values showed that aromatase expression in normal cells was 1.5 times more than in PCOS cells (Fig.3).

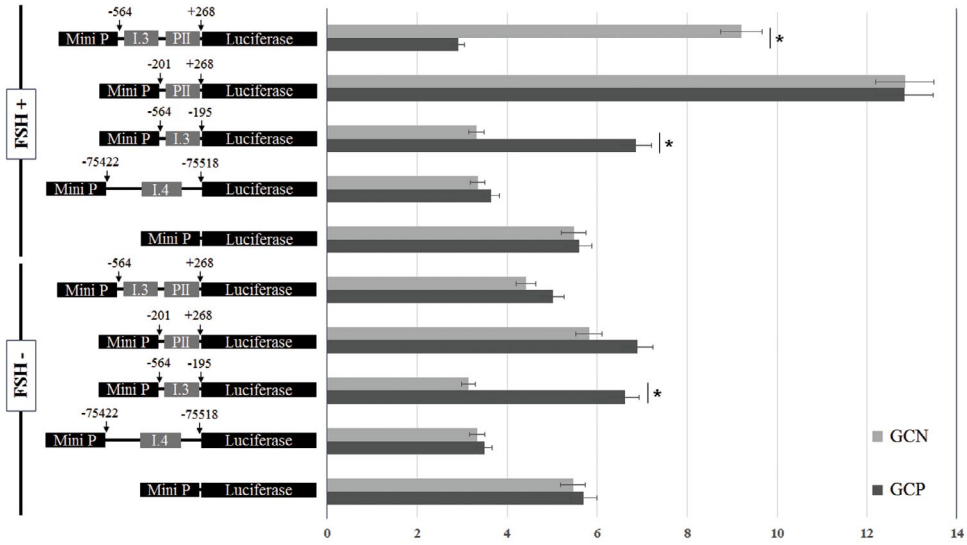

Fig.2: Luciferase assays of several CYP19 promoters constructs under FSH treatment. Relative luciferase activities (right) measured in GCN and GCP (normal and PCOS granulosa cells, respectively) transfected with one pGL4-26-CYP19 construct (PII/I.3, PII, I.3 and I.4; left) were treated with or without FSH. Transfection experiments were replicated three times for each construct. *; Significant differences in activity construct between GCN and GCP (paired sample t test, P<0.05), GCN; Normal granulosa cells, GCP; PCOS granulosa cells, PCOS; Polycystic ovary syndrome, and FSH; Follicle-stimulating hormone.

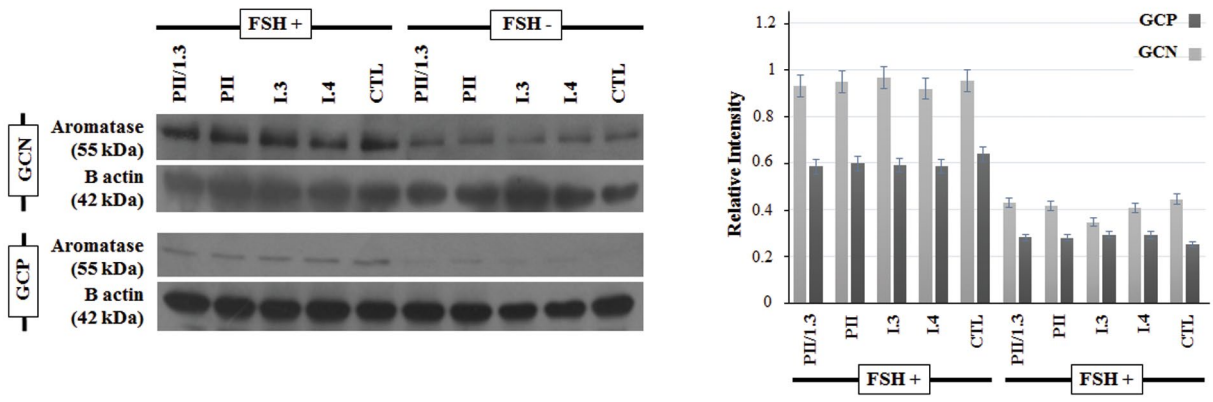

Fig.3: Western blot analysis of aromatase protein expression. **A.** Aromatase expression was investigated in the transfected and treated GCN and GCP. β-actin was used as a loading control. **B.** Histogram for aromatase expression based on western blot results. GCN; Normal granulosa cells, GCP; PCOS granulosa cells, PCOS; Polycystic ovary syndrome, and FSH; Follicle-stimulating hormone.

Discussion

In this study, we showed that in the presence of FSH, the PII promoter is the main promoter that influences ovarian aromatase gene expression; however, the PII promoter activity was affected by promoter region I.3. We also found that the effect of region I.3 on the PII promoter was not similar in the normal and PCOS cells.

According to the previous studies, we investigated 4 promoter regions, PII (-201/+268), PI.3 (-564/-195), PII/I.3 (-564/+268), and I.4 (-75422/-75518), among 11 promoters of the *CYP19A1* gene. Investigation of the role of conserved regulatory sequences in these promoter regions can help to discuss the results.

The PII promoter is coded as the closest promoter to the coding region. This promoter is naturally the main promoter of the ovary, which participates in aromatase expression in seminal vesicles, bladder, testis, and prostate tissues. It was also shown to induce unusual aromatase expression in breast cancer, endometriosis, hepatocellular carcinoma, adrenocortical tumors, and Sertoli and PI.3 to each other and to the coding region, these were considered the promoter region in some studies (21, 22). Therefore, it is considered a relatively strong promoter (8-12). The I.3 promoter is located approximately 200 bp upstream of the PII promoter and acts as a CYP19A1 promoter in breast cancer, adipose tissue, seminal, and blood vessels (8, 9). Due to the proximity of the promoters PII and PI.3 to each other and to the coding region, these were considered the promoter region in some studies (21, 22).

Nevertheless, 1kb upstream of exon II, the three promoter regions PII, I.3, and I.6 are located (23, 24). So far, several conserved regulatory sequences have been identified in this area, indicating the critical role of this region in aromatase gene expression. The most important segments of these regions are the TATA box (-26 to -31), a putative forkhead element (-69 to -82), a conserved region that responds to GATA transcription factors (-165 to -179), and an uncharacterized putative SFRE (-184 to -193) (25-27). The cis-regulatory elements steroidogenic factor-1 (SF-1) and CRE-like sequence (CLS) are located upstream of the PII promoter. CLS responds to both cAMP as an activator and Jun proteins as inhibitors of *CYP1A1* gene expression (28). Other regulatory factors that can be mentioned as the C/EBP conservation sequence are located upstream of SF-1 and CLS (17, 29). There are two conserved sequences for NR5A1/NR5A2 and FOXL2 that bind to the forkhead box and act as a transcription factor. These elements are involved in granulosa cells proliferation, steroid hormones synthesis, and ovary apoptosis regulation. Increased levels of NR5A2, along with forskolin, induce the activity of CYP19A1 and FOXL2 as aromatase inhibitors in the ovary (30). In granulosa cells, cis-elements located upstream of the PII promoter respond to several nuclear receptors, including NURR1 and NGFI-B, that suppress aromatase expression (29). A forkhead element in -516 responds to the mutant FOXL2 (C134W) in granulosa cell tumors, which in turn induces the expression of aromatase in these cells (24). Previous studies investigated the role of some regulatory elements in this area in other cells, which may have a role in ovarian cells, however, they were neglected. For instance, upstream of -211, there are several repressor elements that can inhibit the activity of the PII promoter in MG-63 cells (31). In addition, in upstream of the PII promoter, there are a number of conserved sequences with a silencing role in breast cancer cells. These areas respond to Gata 4 and perhaps other factors but their role is not so far elucidated (27).

The promoter I.4 is located approximately 73 kb upstream of exon II and has been implicated in aromatase expression as the primary promoter in adipose tissue, skin, seminal vesicles, bladder, placenta, bone, and blood vessels (8, 9, 32). Several regulatory sequences in this region are involved in aromatase expression in different tissue cells. For example, glucocorticoid responsive factors in normal breast cells and ROR alpha regulatory factors in breast cancer cells are known as regulatory factors in this area (33-36). However, the effect of the promoter I.4 on the protein expression of the *CYP19A1* gene has not been established in ovarian cells; only in one case, exon I.4 in aromatase transcripts was reported in granulosa cells (18).

Considering the present work results and data reported by previous studies, it can be concluded that the PII promoter is stimulated in the presence of FSH, which leads to aromatase protein expression. Also, inhibitory factors in promoter I.3, which is located upstream of the PII promoter, control the PII promoter and prevent aromatase overexpression resulting in the reduction of the activity of the PII promoter. These results indicated that promoter I.3 acts as enhancer elements (27, 31). However, in the granulosa cells of PCOS individuals, the inhibitory effect of the promoter I.3 is sufficient to inhibit PII promoter activity. Furthermore, aromatase is not sufficiently expressed in these cells leading to PCOS symptoms such as increased androgen and decreased estrogen. Taken together, the data indicate the critical role of the promoter I.3 in the regulation of aromatase gene expression, which has received less attention so far.

This study is a preliminary step to discover how promoter regions are involved in aromatase expression in the normal and PCOS granulosa cells. Therefore, it is likely that nuclear elements interact with the PI.3 region and affect aromatase expression in the normal and PCOS granulosa cells. Further studies are needed to understand the mechanisms of transcriptional regulation in the PII region, in particular I.3, to recognize the nuclear factors that are involved.

In brief, we found that FSH has stimulatory effects on the PII promoter, and a functional relationship between the promoter region I.3 and the PII promoter exists in normal granulosa cells and PCOS. We found that the I.4 promoter was not involved in the expression of aromatase protein, neither in normal nor in PCOS granulosa cells.

These results could help discover the complexity of CYP19 expression in ovarian cells, especially in PCOS granulosa cells.

Acknowledgments

This study has been funded by Royan Institute (91000715). The authors would like to thank colleagues at Royan Institute for Reproductive Biomedicine, Department of Genetics and Genetic Engineering (Tehran, Iran). The authors declare no conflict of interest in this study.

Author's Contributions

Z.H., P.A., S.H., M.Sh.; Contributed to conception and design. Z.H.; Contributed to all experimental work, data and statistical analysis, and interpretation of data. P.A., S.H.; Were responsible for overall supervision. A.A.-Y.; Contributed to concept and design of molecular part. M.K., F.A.; Cooperated with some experimental tests. Z.H.; Drafted the manuscript, which was revised by P.A., A.A.-Y. All authors read and approved the final manuscript.

References

1. Homburg R, Insler V. Ovulation induction in perspective. Hum Reprod Update. 2002; 8(5): 449-462.
2. Matzuk MM, Lamb DJ. The biology of infertility: research advances and clinical challenges. Nat Med. 2008; 14(11): 1197-1213.
3. Macer ML, Taylor HS. Endometriosis and infertility: a review of the pathogenesis and treatment of endometriosis-associated infertility. Obstet Gynecol Clin North Am. 2012; 39(4): 535-549.
4. Baldani DP, Skrgatic L, Ougouag R. Polycystic ovary syndrome: important underrecognised cardiometabolic risk factor in reproductive-age women. Int J Endocrinol. 2015; 2015: 786362.
5. Pangas SA. Regulation of the ovarian reserve by members of the transforming growth factor beta family. Mol Reprod Dev. 2012; 79(10): 666-679.
6. Kidder GM, Vanderhyden BC. Bidirectional communication between oocytes and follicle cells: ensuring oocyte developmental competence. Can J Physiol Pharmacol. 2010; 88(4): 399-413.
7. Stocco C. Aromatase expression in the ovary: hormonal and molecular regulation. Steroids. 2008; 73(5): 473-487.
8. Qiao J, Feng HL. Extra- and intra-ovarian factors in polycystic ovary syndrome: impact on oocyte maturation and embryo developmental competence. Hum Reprod Update. 2011; 17(1): 17-33.
9. Simpson ER, Clyne C, Rubin G, Boon WC, Robertson K, Britt K, et al. Aromatase--a brief overview. Annu Rev Physiol. 2002; 64: 93-127.
10. Stocco C. Tissue physiology and pathology of aromatase. Steroids. 2012; 77(1-2): 27-35.
11. Strauss L, Rantakari P, Sjögren K, Salminen A, Lauren E, Kallio J, et al. Seminal vesicles and urinary bladder as sites of aromatization of androgens in men, evidenced by a CYP19A1-driven luciferase reporter mouse and human tissue specimens. FASEB J. 2013; 27(4): 1342-1350.
12. Strauss L, Rantakari P, Sjögren K, Salminen A, Lauren E, Kallio J, et al. Seminal vesicles and urinary bladder as sites of aromatization of androgens in men, evidenced by a CYP19A1-driven luciferase reporter mouse and human tissue specimens. FASEB J. 2013; 27(4): 1342-1350.
13. Demura M, Reierstad S, Innes JE, Bulun SE. Novel promoter I.8 and promoter usage in the CYP19 (aromatase) gene. Reprod Sci. 2008; 15(10): 1044-1053.
14. Simpson ER, Mahendroo MS, Means GD, Kilgore MW, Hinshelwood MM, Graham-Lorence S, et al. Aromatase cytochrome P450, the enzyme responsible for estrogen biosynthesis. Endocr Rev. 1994; 15(3): 342-355.
15. Sebastian S, Bulun SE. A highly complex organization of the regulatory region of the human CYP19 (aromatase) gene revealed by the human genome project. J Clin Endocrinol Metab. 2001; 86(10): 4600-4602.
16. Conley A, Mapes S, Corbin CJ, Greger D, Walters K, Trant J, et al. A comparative approach to structure-function studies of mammalian aromatases. J Steroid Biochem Mol Biol. 2001; 79(1-5): 289-297.
17. Bulun SE, Lin Z, Imir G, Amin S, Demura M, Yilmaz B, et al. Regulation of aromatase expression in estrogen-responsive breast and uterine disease: from bench to treatment. Pharmacol Rev. 2005; 57(3): 359-83.
18. Bréard E, Roussel H, Lindet Y, Mittre H, Leymarie P. Presence of exon I.4 mRNA from CYP19 gene in human granulosa cells. Mol Cell Endocrinol. 1999; 154(1-2): 187-190.
19. Hosseini E, Mehraein F, Shahhoseini M, Karimian L, Nikmard F, Ashrafi M, et al. Epigenetic alterations of CYP19A1 gene in Cumulus cells and its relevance to infertility in endometriosis. J Assist Reprod Genet. 2016; 33(8): 1105-1113.
20. Hashemian Z, Afsharian P, Farzaneh P, Eftekhari-Yazdi P, Vakhshiteh F, Daneshvar Amoli A, et al. Establishment and characterization of a PCOS and a normal human granulosa cell line. Cytotechnology. 2020; 72(6): 833–845.
21. Michael MD, Kilgore MW, Morohashi K, Simpson ER. Ad4BP/SF-1 regulates cyclic AMP-induced transcription from the proximal promoter (PII) of the human aromatase P450 (CYP19) gene in the ovary. J Biol Chem. 1995; 270(22): 13561-13566.
22. Saitoh M, Yanase T, Morinaga H, Tanabe M, Mu YM, Nishi Y, et al. Tributyltin or triphenyltin inhibits aromatase activity in the human granulosa-like tumor cell line KGN. Biochem Biophys Res Commun. 2001; 289(1): 198-204.
23. Davuluri RV, Suzuki Y, Sugano S, Plass C, Huang TH. The functional consequences of alternative promoter use in mammalian genomes. Trends Genet. 2008; 24(4): 167-177.
24. Attar E, Bulun SE. Aromatase and other steroidogenic genes in endometriosis: translational aspects. Hum Reprod Update. 2006; 12(1): 49-56.
25. Fleming NI, Knower KC, Lazarus KA, Fuller PJ, Simpson ER, Clyne CD. Aromatase is a direct target of FOXL2: C134W in granulosa cell tumors via a single highly conserved binding site in the ovarian specific promoter. PLoS One. 2010; 5(12): e14389.
26. Bates DL, Chen Y, Kim G, Guo L, Chen L. Crystal structures of multiple GATA zinc fingers bound to DNA reveal new insights into DNA recognition and self-association by GATA. J Mol Biol. 2008; 381(5): 1292-1306.
27. Jin T, Zhang X, Li H, Goss PE. Characterization of a novel silencer element in the human aromatase gene PII promoter. Breast Cancer Res Treat. 2000; 62(2): 151-159.
28. Ghosh S, Wu Y, Li R, Hu Y. Jun proteins modulate the ovary-specific promoter of aromatase gene in ovarian granulosa cells via a cAMP-responsive element. Oncogene. 2005; 24(13): 2236-2246.
29. Wu Y, Ghosh S, Nishi Y, Yanase T, Nawata H, Hu Y. The orphan nuclear receptors NURR1 and NGFI-B modulate aromatase gene expression in ovarian granulosa cells: a possible mechanism for repression of aromatase expression upon luteinizing hormone surge. Endocrinology. 2005; 146(1): 237-246.
30. Sahmi F, Nicola ES, Zamberlam GO, Gonçalves PD, Vanselow J, Price CA. Factors regulating the bovine, caprine, rat and human ovarian aromatase promoters in a bovine granulosa cell model. Gen Comp Endocrinol. 2014; 200: 10-7.
31. Enjuanes A, Garcia-Giralt N, Supervía A, Nogués X, Ruiz-Gaspà S, Bustamante M, et al. Functional analysis of the I.3, I.6, pII and I.4 promoters of CYP19 (aromatase) gene in human osteoblasts and their role in vitamin D and dexamethasone stimulation. Eur J Endocrinol. 2005; 153(6): 981-988.
32. Shozu M, Zhao Y, Bulun SE, Simpson ER. Multiple splicing events involved in regulation of human aromatase expression by a novel promoter, I.6. Endocrinology. 1998; 139(4): 1610-1617.
33. Odawara H, Iwasaki T, Horiguchi J, Rokutanda N, Hirooka K, Miyazaki W, et al. Activation of aromatase expression by retinoic acid receptor-related orphan receptor (ROR) alpha in breast cancer cells: identification of a novel ROR response element. J Biol Chem. 2009; 284(26): 17711-17719.
34. Chen S. Aromatase and breast cancer. Front Biosci. 1998; 3: d922-33.
35. Gérard C, Brown KA. Obesity and breast cancer - Role of estrogens and the molecular underpinnings of aromatase regulation in breast adipose tissue. Mol Cell Endocrinol. 2018; 466: 15-30.
36. Ratre P, Mishra K, Dubey A, Vyas A, Jain A, Thareja S. aromatase inhibitors for the treatment of breast cancer: a journey from the scratch. Anticancer Agents Med Chem. 2020; 20(17): 1994-2004.

Original Article

Down-Regulated Expression of Cystathionine β-Synthase and Cystathionine γ-Lyase in Varicocele, and Infertile Men: A Case-Control Study

Fahimeh Akbarian, M.Sc.[1], Marziyeh Tavalaee, Ph.D.[1], Maurizio Dattilio, M.D.[2]*, Mohammad Hossein Nasr-Esfahani, Ph.D.[1, 3]*

1. Department of Animal Biotechnology, Reproductive Biomedicine Research Center, Royan Institute for Biotechnology, ACECR, Isfahan, Iran
2. R&D Department, Parthenogen, Piazza Indipendenza 11, Lugano 6900, Switzerland
3. Isfahan Fertility and Infertility Center, Isfahan, Iran

Corresponding Addresses: R&D Department, Parthenogen, Piazza Indipendenza 11, Lugano 6900, Switzerland
P.O.Box: 8165131378, Department of Animal Biotechnology, Reproductive Biomedicine Research Center, Royan Institute for Biotechnology, ACECR, Isfahan, Iran
Emails: maurizio.dattilo@ parthenogen.ch, mh.nasr-esfahani@royaninstitute.org

Received: 09/September/2020, Accepted: 19/January/2021

Abstract

Objective: Cystathionine β-synthase (CBS) and cystathionine γ-lyase (CSE) are two important enzymes involved in One-Carbon metabolism. These enzymes play important roles in modulating oxidative stress and inflammation in male factor infertility through participating in the synthesis of glutathione (GSH) antioxidants in the trans-sulfuration pathway. Besides, the direct release of hydrogen sulfide (H_2S) has anti-inflammatory and antioxidant effects. Therefore, the expression of *CBS* and *CSE* genes at mRNA levels in infertile and varicocele men was evaluated and compared to the healthy counterparts to clarify their possible role in the pathology of male infertility.

Materials and Methods: In this case-control study, semen parameter assessment (concentration, morphology, and motility of sperms) was performed on 28 men with varicocele, 43 infertile men with abnormal sperm parameters, and 19 fertile men. RNA was extracted from sperm samples followed by cDNA synthesis and real-time polymerase chain reaction (PCR) using *CBS, CSE,* and *GAPDH* primers.

Results: Sperm concentration and motility in infertile and varicocele groups were significantly lower (P=0.001), while spermatoza normal morphology was higher than fertile group (P=0.05). The expression levels of both *CBS* and *CSE* genes in infertile (P=0.04 and P=0.037 respectively) and varicocele (P=0.01 and P=0.046 respectively) groups were significantly lower than fertile group. Additionally, *CBS* gene expression indicated a positive correlation with expression of *CSE* gene (r=0.296, P=0.025) and sperm parameters.

Conclusion: In light of our findings, there is a valid rationale to consider the primary role of *CBS* and *CSE* enzymes impairment in male factor infertility which specifically may point to a deficit in the release of essential antioxidants including the H_2S as a molecular basis of infertility and warrants further investigation.

Keywords: Cystathionine β-Synthase, Cystathionine γ-Lyase, Hydrogen Sulfide, Male Infertility, Oxidative Stress

Cell Journal(Yakhteh), Vol 24, No 4, April 2022, Pages: 176-181

Citation: **Akbarian F, Tavalaee M, Dattilio M, Nasr-Esfahani MH. Down-regulated expression of cystathionine β-synthase and cystathionine γ-lyase in varicocele, and infertile men: a case-control study. Cell J. 2022; 24(4): 176-181. doi: 10.22074/cellj.2022.7775.**

Introduction

According to the WHO, infertility is a global health issue affecting around 15% of couples. Available data suggests that about half of all infertility cases are caused by male factors including lifestyle, genetic, and environment (1, 2). Several lines of evidence have identified oxidative stress as a major contributor to abnormal semen parameters and subsequent male infertility (3). Oxidative stress is mainly occurred due to the imbalance of antioxidant capacity and reactive oxygen species (ROS) content. Increasing the level of ROS could result in the molecular and cellular damage of the reproductive system cells especially spermatozoa with a low amount of cytoplasm and limited repair mechanism potential. Therefore, the high level of ROS could lead to an extreme vulnerability to oxidative stress such as lipid peroxidation of sperm membrane, DNA damage, and apoptosis (1).

Spermatogenesis is a complex process controlled by a large number of genes and interacts with various cell signaling pathways (4). One-carbon metabolism has long been acknowledged to affect spermatogenesis and sperm quality by regulating the biosynthesis of nucleotides and methylations, maintaining genomic integrity, and protecting DNA from damage (5). This folate cofactor-mediated pathway transfers one-carbon (methyl) units for accomplishing the metabolic processes. Folate cycle, methionine cycle, and trans-sulfuration pathway are three main constituent interlinking pathways of one-carbon metabolism (6).

The canonical trans-sulfurations pathway for sulfur amino acid metabolism uses homocysteine as a substrate to generate cysteines for protein synthesis and biosynthesis of glutathione (GSH). GSHs are a family of the most abundant natural antioxidants in human tissues which

are well known as a powerful cellular antioxidant and constitute, together with NADH/NADPX, the main redox buffer of the cells (7, 8). Cystathionine-γ-lyase (CSE) and cystathionine β-synthase (CBS) are trans-sulfuration pathway enzymes known for an unspecific recognition of their substrate. These enzymes allow their substrates to act in a sort of reverse manner, an alternative pathway of CBS and CSE (9). In addiotion, these enzymes are involved in the synthesis of hydrogen sulphide (H_2S). This is a gaseous transmitter with antioxidant and anti-inflammatory properties. H_2S behaves as a powerful reducing substance as the standard two-electron redox potential of H_2S/S0 couple, at pH=7, versus the standard hydrogen electrode, is −0.23 V and is in the same range as that of GSH disulfide/GSH (E°′=−0.262 V) (10). Thus, the transsulfuration pathway is a master regulator of the redox homeostasis in many tissues, which also applies to the testis where the activity of the pathway is well documented (11, 12).

The role of H_2S as a homeostasis modulator is established and several reports proved that it has protective effects against ROS in vascular and neural systems and behaves as a signaling molecule in the regulation of vasodilation and blood pressure (13, 14). Besides its direct ability to neutralize ROS, H_2S also increases the expression of antioxidant enzymes through activation and translocation of the nuclear factor (erythroid-derived 2)-like 2 transcription factor (*NRF2*) (15, 16). Recent studies confirm the role of H_2S release as a homeostatic modulator also in the reproductive system of males and females. Indeed, the vasodilation induced by H_2S occurs at the time of penile erection. Therefore, the H_2S release has been proposed as a target for the treatment of erectile dysfunction (12, 17).

CBS acts at the cross-road of the one-carbon metabolism and is responsible for partitioning homocysteine to either trans-sulfuration, towards GSH and H_2S generation, or re-methylation, feeding the production of activated methyl groups as S-Adenosyl-Methionine (SAMe) (6). SAMe is the main activator of CBS, meaning that antioxidant effectors GSH and H_2S are released only if transmethylations are working (18). H_2S resulting from trans-sulfurations in turn an activator of Methionine Synthase Reductase (MTRR), a key regulator of the folate and methionine cycle (19). Thus, H_2S is the link between the activity of the endogenous antioxidant system and the efficiency of transmethylation reactions. Accordingly, impaired CBS activity is demonstrated to impair the cell methylation (6).

Both CBS and CSE are widely detected in the testes with CSE found mainly in Sertoli cells and immature germ cells and CBS abundant in Sertoli cells, Leydig cells, and germ cells (14), but their relative contribution to H_2S generation within the testes is unknown. However, CBS was identified as a major contributor to H_2S production as it may account for up to 70% of total endogenous H_2S in hypermetabolic cells like astrocytes (7). Moreover, stoichiometric calculations indicate that CSE can be a main source of H_2S in peripheral tissues only in conditions of very high homocysteine as seen in homocystinuria (20).

Several studies have proven that dysfunction of one-carbon metabolism, especially the imbalance of CBS and CSE enzymes in the trans-sulfuration pathway, plays a role in male infertility (14, 21-23) and a specific deficit in the output of H_2S is reported (23). The dysregulated content of CBS and CSE enzymes protein at human semen as well as their expression level at the RNA level in the testis of infertility mouse models were reported previously, however, to the best of our knowledge, there is no report about the specific mechanisms of dysregulation of the trans-sulfuration pathway in human seminal plasma.

This case-control study was undertaken to analyze the expression of *CBS* and *CSE* genes in sperms of infertile men in comparison to healthy fertile counterparts at the RNA level to clarify the connection between these enzymes and male infertility.

Materials and Methods

Design of experiment

This case-control study was conducted following the approval of the Institutional Review Board from the Royan Institute (IR.ACECR.ROYAN.REC.1398.244). Twenty-eight infertile men with varicocele (II or III grade) and 43 infertile men with abnormal sperm parameters (oligozoospermia, asthenozoospermia, teratozoospermia, austenotratozoospermia, oligostenotratozoospermia, and oligosthenospermia) referred to Isfahan Fertility and Infertility Clinic (IFIC) were recruited before receiving any treatments. Nineteen fertile men referring to the same center for family balancing served as fertile controls. Written informed consent was obtained from all subjects before participation in the study.

Semen collection and sperm parameters analysis

Semen samples were collected by masturbation following 3-4 days of sexual abstinence and delivered to the laboratory within 30 minutes after ejaculation. Sperm parameters were analyzed on one portion of the semen samples according to the WHO criteria (24). Briefly, sperm counting chamber (Sperm Processor, India), computer-assisted semen analysis (CASA) software, and Papanicolaou staining were used for assessing the sperm concentration, motility, and abnormal morphology respectively. White blood cells (WBCs) were assessed by peroxidase assay and all the samples showed WBCs below 0.5 million/ml.

RNA expression analysis

The remaining semen samples were washed twice with phosphate-buffered salin (PBS, Sama Tashkhis, Iran) and used for total RNA extraction using YTzol pure RNA (Yekta Tajhiz Azama, Iran) according to the manufacturer's protocol. cDNA was synthesized from extracted total RNA using Yekta Tajhiz cDNA Synthesis Kit (Yekta Tajhiz Azama, Iran). As shown in Table 1, primers

for *CBS*, *CSE,* genes, as well as *GAPDH* housekeeping gene, an internal control, were designed using Gene Runner (version 3.05; Hastings Software, Inc. Hastings, USA). mRNA expression analysis was accomplished via real-time polymerase chain reaction (PCR) by YTA SYBR Green qPCR MasterMix 2X (Yekta Tajhiz Azama, Iran) according to the manufacturer's instruction in StepOnePlus Real-Time PCR System (Applied Biosystems, Foster City, USA). The cycling condition consisted of an initial denaturation at 95˚C for 15 minutes, accompanied by 40 two-steps cycles of 95˚C for 15 seconds and 60˚C for 1 minute. eventually, the process was ended by a dissociation step for documenting the melt of the PCR product.

Statistical analysis

All data in the present study were analyzed by the statistical package for the social sciences for windows, version 26 (SPSS, Inc., Chicago, IL, USA). All parameters had a normal distribution and gene expression was calculated by the $2^{\Delta\Delta Ct}$ method. An independent sample t test was used to compare the mean expression of variables of each group along with the Pearson correlation coefficient test. Data were presented as mean ± standard error of the mean (SEM), and $P<0.05$ was assumed as significant.

Results

Sperm parameters

The conventional sperm parameters are presented as bar charts in Figure 1. The mean sperm concentration (10^6/mL) was significantly lower in varicocele (50.78 ± 6.7, P=0.002) and infertile (30.02 ± 3.8, P=0.000) groups compared to the fertile men (80.23 ± 5.725, Fig.1A). Similarly, motility showed a significant decline in men with varicocele (48.54 ± 3.8, P=0.006) and infertile group (34.52 ± 3.107, P<0.001) compared to the control (63.11 ± 2.816, Fig.1B). On the other hand, the mean percentage of sperm with total abnormal morphology (abnormal head, neck, and tail) was higher in varicocele (96.74 ± 0.3, P=0.018) and infertile (97.13 ± 0.2, P=0.019) groups in comparison with the fertile group (96.06 ± 0.4, Fig.1C).

Gene expression analysis

The comparison between the expression of messenger RNAs of *CBS* and *CSE* genes in healthy, varicocele, and infertile men in Figure 2. indicate a significant lowe expression of *CBS* in varicocele (0.11 ± 0.3, P=0.01) and infertile men (0.52 ± 0.1, P=0.04) in comparison with the fertile counterparts (2.6 ± 0.9, Fig.2A). *CSE* expression also revealed a significant decline in varicocele (0.6 ± 0.08, P=0.046) and infertile men (0.55 ± 0.08, P=0.037) compared to fertile male matched controls (1.6 ± 0.46, Fig.2B).

Table 1: Sequence of designed primers of real-time polymerase chain reaction assay

Gene	Oligonucleotide sequence (5´-3´)	GC (%)	Optimal temperature (˚C)	Size (bp)
CBS	F: GGGCGAAGTGGTCCATCTC	63.16	60	94
	R: GTTGGCAAAGTCATCTACAAGCA	43.48		
CSE	F: GACTCTACATGTCCGAATGG	50	58	149
	R: AACCTGTACACTGACGCTTCA	47.62		
GAPDH	F: CCACTCCTCCACCTTTGACG	60.00	60	107
	R: CCACCACCCTGTTGCTGTAG	60.00		

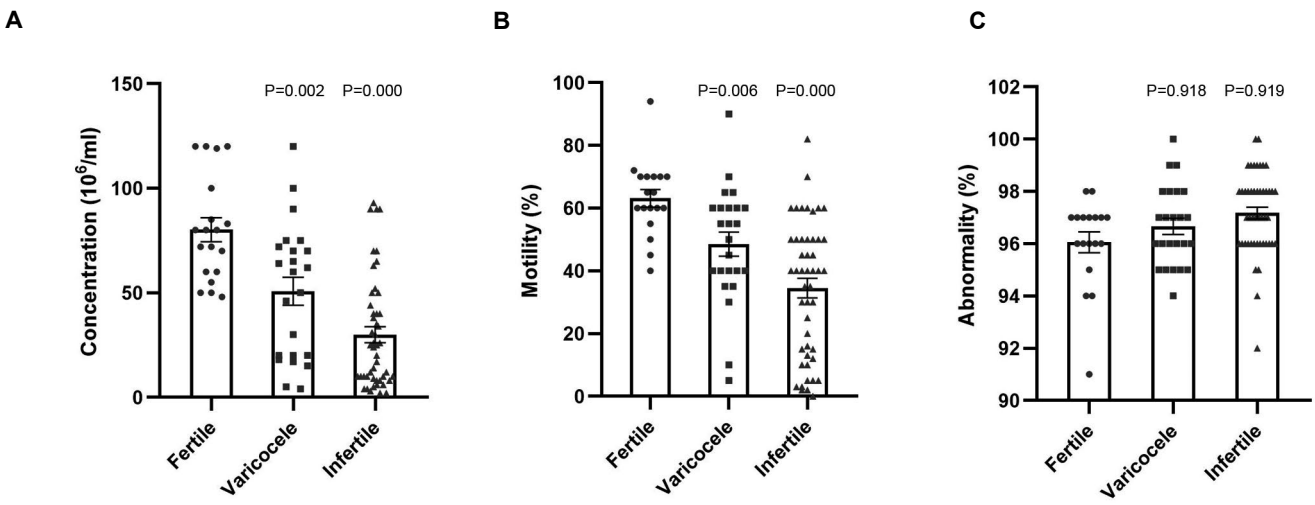

Fig.1: Sperm parameters of fertile, varicocele, and infertile groups. **A.** Sperm concentration (10^6/mL). **B.** Sperm motility (%). **C.** Sperms with the abnormal morphology (%). Data are expressed as means ± standard error of the mean (SEM), significant P values are reported in the figure.

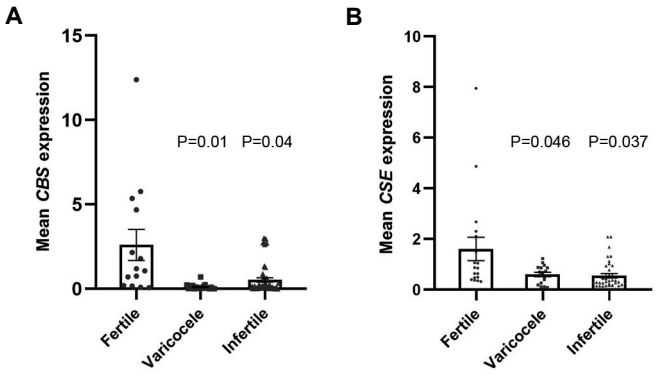

Fig.2: Comparison of mean expression of *CBS* and *CSE* between infertile men (n=43), infertile men with varicocele (n=28), and fertile individuals (n=19). Real-time polymerase chain reaction analysis of **A.***CBS* and **B.** *CSE* genes expression at RNA level relative to the *GAPDH* housekeeping gene (internal control for normalization) between study groups. Values are expressed as mean ± standard error of the mean (SEM), significant P values are reported in the figure.

Correlation of sperm parameters and gene expression

Pearson correlation analysis showed a significant positive correlation between the relative expression of *CBS* and *CSE* mRNAs (r=0.296, P=0.025). The correlation between sperm parameters (sperm concentration, motility, abnormality) and the relative expression of *CBS* and *CSE* genes were also analyzed. As shown in Table 2, a significant positive and negative correlation was observed between *CBS* and sperm concentration and sperm abnormality, respectively. However, no significant correlation between the relative expression of the *CBS* gene with sperm motility and the *CSE* gene with any sperm parameters was observed.

Table 2: Analysis of correlation between different sperm parameters with mRNA expression of *CBS* and *CSE* genes

Sperm parameters		*CBS* expression	*CBE* expression
Sperm concentration	r	0.291*	0.17
	P value	0.01	0.159
Sperm motility	r	0.159	0.155
	P value	0.164	0.205
Sperm abnormality	r	-0.351**	-0.086
	P value	0.002	0.484

*; P<0.05, **; P<0.01, and r; Correlation.

Discussion

In the present study, the decreased expression of *CBS* and *CSE* genes in varicocele and infertile men in comparison with healthy counterparts was documented. These two genes encode core enzymes of the trans-sulfuration pathway, which is a main effector of the endogenous antioxidant system through contributing to GSH generation and direct release of H_2S via CBS and CSE enzymes (7, 9, 11). Accordingly, reduction in the expression of *CBS* and *CSE* in infertile men points to a deficit of the endogenous antioxidant defenses and confirms the relation of male infertility with oxidative stress in addition to the involvement of the H_2S system in sperm DNA methylation.

GSH is produced in trans-sulfuration pathway by CBS and CSE enzymes and its depletion in male infertility are well documented. Naher et al. (25) found that infertile men, despite having the same level of erythrocyte GSH as their fertile controls, had far lower GSH in their seminal plasma indicating a testis-specific defect. Fafula et al. (26) found diminished levels of GSH and oxidized GSH ratio (GSH: GSSG) in the sperm of infertile men. This level decreasing was coupled with a reduction in the activity of GSH peroxidase (GPX) that was interpreted as a consequence of decreased substrate (i.e. GSH) after consumption to counteract primitive oxidative aggression, i.e. The fall of GSH could consider as the consequence, not the cause, of the oxidative damage. This interpretation is questioned by the findings of Wang et al. (23) reporting decreased amounts of CBS protein in infertile men for the first time and also by the findings of the present study at RNA level. According to the data in this study, the low GSH in infertile men is likely due to a decreased synthesis and might be a primary reason for oxidative imbalance and damage.

Wang al. (23) also reported a decreased amount of H_2S in seminal plasma of infertile men and its positive effect on motility from exposure of their sperms to H_2S. The decrease in seminal H_2S was related to the decrease of the CBS protein. However, it could not be established whether the lower amount of the enzyme was due to a primary suppression of the gene or any post-translational modification.

DNA methylation occurs at sperm more than any other cell which is fundamental for appropriate gene expression, DNA compaction, and proper development of the embryo. It is also well-known to contribute to male infertility (22, 27, 28). Hypo-methylation is a common phenomenon in infertile men with varicocele and oligozoospermia although the mechanisms through which hypo-methylation occurs remain unclear (29, 30). In a recent study, in spite of sperm hypomethylation, varicocele patients exert a paradox higher expression of DNA de-novo methylation enzymes DNMT3A and DNMT3B that are likely reverting their activity toward DNA de-methylation during oxidative stress (31). However, decreased generation of H_2S from CBS may also explain the link between male infertility, oxidative stress, and impairment of sperm DNA methylation. The activity of CBS is indeed strictly linked with the activation of transmethylations including DNA methylation, hence epigenetic programming.

The connection between trans-sulfuration and DNA methylation is also supported by animal and clinical models

(22). The administration of cocktails of micronutrients including methyl donors in infertile patients is reported to be effective in reducing both sperm DNA fragmentation, clear oxidative damage, as well as in improving chromatin packaging and protamination (29). Based on the data from Toohey et al., the release of H_2S from CBS (and CSE) is the link between the two pathways and explains why a resumption of the endogenous antioxidant pathways parallels an improved methylation activity (19). This qualifies H_2S as a primary regulator of sperm functions and explains our finding of correlation of *CBS* expression with sperm morphology that is expected to respond to epigenetic regulations, including DNA methylation.

Regarding the role of H_2S as a homeostasis modulator, Nuño-Ayala et al. (32), reported that CBS deficiency leads to pregnancy loss in female mice. The imperative role of H_2S in sustaining the germ cells in normal physiological conditions, especially in heat exposure, was demonstrated in a study by Li et al. (33) on rat testes as the down-regulation of CBS and CSE enzymes were observed following the heat shock injuries. They also showed that the exogenous H_2S exerts protecting effects on germ cells against heat exposure owing to its antioxidant properties, although the administration of a high dose of this gas could have toxic effects. Finally, Morales et al. (16), demonstrated that an H_2S prodrug acts as an antioxidant with recovery effects on spermatogenesis and sperm parameters including sperm count, motility, and morphology in men with oligoasthenozoospermia. Data in this study are showing that the dysregulation of H2S in male infertility is likely dependent on decreased expression of one of the producing enzymes, CBS.

In this study, the gene expression of both the enzymes is also studied and the results showed that *CBS* expression inversely correlated with sperm concentration and normal morphology whereas *CSE* expression did not. A possible explanation is that CSE down-regulation is just the consequence of reduced CBS activity resulting in lower amounts of cystathionine, the CSE substrate. This led our attention to a possible specific CBS defect of H_2S generation. In summary, a major role of CBS down-regulation in the oxidative imbalance of our patients supports the idea that a fall of H_2S generation is involved in male infertility.

A possible limitation of the present study is the expression of another H_2S generating enzyme, 3MST, which is not yet studied. 3MST is well expressed by all cells in the seminiferous tubules with a weaker expression in Leydig cells (33). However, 3MST expression is suppressed in conditions of oxidative stress and is unlikely to contribute to this setting (20). Another possible limitation of this study is not checking GSH and H_2S in the seminal plasma of patients. They could not directly link the lower expression of CBS and CSE to a decreased level of the resulting antioxidant effectors. However, a reduced release of GSH and H_2S in these patients has been well demonstrated by others and was likely to occur also in our model (23, 25, 26).

Conclusion

All things considered, the downregulation of GSH and H_2S releasing enzymes, CBS and CSE, at the RNA level was observed in the present study in men with varicocele or unexplained infertility in addition to the inverse correlation of *CBS* expression with semen parameters. The main role of *CBS* down-regulation points to a specific defect in the H_2S system as well as GSH, which justifies both the oxidative imbalance and the DNA methylation dysregulation in these patients. Although the CBS and CSE proteins were evaluated in human semen previously, this study is the first report of downregulation of *CBS* and *CSE* genes at the RNA level in human samples. Efforts aimed at supporting the activity of CBS and/or the release of H_2S may be of help in the treatment of male infertility.

Acknowledgments

This study was financially supported by the Royan Institute, Iran. We would like to express our gratitude to the staff of the Biotechnology Department of Royan Institute and Fertility and Infertility Center for their full support. The authors declare no conflict of interest.

Authors' Contributions

F.A.; Patients management, preparation of samples and tests, collection, analysis of data, and manuscript writing. M.T.; Design, collection and/or assembly of data, data analysis, interpretation, and manuscript writing. M.D.; Conception, design, interpretation, and manuscript writing. M.H.N.-E.; Conception, design, data analysis, interpretation, manuscript writing and final approval of the manuscript. All authors read and approved the final manuscript.

References

1. Kumar N, Singh AK. Impact of environmental factors on human semen quality and male fertility: a narrative review. Environ Sci Eur. 2022; 34(6): 1-13.
2. Jodar M, Soler-Ventura A, Oliva R; Molecular biology of reproduction and development research group. semen proteomics and male infertility. J Proteomics. 2017; 162: 125-134.
3. Bisht S, Faiq M, Tolahunase M, Dada R. Oxidative stress and male infertility. Nat Rev Urol. 2017; 14(8): 470-485.
4. Nishimura H, L'Hernault SW. Spermatogenesis. Curr Biol. 2017; 27(18): R988-R994.
5. Menezo YJ, Silvestris E, Dale B, Elder K. Oxidative stress and alterations in DNA methylation: two sides of the same coin in reproduction. Reprod Biomed Online. 2016; 33(6): 668-683.
6. Singh K, Jaiswal D. One-carbon metabolism, spermatogenesis, and male infertility. Reprod Sci. 2013; 20(6): 622-630.
7. McBean GJ. The transsulfuration pathway: a source of cysteine for glutathione in astrocytes. Amino Acids. 2012; 42(1): 199-205.
8. Xiao W, Loscalzo J. Metabolic responses to reductive stress. Antioxid Redox Signal. 2020; 32(18): 1330-1347.
9. Renga B. Hydrogen sulfide generation in mammals: the molecular biology of cystathionine-β- synthase (CBS) and cystathionine-γ-lyase (CSE). Inflamm Allergy Drug Targets. 2011; 10(2): 85-91.
10. Mishanina TV, Libiad M, Banerjee R. Biogenesis of reactive sulfur species for signaling by hydrogen sulfide oxidation pathways. Nat Chem Biol. 2015; 11(7): 457-464.
11. Han W, Dong Z, Dimitropoulou C, Su Y. Hydrogen sulfide ameliorates tobacco smoke-induced oxidative stress and emphysema in

mice. Antioxid Redox Signal. 2011; 15(8): 2121-2134.
12. Zhu XY, Gu H, Ni X. Hydrogen sulfide in the endocrine and reproductive systems. Expert Rev Clin Pharmacol. 2011; 4(1): 75-82.
13. Kimura H. Hydrogen sulfide: its production, release and functions. Amino Acids. 2011; 41(1): 113-121.
14. Sugiura Y, Kashiba M, Maruyama K, Hoshikawa K, Sasaki R, Saito K, et al. Cadmium exposure alters metabolomics of sulfur-containing amino acids in rat testes. Antioxid Redox Signal. 2005; 7(5-6): 781-787.
15. Corsello T, Komaravelli N, Casola A. Role of hydrogen sulfide in NRF2- and sirtuin-dependent maintenance of cellular redox balance. Antioxidants (Basel). 2018; 7(10): 129.
16. Morales A, Garza M R G,Valdés O. A randomized clinical study assessing the effects of the antioxidants, resveratrol or SG1002, a hydrogen sulfide prodrug, on idiopathic oligoasthenozoospermia. Asian Pac J Reprod. 2015; 4(2): 106-111.
17. Srilatha B, Muthulakshmi P, Adaikan PG, Moore PK. Endogenous hydrogen sulfide insufficiency as a predictor of sexual dysfunction in aging rats. Aging Male. 2012; 15(3): 153-158.
18. Prudova A, Bauman Z, Braun A, Vitvitsky V, Lu SC, Banerjee R. S-adenosylmethionine stabilizes cystathionine beta-synthase and modulates redox capacity. Proc Natl Acad Sci USA. 2006; 103(17): 6489-6494.
19. Toohey JI. Possible involvement of hydrosulfide in B12-dependent methyl group transfer. Molecules. 2017; 22(4): 582.
20. Kabil O, Banerjee R. Enzymology of H2S biogenesis, decay and signaling. Antioxid Redox Signal. 2014; 20(5): 770-782.
21. Wu Y, Ding R, Zhang X, Zhang J, Huang Q, Liu L, et al. Meet-in-metabolite analysis: a novel strategy to identify connections between arsenic exposure and male infertility. Environ Int. 2021;147:106360.
22. Mohammadi P, Hassani-Bafrani H, Tavalaee M, Dattilo M, Nasr-Esfahani MH. One-carbon cycle support rescues sperm damage in experimentally induced varicocoele in rats. BJU Int. 2018; 122(3): 480-489.
23. Wang J, Wang W, Li S, Han Y, Zhang P, Meng G, et al. Hydrogen sulfide as a potential target in preventing spermatogenic failure and testicular dysfunction. Antioxid Redox Signal. 2018; 28(16): 1447-1462.
24. World Health Organization. WHO laboratory manual for the examination and processing of human semen. 5th ed. 2010. Available from: https://apps.who.int/iris/handle/10665/44261 (09 Sep 2020).
25. Naher ZU, Biswas SK, Mollah FH, Ali M, Arslan MI. Role of glutathione in male infertility. Bangladesh J Med Biochem. 2011; 4(2): 20-25.
26. Fafula RV, Onufrovych OK, Iefremova UP, Melnyk OV, Nakonechnyi IA, Vorobets DZ, et al. Glutathione content in sperm cells of infertile men. Regul Mech Biosyst. 2017; 2(8): 157-161.
27. Stuppia L, Franzago M, Ballerini P, Gatta V, Antonucci I. Epigenetics and male reproduction: the consequences of paternal lifestyle on fertility, embryo development, and children lifetime health. Clin Epigenetics. 2015; 7: 120.
28. Tavalaee M, Razavi S, Nasr-Esfahani MH. Influence of sperm chromatin anomalies on assisted reproductive technology outcome. Fertil Steril. 2009; 91(4): 1119-1126.
29. Bahreinian M, Tavalaee M, Abbasi H, Kiani-Esfahani A, Shiravi AH, Nasr-Esfahani MH. DNA hypomethylation predisposes sperm to DNA damage in individuals with varicocele. Syst Biol Reprod Med. 2015; 61(4): 179-186.
30. Tavalaee M, Bahreinian M, Barekat F, Abbasi H, Nasr-Esfahani MH. Effect of varicocelectomy on sperm functional characteristics and DNA methylation. Andrologia. 2015; 47(8): 904-909.
31. Rashidi M, Tavalaee M, Abbasi H, Nomikos M, Nasr-Esfahani MH. Increased de novo DNA methylation enzymes in sperm of individuals with varicocele. Cell J. 2021; 23(4): 389-396.
32. Nuño-Ayala M, Guillén N, Arnal C, Lou-Bonafonte JM, de Martino A, García-de-Jalón JA, et al. Cystathionine β-synthase deficiency causes infertility by impairing decidualization and gene expression networks in uterus implantation sites. Physiol Genomics. 2012; 44(14): 702-716.
33. Li G, Xie ZZ, Chua JM, Wong PC, Bian J. Hydrogen sulfide protects testicular germ cells against heat-induced injury. Nitric Oxide. 2015; 46: 165-171.

Original Article

COVID-19 and Endocrine System: A Cross-Sectional Study on 60 Patients with Endocrine Abnormality

Negin Hadisi, M.Sc.[1, 2], Hadi Abedi, B.Sc.[2], Majid Shokoohi, Ph.D.[3], Seval Tasdemir, M.D.[4], Shahriyar Mamikhani, M.D.[2], Shahla Meshgi, M.D.[5], Arian Zolfagharzadeh, M.D.[6], Leila Roshangar, Ph.D.[1]*

1. Stem Cell Research Center, Tabriz University of Medical Sciences, Tabriz, Iran
2. Ahar Bagher-al-Olum General Hospital, Ahar, Iran
3. Clinical Research Development Unit of Tabriz Valiasr Hospital, Tabriz University of Medical Sciences, Tabriz, Iran
4. Fertijin IVF Center Nispetiye Cad Bebek Yokusu Sokak, Etiler, Istanbul, Turkey
5. Cardiovascular Research Center, Tabriz University of Medical Sciences, Tabriz, Iran
6.Tabriz Imam Reza General Hospital, Tabriz, Iran

**Corresponding Address: P.O.Box: 5138664393, Stem Cell Research Center, Tabriz University of Medical Sciences, Tabriz, Iran*
Email: lroshangar@yahoo.com

Received: 20/May/2021, Accepted: 31/January/2021

Abstract

Objective: COVID-19 is an infectious disease that has become pandemic with a high mortality rate. This study aims to provide new insight into the relations between SARS-CoV-2 and the Endocrine system.

Materials and Methods: In this cross-sectional study, we have hospitalized 60 patients with a positive SARA-CoV-2 PCR test. The information of complete blood count and endocrine hormones was obtained when the patients were admitted to the hospital or for a maximum of 4 days onset the hospitalization.

Results: Of 60 patients with COVID-19, forty-four (73.33%) had at least one abnormality mean item >×3. In total, 26 (43.33%), 21 (35%), 18 (30%), 13 (21.67%), 31 (51.67%), 12 (20%), 30 (50%), 25 (41.67%) patients having estradiol, follicle stimulating hormone (FSH), luteinizing hormone (LH), prolactin, progesterone, testosterone, cortisol and thyroid stimulating hormone (TSH) abnormal test results, respectively. There was no change in creatinine levels. FSH has shown drastic changes in both sexes' intensity (F: 769, P<0.0001). Although TSH had many abnormalities in women, analysis has shown no significant P value (P=0.4558). Furthermore, prolactin and testosterone mean level in men and the estradiol mean level in women have shown no significant P value (P=0.2077, P=0.1446, P=0.1351, respectively).

Conclusion: Results suggest that COVID-19 affects directly or non-directly glands and related hormones.

Keywords: COVID-19, Endocrine System, SARS-CoV-2

Cell Journal(Yakhteh), Vol 24, No 4, April 2022, Pages: 182-187

Citation: Hadisi N, Abedi H, Shokoohi M, Tasdemir S, Mamikhani Sh, Meshgi Sh, Zolfagharzadeh A, Roshangar L. COVID-19 and endocrine system: a cross-sectional study on 60 patients with endocrine abnormality. Cell J. 2022; 24(4): 182-187. doi: 10.22074/cellj.2022.8079.

Introduction

Coronaviruses are a common virus within animals and humans that cause multiple system infections in both species, predominantly humans respiratory tract infections, such as severe acute respiratory syndrome (SARS) and the Middle East respiratory syndrome (MERS). Coronaviruses also cause enteric, hepatic, and neurologic diseases (1-3). Since late December 2019, a newfound virus has become prevalent in Wuhan, China, previously described as (2019-nCoV), which subsequently affected all countries worldwide (4, 5).

The worldwide health organization labeled the COVID-19 as a pandemic worldwide that has led to thousands of deaths, albeit most of the cases have mild symptoms, more severe symptoms have caused respiratory failure, septic shock, and multiple organ failure dysfunctions (6). It appears that 93.1% of the sequence identity of the spike gene of the virus is relative to the RaTG13 of Bat coronaviruses. However, the other SARS-CoV and SSRS-CoVs have less than 80% manifested sequence identity (7). A homometric spike glycoprotein with S1 and S2 subunits in each spike monomer operates as cellular receptors to bind the hostage. A cascade of events occurs by binding the receptors leading to the fusion between viral membrane and cell. Cryo-EM studies of the SARS-CoV spike with ACE2 cell receptor have shown that glycan-RBD (a hexapeptide in the receptor-binding domain) enforces the separation of the S1 with ACE2 as a necessary action for membrane fusion through actuating the S2 subunit from mutable perfusion to a more post-fusion state (8-13). A required regularization of the renin-angiotensin system, named angiotensin-converting enzyme 2 (ACE2), has been known as a homolog of the metalloprotease angiotensin-converting enzyme ACE (14, 15).

The expression and presence of the ACE2 within the internal organs may assume to be the potential path of the entrance of the COVID-19 virus. Highly enriched expression and distribution of ACE2 at the surface of type 2 alveolar cells of the lung, oral mucosa, tongue, stratified and upper esophagus epithelial cells, colon and ileum absorptive enterocytes, myocardial cells, cholangiocytes, proximal tubule cells of the kidney, bladder urothelial cells, seminiferous duct cells in the testis and leydig cells have been detected (16-21). These uncoverings demonstrate that organs with high expression of ACE2

receptors are exposed to the high risk of 2019-nCoV infection (18). Moreover, hormonal disorders can amplify cytokine storms and organ failure (22).

However, the data of other organs has not been comprehensively analyzed. Hence, this study aims to report the hormonal sex, adrenal, ovary, hypothalamus, thyroid, and pituitary gland function and their parameters in patients with COVID-19 hospitalized to the Bagher-Al-Olum hospital in Ahar, Iran. More potential therapies would be recognized with a better concentrate on pathogenesis and affected human physiology, which might intercept glands failure in patients with SARS-CoV-2.

Study criteria and design

We conducted a cross-sectional study of patients admitted to the Bagher-Al-Olum Hospital of Ahar. As the WHO interim guidance (23). From November 12, 2020, to December 18, 2020, 85 infected patients were identified; however, only 60 were placed in this study. All of the patients were in reproduction age. Those who had abnormal CT-Scan, and CBC and Diff test results with a signed consent form, from admission to November 12, 2020, were enrolled in the study. Also, we extracted 60 normal laboratory test results from the hospital database (HIS) to set as the control group for reaching an accurate comparative study. Women with menstrual disorders and patients using medications that may affect hormonal results were excluded from the study. This study has taken approval from Tabriz University of Medical Sciences Ethics Committee, Iran (IR.TBZMED.REC.1399.129).

Confirmation and severity of SARS-CoV-2

Hospitalization of patients was based on confirmation of positive real-time polymerase chain reaction (PCR), chest CT-Scan, and abnormal CBC and Diff tests. All patients stated no history of glands disease, and their odd results were likely due to SARS-CoV-2 disease. Nasopharyngeal and throat specimens were collected by swab from dubious patients to evaluate their E gene expression by RT-PCR. According to the Infectious Diseases Society of America/ American Thoracic Society (IDSA/ATS) guideline (24), Pneumonia was defined. Combinations of azithromycin, Hydroxychloroquine, Kaletra, Vitamin C, and Interferon 1-B were applied for treatment.

Statistical analysis

GraphPad Prism version 8.4.3 (San Diego, California, USA) was used for statistical analysis. Median for continuous variables were compared using independent group t tests when the data were normally distributed; confidence interval (CI) and Significance were set as a $P<0.05$ for each group; otherwise, the Mann-Whitney U test was used. Also, an ANOVA test was performed to compare the mean among several independent groups, and F statistics were reported for the ratio of changes Between Groups to Within Groups.

Results

Clinical characteristic of patients with COVID-19

Blood samples due to precise analysis of the cortisol were collected at 8 AM. Of 60 patients with COVID-19**,** 26 (43.33%) had abnormal estradiol test, 21 (35%) had abnormal follicle stimulating hormone (FSH) test, 18 (30%) had abnormal luteinizing hormone (LH) test, 13 (21.67%) had abnormal prolactin test, 31 (51.67%) had abnormal progesterone test, 12 (20%) had abnormal testosterone test, 30 (50%) had abnormal cortisol test, 25 (41.67%) had abnormal thyroid stimulating hormone (TSH) test, and no changing in creatinine levels was observed. Twenty (33.33%) extended intensive disease, and 40 (66.67%) had the moderate disease during confinement.

Clinical characteristics of patients

At admission, about 51 (85%) of the patients had abnormal CBC and Diff test results, 35 (58.33%) fever, cough 45 (75%), body aches 49 (81.67%), headache 49 (81.67%), insomnia 27 (45%), dysgeusia 25 (41.67%), ageusia 18 (30%) in both sexes. Almost all 27 women had menstrual disorder such, polymenorrhea 12 (40%), oligomenorrhea 4 (13.33%), metrorrhagia 7 (23.33%), menometrorrhagia 4 (13.33%), and 3 (10%) had no change in their menstrual hygiene.

Results by statistical analysis

The average age of all patients with COVID-19 was almost 41 years old, 30 (50%) were male, and 30 (50%) were female. In total, for 60 patients, laboratory results have shown that 26 (43.33%), 21 (35%), 18 (30%), 13 (21.67%), 31 (51.67%), 12 (20%), 30 (50%), 25 (41.67%) patients having estradiol, FSH, LH, prolactin, progesterone, testosterone, cortisol and TSH abnormal test results, respectively. Of 60 patients, forty-four (73.33%) had at least one abnormality mean Item >×3, of which 26 were women, and 18 were confined in the intensive care unit (ICU) (Fig.1).

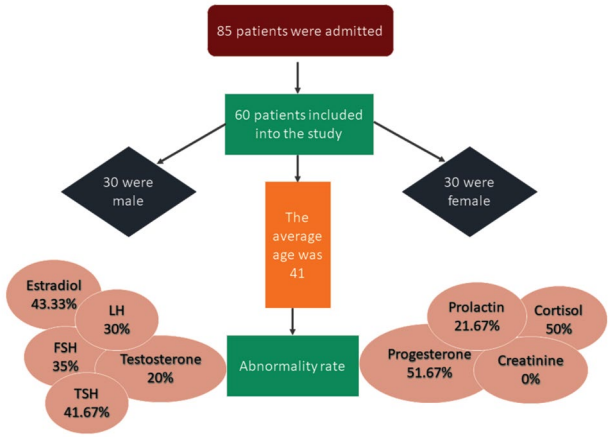

Fig.1: Flowchart of the study. FSH; Follicle stimulating hormone, LH; Luteinizing hormone, and TSH; Thyroid stimulating hormone.

Table 1 shows the P value, minimum, maximum, and mean for all hormones in males and females. The serum level of FSH value in Infected women was >2× of normal control women (CI: 4.422-15.83, P=0.0008). Likewise, males had almost >×2 FSH mean levels than healthy control males (CI: 1.691-7.891, P=0.0030), and women had ×1-2 FSH elevated mean levels than infected men ($F_{3,116}$: 9.769, P<0.0001). The average LH mean value for both infected women and men were almost ×2 normal levels (female CI: 1.575-9.993, P=0.0079, male CI: 1.376-5.076, P=0.0009), also males had almost > ×1 rose ($F_{3,116:}$ 12.42, P<0.0001) testosterone in both infected sex had a slight change. The mean of the infected men has shown ×1-2 decreased levels compared with normal control men (CI: -127.0-19.07, P=0.1446). Contrariwise, the infected women have shown ×1-2 increased levels of testosterone (CI: 3.653-29.73, P=0.0130). Females had >×1 changed testosterone mean level value than males ($F_{3.116}$: 51.75, P<0.0001).

Table 1: Hypothalamus-pituitary axis hormones range between normal, and infected patients

Hormones		Women				Men			
		Normal	Infected	Normal range	P value	Normal	Infected	Normal range	P value
FSH	Min	1.2	1.5	1.2-9.0 mIU/mL	0.0008	1.18	1.26	0.7-11.1	0.0030
	Max	9	51.5			17.92	25		
	Median	5.750	8.005			3.820	6.425		
LH	Min	0.8	1.84	0-14.7 mIU/mL	0.0079	1	1.6	0.8-7.6	0.0009
	Max	14.6	40.2			7.58	19.8		
	Median	8.100	9.850			3.525	5.685		
Testosterone	Min	1.01	17.5	ND-73 Ng/dl	0.013	130	16.6	20-49: 72 –853	0.1446
	Max	70.1	100.7			600	560	>50: 129 – 767	
	Median	20.50	22.90			251.0	232.0		
Progesterone	Min	0.73	0.1	0.72 -17.8 Ng/mL	0.0299	0.27	0.80	0.27 – 0.90	<0.0001
	Max	17.5	25.8			0.9	0.57		
	Median	11.02	1.175			0.5400	0.2550		
Estradiol	Min	65.5	0.28	72 -246 Pg/mL	0.1351	12	18.3	0-56	0.0124
	Max	245	403			55	250		
	Median	99.00	78.15			31.57	39.85		
Prolactin	Min	45	45	40 – 530 mIU/L	0.0013	55	62	53 – 360	0.2077
	Max	522	823			356	578		
	Median	261.5	407.0			224.5	187.5		
Cortisol	Min	3.7	0.19	3.7- 19.4 Micg/dl	0.0016	3.7	1	3.7- 19.4	0.0087
	Max	12.25	43			12.4	29		
	Median	6.735	11.70			8.90	10.23		
TSH	Min	0.33	0.1	0.3-5.2 Micg/dl	0.4558	0.32	0.1	0.32 – 5.2	0.0104
	Max	5.2	8			5.23	8.2		
	Median	3.010	2.500			2.465	1.160		

FSH; Follicle stimulating hormone, LH; Luteinizing hormone, TSH; Thyroid stimulating hormone, Min; Minimum, and Max; Maximum.

Although progesterone mean levels of women dropped ×1-2 compared with the Healthy control group (CI: -7.140 to-0.3000, P=0.0299), males have experienced ×2-3 decreased levels mean value of progesterone (CI: -0.3923 to -0.2037, P<0.0001). The decreased mean levels of males were ×1-2 females ($F_{3,116}$: 24.21, P<0.0001). Prolactin mean levels were elevated in both sexes, infected females experienced prolactin (PRL) levels ×1-2 Normal control group (CI: 58.03-227.9, P=0.0013). Likewise, males had ×1-2 elevated PRL mean level than the healthy control group (CI: -24.42 -109.9, P=0.2077). Women had ×1-1.5 enhancement PRL mean level than men ($F_{3,116}$: 9.134, P<0.0001). Furthermore, females had a minor reduction in their estradiol mean levels (CI: -55.03-6.800, P=0.1351), but Infected men experienced ×1-2 Increased mean levels (CI: 5.980-47.41, P=0.0124). Males had ×1-2 raised Estradiol mean levels than infected women ($F_{3,116}$: 14.37, P<0.0001). Both sexes experienced ×1-2 ascent mean levels of cortisol (female CI: 2.423 to 9.833, P=0.0016, male CI: 1.260 to 8.303, P=0.0087). Women had >×1 increased mean level cortisol than infected men ($F_{3,116}$: 6.177, P=0.0006). TSH for both sexes had a slight reduction. Female mean level TSH in women has dropped almost ×1 (CI: -1.230-0.8000, P=0.4558). Men have experienced ×1-2 dropped mean level than normal control (CI: -1.910 to -0.2200, P=0.0104). Also, men had ×1-2 decreased mean level of TSH than infected women ($F_{3,116}$: 0.5781, P=0.6306), as shown in Figures 2 and 3.

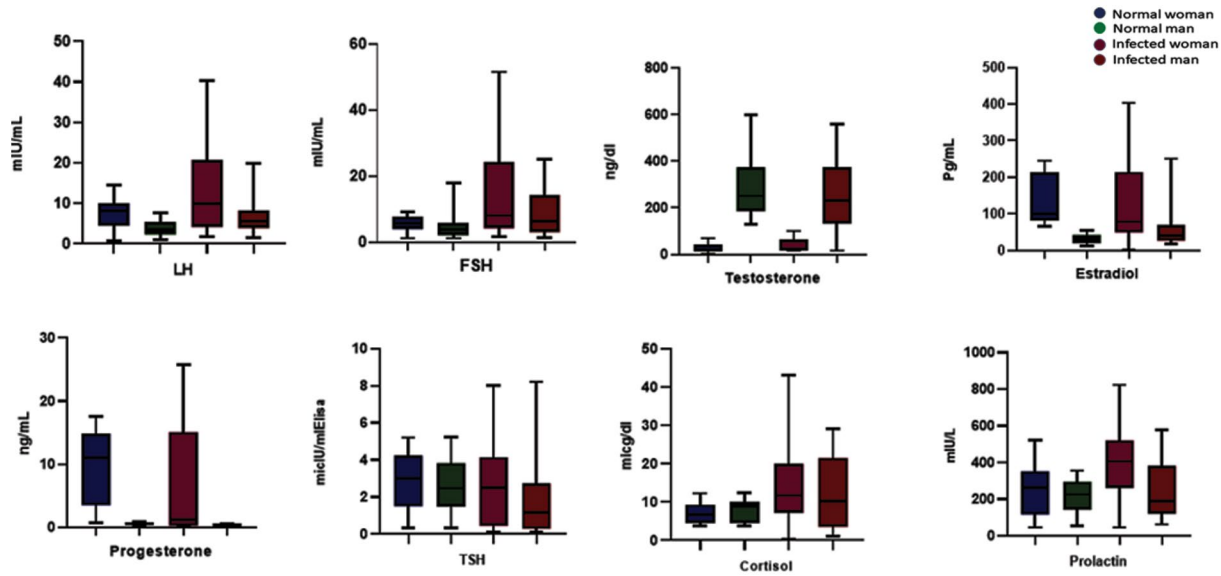

Fig.2: The hormonal changes in both sexes compared to the normal range of healthy individuals. FSH; Follicle stimulating hormone, LH; Luteinizing hormone, and TSH; Thyroid stimulating hormone.

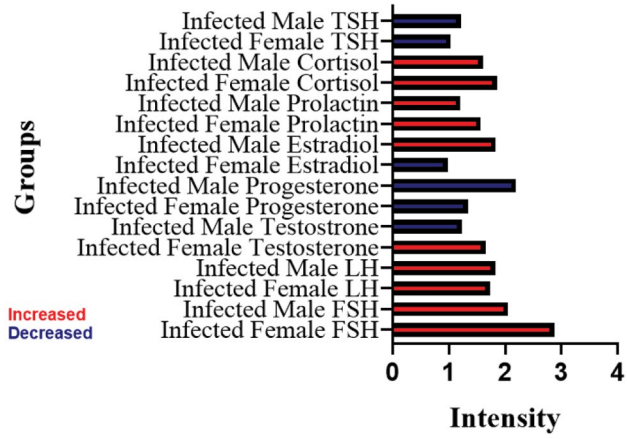

Fig.3: Hormone changes based on the intensity of increase and decrease. FSH; Follicle stimulating hormone, LH; Luteinizing hormone, and TSH; Thyroid stimulating hormone.

Discussion

Our study has comprehensively investigated most of the hormones, that had not been measured during Covid-19 disease. Based on our findings, most of the studied female cases had abnormal changes in their hormones compared with the studied males. The first hormone that showed increasing, and decreasing changes in both sexes was estradiol. Many reasons indicate the absence of estrogen is a consequence of dysfunction or toxicity of the hypothalamus-pituitary axis and ovary (25, 26), leading to the coronary artery and renal diseases, osteoporosis, changes in verbal memory performance and mood, and IL-6 production, which have been recognized as a critical factor in cytokine storm that occurs in Covid-19, osteoclasts, and dysgeusia (27-32). Likewise, increasing estradiol levels will affect the thyroid and enhance iodide concentration, thrombotic**,** ischemic stroke, and elevations of breast cancer risk (33-36). Firstly, Estradiol's abnormal levels in patients might directly result from the damaged ovary, hypothalamus-pituitary axis, FSH, and LH abnormalities. Secondly, maybe as a derivative result of dysgeusia led by the virus itself or antiviral drugs or a combination of both. The next and more forgotten hormone in men is progesterone, which showed only decreasing changes. Progesterone is an essential hormone in men that influences spermatogenesis, sperm capacitation/acrosome reaction, and testosterone biosynthesis in the Leydig cells. Besides, the nervous system has the capacity to bio-convert progesterone into its active metabolite allopregnanolone. Other progesterone effects include blocking gonadotropin secretion, sleep improvement, and effects on tumors in the central nervous system (CNS) (meningioma, fibroma), and effects on the immune system, cardiovascular system, and kidney function, adipose tissue, behavior, and respiratory system (37, 38). As we know, in women, progesterone saves the pregnancy, regulates the period, and the ovary produces the most amount of it; also, adrenals generate a slight amount of progesterone. The abnormal amount of progesterone in both sexes is probably a result of impairment of the ovary, adrenal, or hypothalamus-pituitary axis.

Both genders (male and female) had almost equal abnormalities, suggesting that adrenal and or hypothalamus-pituitary axis are most likely to be involved in the virus attack, rather than women hormons secretion. Testosterone was among those hormones with fewer fold changes. Still, there is a need to enhance the statistical community to determine whether it is an effect of SARS-CoV-2 or not since it is an essential hormone in reproductive health. Moreover, the levels of FSH, LH, TSH, and prolactin showed significant changes. The results of the current study suggests that hypothalamus-pituitary axis was infected and affected by the virus, which consequently leads to cardiovascular disease, blood pressure, and Metabolic disease (39). However, a sudden increase in estrogen and progesterone can cause negative feedback of FSH and LH hormones. Also, the abnormal TSH level might be negative feedback toward T3 and T4 amount and probably reflects the thyroid gland injury. The excess of Cortisol secretion on the immune system, blood pressure, fat deposition, and symptoms and disease is well documented. Therefore, the abnormal level of cortisol and progesterone have been found in this study confirmed the hypothesis of adrenal damage. We will next determine whether these changes are the results of cytokine storm, Stress caused by fear of illness, or the amount of CRH and ACTH released by the hypothalamus and pituitary glands. There is a need to measure the CRH, ACTH, GNRH, T3, and T4 in more samples to endorse the damage of cerebral glands, thyroid, and virus access into the brain.

Conclusion

These results suggested that COVID-19 affects directly or non-directly glands and related hormones.

Acknowledgments

We want to thank Dr. Shahriyar Mamikhani, Dr. Mohammad Hakkaki Fard for all they did during COVID-19 on the quarantine section and saving lives. Although Dr. Mohammad Mirzapour, Mr. Saeid Abdi, and Ms. Helma Mohtadifar supported our study and provided us with all the equipment, we needed. This study financially supported by the Tabriz University of Medical Sciences. The authors declare no conflicts of interest.

Authors' Contributions

N.H., L.R.; Had the idea for and designed the study. All authors had full access to all data in the study and took responsibility for the data's integrity and accuracy. N.H., M.Sh., S.T.; Contributed to the writing of the report and analysis. H.A.; Contributed to the blood sampling of patients at the infectious ward and reporting of results. Sh.Ma.; Contributed as a supervising physician. A.Z., Sh.Me.; Had contributed to the clinical trials assessing. All authore read and approved the final manuscript.

References

1. Jiang F, Deng L, Zhang L, Cai Y, Cheung CW, Xia Z. Review of the clinical characteristics of coronavirus disease 2019 (COVID-19). J Gen Intern Med. 2020; 35(5): 1545-1549.
2. Drosten C, Günther S, Preiser W, Van Der Werf S, Brodt HR, Becker S, et al. Identification of a novel coronavirus in patients with severe acute respiratory syndrome. N Engl J Med. 2003; 348(20): 1967-1976.
3. Zaki AM, van Boheemen S, Bestebroer TM, Osterhaus AD, Fouchier RA. Isolation of a novel coronavirus from a man with pneumonia in Saudi Arabia. N Engl J Med. 2012; 367(19): 1814-1820.
4. Wu F, Zhao S, Yu B, Chen YM, Wang W, Song ZG, et al. A new coronavirus associated with human respiratory disease in China. Nature. 2020; 579(7798): 265-269.
5. Huang C, Wang Y, Li X, Ren L, Zhao J, Hu Y, et al. Clinical features of patients infected with 2019 novel coronavirus in Wuhan, China. Lancet. 2020; 395(10223): 497-506.
6. Wu Z, McGoogan JM. Characteristics of and important lessons from the coronavirus disease 2019 (COVID-19) outbreak in china: summary of a report of 72314 cases from the chinese center for disease control and prevention. JAMA. 2020; 323(13): 1239-1242.
7. Zhou P, Yang XL, Wang XG, Hu B, Zhang L, Zhang W, et al. A pneumonia outbreak associated with a new coronavirus of probable bat origin. Nature. 2020; 579(7798): 270-273.

8. Dimitrov DS. The secret life of ACE2 as a receptor for the SARS virus. Cell. 2003; 115(6): 652-653.
9. Gui M, Song W, Zhou H, Xu J, Chen S, Xiang Y, et al. Cryo-electron microscopy structures of the SARS-CoV spike glycoprotein reveal a prerequisite conformational state for receptor binding. Cell Res. 2017; 27(1): 119-129.
10. Song W, Gui M, Wang X, XiangY. Cryo-EM structure of the SARS coronavirus spike glycoprotein in complex with its host cell receptor ACE2. PLoS Pathog. 2018; 14(8): e1007236.
11. Kirchdoerfer RN, Wang N, Pallesen J, Wrapp D, Turner HL, Cottrell CA, et al. Stabilized coronavirus spikes are resistant to conformational changes induced by receptor recognition or proteolysis. Sci Rep. 2018; 8(1): 15701.
12. Yuan Y, Cao D, Zhang Y, Ma J, Qi J, Wang Q, et al. Cryo-EM structures of MERS-CoV and SARS-CoV spike glycoproteins reveal the dynamic receptor binding domains. Nat Commun. 2017; 8: 15092.
13. Struck AW, Axmann M, Pfefferle S, Drosten C, Meyer B. A hexapeptide of the receptor-binding domain of SARS corona virus spike protein blocks viral entry into host cells via the human receptor ACE2. Antiviral Res. 2012; 94(3): 288-296.
14. Donoghue M, Hsieh F, Baronas E, Godbout K, Gosselin M, Stagliano N, et al. A novel angiotensin-converting enzyme-related carboxypeptidase (ACE2) converts angiotensin I to angiotensin 1-9. Circ Res. 2000; 87(5): E1-9.
15. Prabakaran P, Xiao X, Dimitrov DS. A model of the ACE2 structure and function as a SARS-CoV receptor. Biochem Biophys Res Commun. 2004; 314(1): 235-241.
16. Xu H, Zhong L, Deng J, Peng J, Dan H, Zeng X, et al. High expression of ACE2 receptor of 2019-nCoV on the epithelial cells of oral mucosa. Int J Oral Sci. 2020; 12(1): 8.
17. Zou X, Chen K, Zou J, Han P, Hao J, Han Z. Single-cell RNA-seq data analysis on the receptor ACE2 expression reveals the potential risk of different human organs vulnerable to 2019-nCoV infection. Front Med. 2020; 14(2): 185-192.
18. Zhao Y, Zhao Z, Wang Y, Zhou Y, Ma Y, Zuo W. Single-cell rna expression profiling of ACE2, the receptor of SARS-CoV-2. Am J Respir Crit Care Med. 2020; 202(5): 756-759.
19. Zhang H, Kang Z, Gong H, Xu D, Wang J, Li Z, et al. The digestive system is a potential route of 2019-nCov infection: a bioinformatics analysis based on single-cell transcriptomes. Gut. 2020; 69: 1010-1018.
20. Chai X, Hu L, Zhang Y, Han W, Lu Z, Ke A, et al. Specific ACE2 expression in cholangiocytes may cause liver damage after 2019-nCoV infection. bioRxiv. 2020.
21. Fan C, Lu W, Li K, Ding Y, Wang J. ACE2 expression in kidney and testis may cause kidney and testis infection in COVID-19 patients. Front Med (Lausanne). 2021; 7: 563893.
22. Marazuela M, Giustina A, Puig-Domingo M. Endocrine and metabolic aspects of the COVID-19 pandemic. Rev Endocr Metab Disord. 2020; 21(4): 495-507.
23. World Health Organization. Clinical management of severe acute respiratory infection (SARI) when COVID-19 disease is suspected: interim guidance, 13 March 2020. World Health Organization; 2020. Available from: https://apps.who.int/iris/handle/10665/331446 (12 March 2022).
24. Mandell LA, Wunderink RG, Anzueto A, Bartlett JG, Campbell GD, Dean NC, et al. Infectious diseases society of america/american thoracic society consensus guidelines on the management of community-acquired pneumonia in adults. Clin Infect Dis. 2007; 44 Suppl 2: S27-S72.
25. Oliveira FR, Ferreira JR, dos Santos CM, Macêdo LE, de Oliveira RB, Rodrigues JA, et al. Estradiol reduces cumulative mercury and associated disturbances in the hypothalamus-pituitary axis of ovariectomized rats. Ecotoxicol Environ Saf. 2006; 63(3): 488-493.
26. Tanaka T, Utsunomiya T, Utsunomiya H, Umesaki N. Irinotecan HCl, an anticancer topoisomerase I inhibitor, frequently induces ovarian failure in premenopausal and perimenopausal women. Oncol Rep. 2008; 19(5): 1123-1133.
27. Collins P, Rosano GM, Sarrel PM, Ulrich L, Adamopoulos S, Beale CM, et al. 17 beta-Estradiol attenuates acetylcholine-induced coronary arterial constriction in women but not men with coronary heart disease. Circulation. 1995; 92(1): 24-30.
28. Antus B, Hamar P, Kokeny G, Szollosi Z, Mucsi I, Nemes Z, et al. Estradiol is nephroprotective in the rat remnant kidney. Nephrol Dial Transplant. 2003; 18(1): 54-61.
29. Fink HA, Ewing SK, Ensrud KE, Barrett-Connor E, Taylor BC, Cauley JA, et al. Association of testosterone and estradiol deficiency with osteoporosis and rapid bone loss in older men. J Clin Endocrinol Metab. 2006; 91(10): 3908-3915.
30. Wolf OT, Kudielka BM, Hellhammer DH, Törber S, McEwen BS, Kirschbaum C. Two weeks of transdermal estradiol treatment in postmenopausal elderly women and its effect on memory and mood: verbal memory changes are associated with the treatment induced estradiol levels. Psychoneuroendocrinology. 1999; 24(7): 727-741.
31. Girasole G, Jilka RL, Passeri G, Boswell S, Boder G, Williams DC, et al. 17 beta-estradiol inhibits interleukin-6 production by bone marrow-derived stromal cells and osteoblasts in vitro: a potential mechanism for the antiosteoporotic effect of estrogens. J Clin Invest. 1992; 89(3): 883-891.
32. LoRusso PM, Piha-Paul SA, Mita M, Colevas AD, Malhi V, Colburn D, et al. Co-administration of vismodegib with rosiglitazone or combined oral contraceptive in patients with locally advanced or metastatic solid tumors: a pharmacokinetic assessment of drug-drug interaction potential. Cancer Chemother Pharmacol. 2013; 71(1): 193-202.
33. Boccabella AV, Alger EA. Influence of estradiol on thyroid: serum radioiodide concentration ratios of gonadectomized and hypophysectomized rats. Endocrinology. 1964; 74: 680-688.
34. Bagot CN, Leishman E, Onyiaodike CC, Jordan F, Gibson VB, Freeman DJ. Changes in laboratory markers of thrombotic risk early in the first trimester of pregnancy may be linked to an increase in estradiol and progesterone. Thromb Res. 2019; 178: 47-53.
35. Hu J, Lin JH, Jiménez MC, Manson JE, Hankinson SE, Rexrode KM. Plasma estradiol and testosterone levels and ischemic stroke in postmenopausal women. Stroke. 2020; 51(4): 1297-1300.
36. Lyytinen H, Pukkala E, Ylikorkala O. Breast cancer risk in postmenopausal women using estradiol–progestogen therapy. Obstet Gynecol. 2009; 113: 65-73.
37. Oettel M, Mukhopadhyay AK. Progesterone: the forgotten hormone in men? Aging Male. 2004; 7(3): 236-257.
38. Guennoun R, Labombarda F, Gonzalez Deniselle MC, Liere P, De Nicola AF, Schumacher M. Progesterone and allopregnanolone in the central nervous system: response to injury and implication for neuroprotection. J Steroid Biochem Mol Biol. 2015; 146: 48-61.
39. Xiong F, Zhang L. Role of the hypothalamic-pituitary-adrenal axis in developmental programming of health and disease. Front Neuroendocrinol. 2013; 34(1): 27-46.

Original Article

Improved Healing of Colonic Anastomosis with Allotransplantation of Axillary Skin Fibroblasts in Rats

Narges Sufian, D.V.M.[1], Mehdi Behfar, D.V.Sc.[1]*, Ali-Asghar Tehrani, Ph.D.[2], Hassan Malekinejad, Ph.D.[3, 4]

1. Department of Surgery and Diagnostic Imaging, Faculty of Veterinary Medicine, Urmia University, Urmia, Iran
2. Department of Pathobiology, Faculty of Veterinary Medicine, Urmia University, Urmia, Iran
3. Department of Pharmacology and Toxicology, School of Pharmacy, Urmia University of Medical Sciences, Urmia, Iran
4. Experimental and Applied Pharmaceutical Sciences Research Center, Urmia University of Medical Sciences, Urmia, Iran

**Corresponding Address: P.O.Box: 57153-1177, Department of Surgery and Diagnostic Imaging, Faculty of Veterinary Medicine, Urmia University, Urmia, Iran*
Email: m.behfar@urmia.ac.ir

Received: 07/November/2020, Accepted: 13/April/2021

Abstract

Objective: Colonic anastomosis is associated with serious complications leading to significant morbidity and mortality. Fibroblasts have recently been introduced as a practical alternative to stem cells because of their differentiation capacity, anti-inflammatory, and regenerative properties. The aim of this study was to evaluate the effects of intramural injection of fibroblasts on the healing of colonic anastomosis in rats.

Materials and Methods: Inbred mature male Wistar rats were used in this experimental study (n=36). Fibroblasts were isolated from the axillary skin of a donor rat. In the sham group, manipulation on descending colon was done during laparotomy. A 5 mm segment of the colon was resected, and end-to-end anastomosis was performed. In the control group, 0.5 ml of phosphate buffer saline (PBS) was injected into the colonic wall and in the treatment group, 1×10^6 fibroblasts were transplanted. Following euthanasia on day 7, intra-abdominal adhesion, leakage and peritonitis were evaluated by necropsy. Mechanical properties were assessed using bursting pressure and tensile tests. Inflammation, angiogenesis, and collagen deposition were examined histopathologically.

Results: The mean scores for adhesion and leakage were decreased in the treatment group versus control samples. Lower infiltration of inflammatory cells was observed in the treatment group (P=0.03). Angiogenesis and collagen deposition scores were significantly increased in the fibroblast transplanted group (P=0.03). Tensile mechanical properties of the colon were significantly increased in the treatment group compared to the control sample (P=0.01). There was no significant difference between the control and treatment groups in terms of bursting pressure (P=0.10). Positive weight changes were found in sham and treatment groups, but the control rats lost weight after 7 days.

Conclusion: The results suggested that allotransplantation of dermal fibroblasts could improve the necroscopic, histopathological, and biomechanical indices of colonic anastomosis repair in rats.

Keywords: Allogeneic Transplantation, Colorectal Surgery, Fibroblasts, Rats, Wound Healing

Cell Journal(Yakhteh), Vol 24, No 4, April 2022, Pages: 188-195

Citation: Sufian N, Behfar M, Tehrani AA, Malekinejad H. Improved healing of colonic anastomosis with allotransplantation of axillary skin fibroblasts in rats. Cell J. 2022; 24(4): 188-195. doi: 10.22074/cellj.2022.7861.

Introduction

Anastomosis following colonic resection is performed as a standard treatment for colon neoplastic lesions and chronic ulcerative colitis. Anastomosis is often associated with severe complications such as leakage, dehiscence, and infection (1). Reportedly, the incidence of anastomotic leak ranges from 0.5 to 30% (2). Sepsis and mortality are considered the most severe consequences of anastomotic leakage (3). It is believed that the mechanical stress for defecation and high luminal microbial load are the causes of these complications (4). Different anastomotic devices like staplers, various surgical techniques, and intensive preoperative care have been adopted to decrease the complications, however, fast and safe healing of the anastomosis is still a major concern for colorectal surgeons.

As an alternative strategy, cell-based therapy benefits transplanting multipotent cells to improve the healing process and decrease the rate of complication. Naturally, stromal cells migrate from bone marrow to the site of injury and based on the environmental signals, they differentiate into fibroblasts to deposit collagen and extracellular matrix proteins (5). The multilineage differentiation potentials and minimal immunogenicity of stromal cells are reported to result in the extensive application of these cells in cell-based regenerative medicine.

Although promising results were obtained following transplantation of mesenchymal stromal cells (MSCs) and significant improvement was observed in histological and mechanical properties of the anastomoses in several studies (6, 7), the invasive and painful procedure of bone marrow harvest, time-consuming and expensive multistep procedures for isolation, characterization and expansion can limit MSCs application.

Isolation of adipose-derived stromal cells (ASCs) is performed less invasively, and higher cell yield can be obtained compared to bone marrow. However, their short life span necessitates multiple passages to reach a therapeutic dose. Reportedly, ASCs rapidly undergo

replicative senescence after multiple *in vitro* passages (8). The cellular senescence reduces differentiation capacity and predisposes genomic instability and malignant transformation, thus, the application of ASCs in cell therapy could be challenging. Due to these limitations, the clinical application of MSCs is still being investigated to find the best cell type and method for isolation and expansion.

Fibroblasts are known as the resident mesenchymal stromal/stem cells in connective tissues (9), a key player in wound healing by producing extracellular matrix and collagen fibers (10). Also, fibroblasts enhance angiogenesis in the healing tissue through different growth factors (11). Fibroblasts transform into myofibroblasts that are responsible for wound contraction (12). It seems that MSCs could be practically replaced with fibroblasts due to their anti-inflammatory, regenerative and immune-modulatory properties. In addition, fibroblasts could be easily harvested in large quantities using a cutaneous punch biopsy. The expansion and culture of fibroblasts are markedly easier and require a shorter doubling time compared to MSCs (13). However, there are a few drawbacks in fibroblast cultures such as slow growth especially in their older populations, and susceptibility to mycoplasma contamination (14). Previous studies have shown that fibroblasts transplantation improved skin wound healing in a variety of animal models (15, 16).

To the best of the authors' knowledge, the effects of fibroblasts allotransplantation on colon anastomosis have not been studied, yet. In this study, allogeneic dermal fibroblasts were transplanted into the wall of the colon after surgical anastomosis, and necroscopic, histopathological, and mechanical aspects of repairs were studied.

Materials and Methods

All experimental protocols were performed based on the Iranian guidelines of animal welfare and approved by the Ethics Committee in Urmia University, Faculty of Veterinary Medicine, Urmia, Iran (IR-UU-AEC-3/1024/AD).

Study design

In this experimental study, 36 inbred adult male Wistar rats weighing 220.00 ± 30.00 g were obtained from the Laboratory Animal Center of the Faculty of Veterinary Medicine, Urmia University, Urmia, Iran. The rats were housed in plastic cages in a group of two and fed standard commercial pellets and had free access to a bottle of water. The rats were randomly divided into three groups of sham, control, and treatment (n=12). The mean body weight of rats in each group was recorded as baseline values to compare to the post-operative weights at the end of the study. All chemicals for this analysis were purchased from Sigma-Aldrich (Darmstadt, Germany) unless otherwise stated.

Fibroblast isolation

To isolate dermal fibroblast, 1 cm^2 of skin was harvested from a randomly selected donor out of the sham rats. In this regard, the rat was anesthetized using intraperitoneal (IP) injection of 90 mg/kg ketamine hydrochloride (Alfasan, Woerden, Netherlands) and 5 mg/kg xylazine hydrochloride (Alfasan, Woerden, Netherlands). The right axillary region was prepared aseptically, and the skin sample was excised using a 10 scalpel blade and placed in phosphate buffer saline (pH=7.2, Gibco, Grand Island, USA). Then, the donor site was sutured using a 3-0 nylon (SPUA, Iran) with a simple interrupted pattern. The skin sample was cut into small pieces, then placed in 10 ml of DMEM/F12 medium supplemented with antibiotic/antimycotic agents (Gibco, USA), and digested enzymatically with medium containing 10% collagenase type II (Sigma-Aldrich, USA) for 90 minutes at 37˚C. Then, 10 ml of culture medium containing 10% fetal bovine serum (FBS, Gibco, USA) was added to stop digestion. Using a 70 µm cell strainer (BD Falcon™, BD Biosciences, USA), the tissue suspension was filtered. The resulting suspension was centrifuged at 700 g for 5 minutes. After 5 minutes, the supernatant was gently removed, and the pellet was re-suspended by pipetting in a complete culture medium. The pellet was then cultured in a cell culture flask (T25, SPL life Sciences, Seoul, Korea) containing DMEM, 15% FBS, penicillin (100 IU/ml, Sigma-Aldrich, USA), and streptomycin (100 µg/ml, Sigma-Aldrich, USA) and then it was placed in 37˚C and 5% CO_2 incubator. The fibroblast started to exit tissue fragments within 2-5 days and on day 14 the first subculture was performed. Non-adherent cells were discarded before medium replacement and subculture processes; therefore, morphological methods were used to confirm the fibroblast characteristics of the isolated cells. The isolated cells were large, adherent with lamellipodia that are well-known characteristics of skin fibroblasts (17). To characterize the fibroblasts, the cell migration rate, the pattern of migration, and *in vitro* hydroxyproline concentration were evaluated.

Cell migration

The pattern and rate of migration were evaluated through a scratch wound healing assay as previously described by Jonkman et al. (18). In this regard, 1×10^6 cells/well were seeded in a 6-well plate with 2 ml of DMEM until 90% confluence was reached. Then, a linear scratch wound was created in the monolayer with a sterile 200 µl plastic micropipette tip. Any cellular debris was removed by washing the plate with phosphate buffer saline (PBS, Sigma-Aldrich, USA). Then, 2 ml of fresh medium were added to the cultures which were then incubated at 37˚C inside an incubator with a 5% CO_2 humidified atmosphere for 24 hours. Cell migration was determined after 24 hours using an inverted microscope equipped with a digital camera. The wound width was measured at predetermined time points and average widths were recorded. The migration rate was calculated using the

below equation (19):

Migration rate (μm/hours)=W(t1)W(t2)/Δt
where, W(t1) is the initial wound width, W(t2) is the final wound width, and Δt is the duration of migration.

In vitro hydroxyproline assay

To determine hydroxyproline concentration, the cells were homogenized using KCl (150 mM, pH=7.40). The homogenate (0.5 ml) was digested in 1 ml of 6 N HCl at 120˚C for 8 hours. Then, to oxidize the free hydroxyproline, citrate/acetate buffer (50 μl, pH=6) and 1 ml of chloramine-T solution (282 mg of chloramine-T, 2.00 ml of n-propanol, 2 ml of H_2O, and 16 ml of citrate/acetate buffer) were added to 50 μl of samples and kept at room temperature for 20 minutes. 1 ml of Ehrlich's solution was added to each sample, and then the samples were placed in a water bath at 65˚C for 15 minutes. After cooling to room temperature, the sample absorbance was measured with a microplate reader (Stat Fax® 2100; Awareness Technology Inc., USA) at 550 nm. A concentration range of 0.00 to 10.00 μg/ml hydroxyproline standard was used to establish a standard curve (20).

Cell viability

Before transplantations, the cell viability was assessed by the trypan blue dye exclusion test. Briefly, the fibroblasts were trypsinized and centrifuged (200 g for 8 minutes). The pellet was suspended in DMEM and 20 μL of the cell suspension was mixed with 0.4% trypan blue solution in the ratio of 1:10. Live (colorless) and dead (stained blue) cells were counted in a Neubauer chamber to determine cell viability.

Surgery

Under general anesthesia, the caudal abdomen was prepared for aseptic surgery and opened through a ventral midline incision. Descending colon was carefully exteriorized and manipulated for 10 minutes in the sham group and then was returned to its anatomic position. The abdominal incision was then sutured using 3-0 nylon suture (SPUA ,Iran) in a simple continuous pattern. In control and treatment groups, to avoid intraabdominal contamination, saline-soaked gauze was used to isolate the colon. Then, a 5 mm segment of the descending colon was excised. Subsequently, end-to-end anastomosis was performed using 10 simple interrupted 6-0 nylon sutures (SPUA, Iran, Fig.1A). The anastomosis was tested for leakage by injecting 1 ml of sterile saline intraluminally while the colon was occluded proximal and distal to the anastomosis (Fig.1B). Additional sutures were placed if necessary. The rats in the control group were injected 0.5 ml PBS intramurally (into the colonic wall) at both sides of anastomosis. In the treatment group, 1×10^6 homologous dermal fibroblasts suspended in 0.5 ml PBS, as the carrier, were injected in the same fashion (Fig.1C). Then, the abdomen was closed as mentioned above.

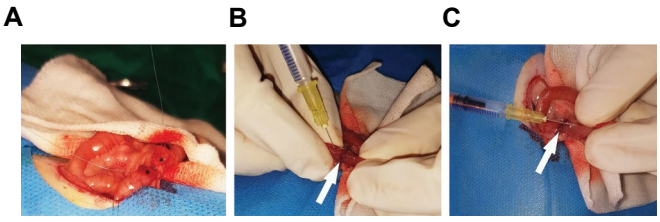

Fig.1: The surgical procedure of colonic anastomosis in rats. **A.** Asterisks show the transected ends of the descending colon and the first suture was passed through both ends. **B.** The white arrow shows the complete anastomosis which was followed by a leak test with the injection of normal saline into the lumen of the colon. **C.** Fibroblasts were injected intramurally (into the colonic wall) at both sides of the anastomotic site (white arrow) in the treatment group.

Sampling

On day 7, the rats were euthanized by anesthetic overdose (IP injection of 300 mg/kg ketamine hydrochloride and 30 mg/kg xylazine hydrochloride). Before necropsy, the rats' bodyweight was measured to evaluate the catabolic and the anabolic states postoperatively and was compared to the baseline values. The abdomen was re-opened and after gross examinations, the colon (n=6, including the anastomotic site) was harvested and then divided into two longitudinal halves using a scalpel blade. One half was tested for mechanical tensile test and the other half was evaluated by histopathology. Six other samples were harvested en bloc for bursting pressure.

Macroscopic evaluations

Any peri-anastomotic adhesion formation, abscess, and peritonitis were scored as described previously (21). Adhesion severity was classified as none: no adhesion (score=0), mild: adhesions formation between the anastomotic site and the greater omentum (score=1), moderate: adhesions between anastomotic site, greater omentum and small intestines (score=2), and severe: extensive adhesions (score=3). The scoring system of Wu et al. was used to evaluate the severity of leakage from the anastomosis, in which score 0 indicates no leakage, score 1 indicates mild leakage associated with abscess around the anastomotic site, score 2 represents moderate leakage and presence of intra-abdominal feces leading to peritonitis with or without abscess formation, and 3=death due to severe leakage (22).

Mechanical evaluation

The second half-strips from each group (n=6) were subjected to mechanical testing. Each sample was mounted on an STM-5 tensile machine (Santam Engineering Design Co., Tehran, Iran) supplied with a 20 kg load cell (Bongshin Loadcell Co. Ltd., Seoul, South Korea). The constant velocity of 20 mm/minutes was used for the tensile test until breakage. A load-displacement curve and the following mechanical properties were obtained: maximum load (N), load in yield point (N), and energy absorption (J). Figure 2 shows the diagrams of load-displacement curves of the experimental groups.

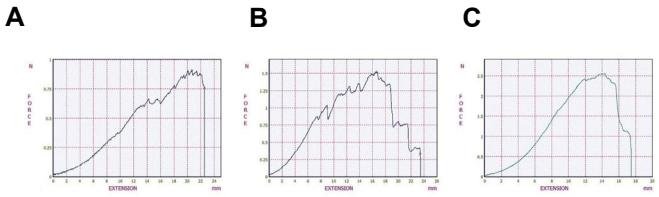

Fig.2: The load-displacement curve of colon samples during the tensile test under the constant velocity of 20 mm/minutes. **A.** Control group, **B.** Treatment group, and **C.** Sham group.

Bursting pressure

The bursting pressure test was done *ex vivo*. The anastomoses (n=6 from each group) were resected en bloc as well as a 15 mm segment of the intact colon on each side. After washing out the feces, the proximal end was ligated by a 2-0 Dexon suture (SPUA, Iran), and the distal end of the colon was secured to an intravenous catheter and attached to the bursting pressure measurement apparatus thorough a T-shaped three-way. The colon was placed in a water-filled container and a constant oxygen flow (1 L per minutes) was used to inflate it. A manometer was used to measure the bursting pressures. It was recorded when bubbles were observed at the anastomotic site, or a sudden pressure decrease was noted on the manometer.

Histopathological assessment

The longitudinal strips of the colon (n=6) from the control and treatment groups were formalin-fixed and paraffin-embedded. Five µm sections were stained with hematoxylin and eosin (H&E). Infiltration of inflammatory cells and neovascularization were scored as described in a previous study (23). Collagen content was scored according to modified Ehrlich & Hunt in Masson's trichrome (MTC) stained sections. For MTC stain, Masson Kit (HT15, Sigma-Aldrich, USA) was used. In brief, the sections were deparaffinized, rehydrated, and immersed in Bouin's solution at 56˚C for 15 minutes. The slides were washed using tap water for 5 minutes then stained in Weigert's hematoxylin for 5 minutes. After washing with water, the slides were stained in the Biebrich scarlet-acid fuchsin. Then, the slides were incubated for 5 minutes in the phosphotungstic-phosphomolybdic acid. The slides were stained using aniline blue for 5 minutes and finally were fixed in acetic acid for 2 minutes. Then the slides were rinsed in distilled water, dehydrated with methanol, and mounted.

Accordingly, score 0=no evidence, score 1=occasional collagen fibers, score 2=light scattering, score 3=abundant collagen fibers, and score 4=dense collagen bundles under 100× magnification (24). All sections were coded and examined blindly blindly by two observers and the results were presented as the mean score.

Statistical analysis

The semi-quantitative scores were analyzed using Kruskal Wallis followed by Mann-Whitney test and the results were shown as the mean and interquartile range (25 and 75% quartile). The quantitative results were analyzed using one-way ANOVA and Tukey post hoc test for multiple comparisons. The experimental data were presented as mean ± standard deviation (SD). All statistical analyses were done in Minitab (version 16.0, Minitab Inc., Boston, USA), and $P<0.05$ were considered as statistical significance.

Results

Culture properties

Morphologically, the cultured cells had a spindle-shaped cell body with flat elongated oval nuclei and long lamellipodia. In the scratch assay, the cells were loosely connected during migration which was the characteristic of fibroblasts (Fig.3). The migration rate of fibroblast in the culture plate was 26.5 µm/hours. *In vitro* hydroxyproline content after 48 hours culture was 1.20 ± 0.12 mg/ml of cell homogenate. According to the trypan blue exclusion assay, cell viability was above 95% before transplantations.

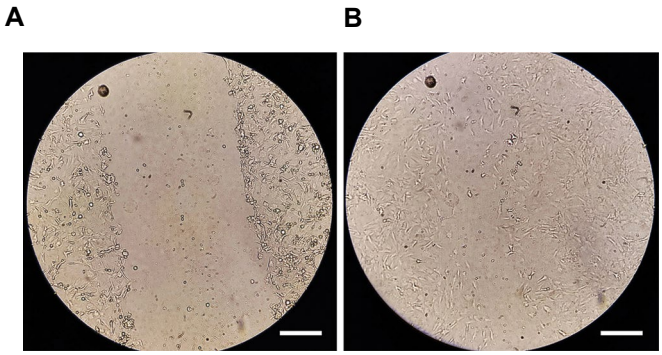

Fig.3: The *in vitro* wound-healing assay. **A.** Scratch assay on monolayer fibroblast culture (0 hour). **B.** Fibroblasts migrated after 24 hours to close the distance between two edges of the wound (scale bars=300 µm).

Bodyweight

After 7 days, an increase in the body weight was observed in the sham (19.66 ± 3.24 g) and treatment (6.50 ± 3.24 g) groups versus their preoperative values. However, a decrease in body weights of the control rats was observed (4.83 ± 1.38 g) when compared to the baseline values. Significant differences were found among the three groups in terms of post-operative body weight change ($P<0.001$).

Macroscopic necropsy findings

No adhesion was observed in the sham group (score 0). Adhesion formation was detected in the control group (mean score=2, range 1-3) in which the adhesions

were formed mostly to small intestines and omentum. In the fibroblast transplanted group, mild adhesions to the omentum were observed (mean score=0.5, range 0-1, Fig.4). The semi-qualitative statistical comparison showed that adhesions were significantly lower in the fibroblast transplanted group in comparison with the control samples (P=0.03). In control rats, mild to moderate anastomotic leakage into the abdomen were observed (mean score=1, range 0-2). No leakage was found in sham and treatment groups (score 0). Statistical analysis showed a significant increase in the extent of leakage between the control group (P=0.00) compared to sham and treatment groups. Peritonitis was not observed in the samples (score 0). Statistically, no significant changes were observed among the three groups for peritonitis (P=0.10).

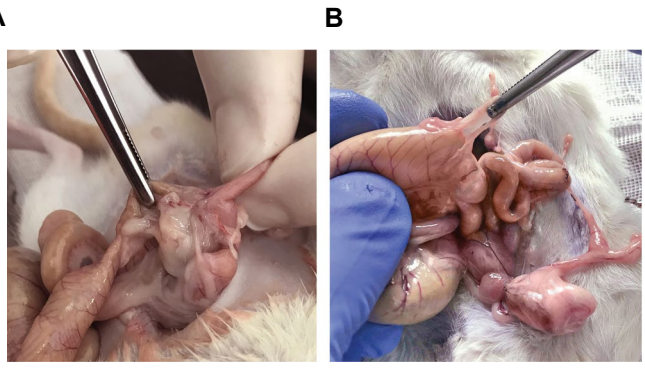

Fig.4: After euthanasia, the rats underwent necropsy to evaluate the adhesion score. **A.** Moderate adhesion was observed in the control group. The colon anastomotic site was covered by small intestines and greater omentum and precise sharp dissection were required for sampling. **B.** In the treatment group, mild omental adhesions were found around the colon anastomosis. Using blunt dissection and mild traction the omentum was easily detached from the colon.

Mechanical properties

Statistical analysis of tensile test showed a significant increase in the mechanical properties of repairs including maximum load, yield load and energy absorption in the fibroblast received group when compared to the control group (P=0.01). Figure 5 represents the results of mechanical properties in the experimental groups.

Bursting pressure

In the sham group, the bursting pressure (228.5 ± 24.90 mm Hg) was significantly higher in comparison with the other experimental groups (P=0.01). According to the statistical analysis, no significant difference was observed between the control (142.67 ± 34.51 mm Hg) and treatment (150.00 ± 15.65 mm Hg) groups (P=0.15).

Histopathology findings

A significant reduction of infiltrated inflammatory cells was observed in the treatment group compared to the control group (P=0.03, Fig.6). The mean score for infiltration of inflammatory cells was 3 (range=1-4) in the control group versus 1.5 (range=1-2) in the treatment group. In terms of angiogenesis, a significantly lower score was obtained in the control group (mean=2.5, range: 1-3) as compared to the treatment group (mean=3.5, range: 3-4, P=0.03). According to the MTC staining, fibroblast transplantation resulted in a significant increase in collagen deposition (P=0.001) with a parallel orientation of collagen bundles within the granulation tissue. In contrast, the haphazard orientation of collagen bundles was observed in control samples (Fig.6). The mean score for collagen deposition were 1.5 (range=1-3) in control group versus 3.5 (range=3-4) for treatment group. The difference between these two groups was statistically significant (P=0.02).

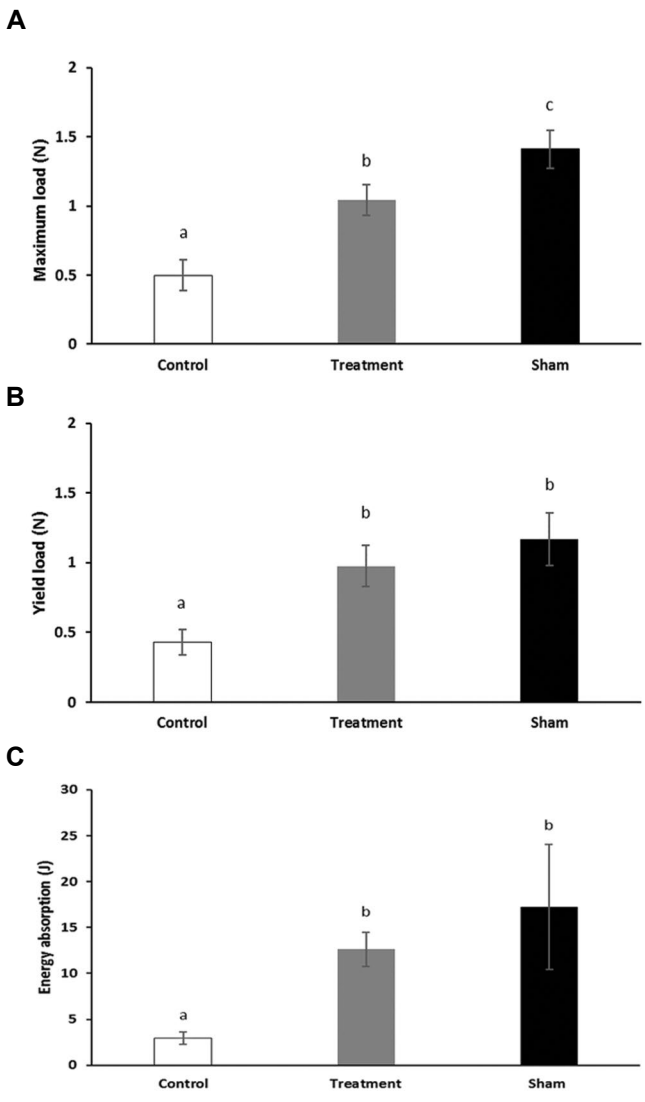

Fig.5: Mechanical properties of colon anastomosis of different groups derived from the load-displacement curves. **A.** Maximum load, **B.** Yield load, and **C.** Energy absorption. Data are presented as mean ± standard deviation. abc; Different letters indicate significant differences among the groups at P<0.05.

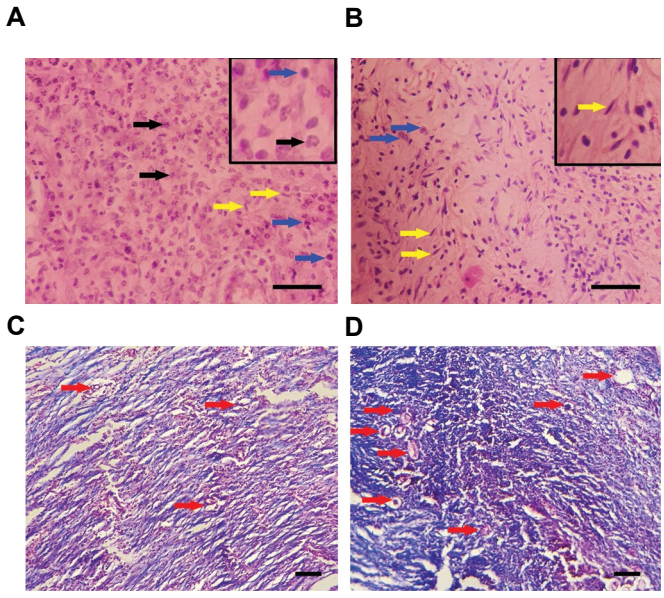

Fig.6: Photomicrograph of granulation tissue in the colon anastomotic site. A significant increase in the infiltration of inflammatory cells was observed in **A.** The control group compared to **B.** The fibroblast transplanted group (H&E, 400×, Insets 1000×). Neutrophils and lymphocytes are shown with black and blue arrows, respectively. Yellow arrows show mature fibroblasts within the granulation tissue. Masson's trichrome staining of colon anastomotic site in **C.** The control group and **D.** Treatment groups. Collagen bundles were sparse and randomly oriented within the granulation tissue of the control group. However, in the fibroblast transplanted group, a dense network of collagen bundles was observed. Blue areas indicate collagen deposition (MTC, 40×). Red arrows show newly formed vessels within the granulation tissue. The number of new vessels was significantly higher in the treatment group (MTC, 40×, scale bars=100 µm).

Discussion

Anastomotic dehiscence and leakage are known as the most serious complications of colorectal colon anastomosis (25) which often occur during the first-week post-operation (4). Following anastomosis, the tensile strength of the anastomotic site is reduced due to inflammatory responses. To prevent dehiscence collagen synthesis is crucial to provide compensatory strength (6). Collagen is synthesized by fibroblasts, which are the main cell type within the stroma. By providing structural scaffolding and modulating the secretion of growth factors, the fibroblasts have a critical role in wound remodeling and homeostasis (26). Here, we examined the effects of intramural transplantation of allogeneic fibroblasts on the healing of colonic anastomosis in a rat model.

In the present study, the isolated and cultured cells were verified as fibroblasts based on their spindle-shaped morphology as the defining characteristics of fibroblasts (27), plastic-adherence properties (28), cell migration pattern, (29), and *in vitro* hydroxyproline synthesis (30). *In vitro* scratch assay is a well-developed method to examine cell migration because it is easy to perform on adherent cell lines including fibroblasts, epithelial and endothelial cell lines (31). According to Suarez-Arnedo et al. (19), the most important advantages of the scratch assay are the low requirements of specialized equipment and costly reagents. Reportedly, the above-mentioned cell lines can be determined based on their pattern of migration in which a loosely connected population indicates the fibroblasts. Whereas the epithelial and endothelial cells are embedded in sheets of cells during migration (29).

The present study revealed that fibroblast transplantation resulted in a lower adhesion and leakage score. Reduced inflammation, improved angiogenesis, and organized collagen deposition were detected in the fibroblast treated group. The transplantation also improved the mechanical properties of the repairs after 7 days.

Previously, promising results were obtained following systemic injection of stromal cells in experimental colonic anastomosis (7). The systemic transplantation of cells can significantly reduce the rate of cellular engraftment (32), in contrast, local transplantation of stem cells would improve the effectiveness of cell therapy. In the literature, there are few studies addressing the effects of intramural injection of cells on the healing of intestinal anastomosis. According to Shen et al. (33), submucosal injection of bone marrow stromal cells could prevent degenerative changes of the small intestine in rats (33). Adas et al. (7) reported that injection of bone marrow stromal cells could accelerate the healing of ischemic model colonic anastomosis in rats through improving the histopathological parameters and elevating the bursting pressure. Yoo et al. (34) transplanted ASCs in a rat colonic anastomosis model and reported higher bursting pressure, increased collagen deposition, improved angiogenesis, and minimal bodyweight loss in comparison with the control group.

Although MSCs are used as the ideal source for cell-therapy, there are major shortcomings in practice. To reach a therapeutic number of cells, multiple *in vitro* expansions are required which increase the possibility of mutagenesis and dysfunction of the cells. The *in vitro* expansions also would increase the duration and cost of treatment. Fibroblasts could be easily isolated in large quantities compared to the mesenchymal stromal cells. A shorter doubling time is required for fibroblast expansion which could effectively reduce the cost of treatment (13).

Fibroblasts are believed to be an important source of anti-inflammatory mediators (35). Inflammation is a critical phase during the healing process; however, prolonged inflammation may lead to massive collagen degradation in the repair site. A Short inflammatory phase provides the early commencement of the proliferation phase and early collagen synthesis. Collagen deposition is the key player in the prevention of anastomotic leakage (36). Mechanical stress from the strong colonic wall motility increases the potential for dehiscence and leakage after anastomosis.

The anastomotic site should also possess sufficient strength to resist the mechanical stress during the fecal passage. In this regard, the bursting pressure and tensile strength tests are used to evaluate the anastomotic strength. The bursting pressure reflects the resistance of the anastomotic site against the increased intraluminal pressure, and the tensile strength represents the anastomotic resistance to longitudinal forces resulted

from contractions of the intestinal muscular layer (37).

It has been reported that the evaluation of bursting pressure is reliable only during the early phase of anastomotic repair (i.e., the first three days) (38). In this study, no statistical difference was found between the control and treatment groups. Thus, we assumed that measurement on day 7, was too late to observe any changes.

According to Iwanaga et al., the tensile strength test is the standard method of assessing the biological aspects of anastomotic repair (39). In this study, the maximum load and yield load were significantly higher in response to fibroblast transplantation suggesting a higher tolerance against colonic motility and therefore greater resistance to the dehiscence and leakage. Low energy-absorption may lead to an increased risk of tissue overload (e.g. dehiscence) under mechanical stress. The tensile test in this study revealed higher energy-absorbing capacity in fibroblast transplanted samples when compared to the controls. Sufficient energy-absorbing capacity is required to store and release the mechanical forces without damage to the anastomotic site (40).

In the present study, following anastomosis the mean bodyweights were decreased in both experimental groups compared to the sham rats, however, the change was lower in the fibroblast treated group. It has been reported that bodyweight loss is directly linked to decreased anastomotic strength and lower deposition of collagen. Thus, it could be stated that fibroblast transplantation could prevent the adverse outcomes of an inferior anastomosis leading to the catabolic state after the surgery.

Conclusion

The present study provided strong pieces of evidence on the ameliorative effects of fibroblast transplantation on the healing of colonic anastomosis in rats. Our results showed that serious complications of colonic anastomosis could be avoided by intramural fibroblast transplantation.

Acknowledgments

The authors wish to thank Dr. Ramin Mazaheri-Khameneh and Miss Aylar Alenabi for their excellent technical assistance. The financial support of the Research Dean of Urmia University is also gratefully acknowledged (Grant No. 97-40/PD3). The authors declare no conflict of interest regarding the publication of this manuscript.

Authors' Contributions

M.B., H.M.; Contributed to conception and design. N.S.; Contributed to the experimental work and drafted the manuscript. A.-A.T., H.M.; Data acquisition. M.B.; Contributed to data analysis revision and final approval of the manuscript. All authors read and approved the final manuscript.

References

1. Slieker JC, Daams F, Mulder IM, Jeekel J, Lange JF. Systematic review of the technique of colorectal anastomosis. JAMA Surg. 2013; 148(2): 190-201.
2. Blanco-Colino R, Espin-Basany E. Intraoperative use of ICG fluorescence imaging to reduce the risk of anastomotic leakage in colorectal surgery: a systematic review and meta-analysis. Tech Coloproctol. 2018; 22(1): 15-23.
3. Thomas MS, Margolin DA. Management of colorectal anastomotic leak. Clin Colon Rectal Surg. 2016; 29(2): 138-144.
4. Bhat AH, Parray FQ, Chowdri NA, Wani RA, Thakur N, Nazki S, et al. Mechanical bowel preparation versus no preparation in elective colorectal surgery: A prospective randomized study. Int J Surg Open. 2016; 2: 26-30.
5. El-Said MM, Emile SH. Cellular therapy: a promising tool in the future of colorectal surgery. World J Gastroenterol. 2019; 25(13): 1560-1565.
6. Maruya Y, Kanai N, Kobayashi S, Koshino K, Okano T, Eguchi S, et al. Autologous adipose-derived stem cell sheets enhance the strength of intestinal anastomosis. Regen Ther. 2017; 7: 24-33.
7. Adas G, Arikan S, Karatepe O, Kemik O, Ayhan S, Karaoz E, et al. Mesenchymal stem cells improve the healing of ischemic colonic anastomoses (experimental study). Langenbecks Arch Surg. 2011; 396(1): 115-126.
8. Palumbo P, Lombardi F, Siragusa G, Cifone MG, Cinque B, Giuliani M. Methods of isolation, characterization and expansion of human adipose-derived stem cells (ASCs): an overview. Int J Mol Sci. 2018; 19(7): 1897.
9. Hutchison N, Fligny C, Duffield JS. Resident mesenchymal cells and fibrosis. Biochim Biophys Acta. 2013; 1832(7): 962-971.
10. Thangapazham RL, Darling TN, Meyerle J. Alteration of skin properties with autologous dermal fibroblasts. Int J Mol Sci. 2014; 15(5): 8407-8427.
11. Nakamichi M, Akishima-Fukasawa Y, Fujisawa C, Mikami T, Onishi K, Akasaka Y. Basic fibroblast growth factor induces angiogenic properties of fibrocytes to stimulate vascular formation during wound healing. Am J Pathol. 2016; 186(12): 3203-3216.
12. Darby IA, Laverdet B, Bonté F, Desmoulière A. Fibroblasts and myofibroblasts in wound healing. Clin Cosmet Investig Dermatol. 2014; 7: 301-311.
13. Ichim TE, O'Heeron P, Kesari S. Fibroblasts as a practical alternative to mesenchymal stem cells. J Transl Med. 2018; 16(1): 212.
14. Auburger G, Klinkenberg M, Drost J, Marcus K, Morales-Gordo B, Kunz WS, et al. Primary skin fibroblasts as a model of parkinson's disease. Mol Neurobiol. 2012; 46(1): 20-27.
15. Mizoguchi T, Ueno K, Takeuchi Y, Samura M, Suzuki R, Murata T, et al. Treatment of cutaneous ulcers with multilayered mixed sheets of autologous fibroblasts and peripheral blood mononuclear cells. Cell Physiol Biochem. 2018; 47(1): 201-211.
16. Motamed S, Taghiabadi E, Molaei H, Sodeifi N, Hassanpour SE, Shafieyan S, et al. Cell-based skin substitutes accelerate regeneration of extensive burn wounds in rats. Am J Surg. 2017; 214(4): 762-769.
17. Seluanov A, Vaidya A, Gorbunova V. Establishing primary adult fibroblast cultures from rodents. J Vis Exp. 2010; (44): 2033.
18. Jonkman JE, Cathcart JA, Xu F, Bartolini ME, Amon JE, Stevens KM, et al. An introduction to the wound healing assay using live-cell microscopy. Cell Adh Migr. 2014; 8(5): 440-451.
19. Suarez-Arnedo A, Torres Figueroa F, Clavijo C, Arbeláez P, Cruz JC, Muñoz-Camargo C. An image J plugin for the high throughput image analysis of in vitro scratch wound healing assays. PLoS One. 2020; 15(7): e0232565.
20. Ghayemi N, Sarrafzadeh-Rezaei F, Malekinejad H, Behfar M, Farshid AA. Effects of rabbit pinna-derived blastema cells on tendon healing. Iran J Basic Med Sci. 2020; 23(1): 13-19.
21. Malekolkalami M, Behfar M, Tehrani AA. Effect of short term oral administration of silymarin on healing of colonic anastomosis in rats. Iran J Vet Surg. 2020; 15(2): 106-114.
22. Wu Z, Daams F, Boersema GS, Vakalopoulos KA, Lam KH, van der Horst PH, et al. Colorectal anastomotic leakage caused by insufficient suturing after partial colectomy: a new experimental model. Surg Infect (Larchmt). 2014; 15(6): 733-738.
23. Lorenzi T, Trombettoni MMC, Ghiselli R, Paolinelli F, Gesuita R, Cirioni O, et al. Effect of omiganan on colonic anastomosis healing in a rat model of peritonitis. Am J Transl Res. 2017; 9(7): 3374-3386.
24. Tallón-Aguilar L, Lopez-Bernal Fde A, Muntane-Relat J, García-Martínez JA, Castillo-Sanchez E, Padillo-Ruiz J. The use of TachoSil as sealant in an experimental model of colonic perforation. Surg Innov. 2015; 22(1): 54-60.
25. Kosmidis C, Efthimiadis C, Anthimidis G, Basdanis G, Apostolidis S, Hytiroglou P, et al. Myofibroblasts and colonic anastomosis

healing in Wistar rats. BMC Surg. 2011; 11: 6.
26. Mukaida N, Sasaki S. Fibroblasts, an inconspicuous but essential player in colon cancer development and progression. World J Gastroenterol. 2016; 22(23): 5301-5316.
27. Sun Y, Kim DH, Simmons CA. Integrative mechanobiology: micro- and nano-techniques in cell mechanobiology. UK: Cambridge University Press; 2015; 269.
28. Shafiei F, Tavangar MS, Razmkhah M, Attar A, Alavi AA. Cytotoxic effect of silorane and methacrylate based composites on the human dental pulp stem cells and fibroblasts. Med Oral Patol Oral Cir Bucal. 2014; 19(4): e350-358.
29. Liang CC, Park AY, Guan JL. In vitro scratch assay: a convenient and inexpensive method for analysis of cell migration in vitro. Nat Protoc. 2007; 2(2): 329-333.
30. Restu Syamsul H, Indra K, Yurika S. Allogeneic human dermal fibroblasts are viable in peripheral blood mononuclear co-culture. Universa Medicine. 2014; 33: 91-99.
31. Vang Mouritzen M, Jenssen H. Optimized scratch assay for in vitro testing of cell migration with an automated optical camera. J Vis Exp. 2018; (138): 57691.
32. Parekkadan B, Milwid JM. Mesenchymal stem cells as therapeutics. Annu Rev Biomed Eng. 2010; 12: 87-117.
33. Shen ZY, Zhang J, Song HL, Zheng WP. Bone-marrow mesenchymal stem cells reduce rat intestinal ischemia-reperfusion injury, ZO-1 downregulation and tight junction disruption via a TNF-α-regulated mechanism. World J Gastroenterol. 2013; 19(23): 3583-3595.
34. Yoo JH, Shin JH, An MS, Ha TK, Kim KH, Bae KB, et al. Adipose-tissue-derived stem cells enhance the healing of ischemic colonic anastomoses: an experimental study in rats. J Korean Soc Coloproctol. 2012; 28(3): 132-139.
35. Flavell SJ, Hou TZ, Lax S, Filer AD, Salmon M, Buckley CD. Fibroblasts as novel therapeutic targets in chronic inflammation. Br J Pharmacol. 2008; 153 Suppl 1: S241-S246.
36. Shogan BD, Belogortseva N, Luong PM, Zaborin A, Lax S, Bethel C, et al. Collagen degradation and MMP9 activation by Enterococcus faecalis contribute to intestinal anastomotic leak. Sci Transl Med. 2015; 7(286): 286ra68.
37. Hendriks T, Mastboom WJ. Healing of experimental intestinal anastomoses. Parameters for repair. Dis Colon Rectum. 1990; 33(10): 891-901.
38. Ho YH, Ashour MA. Techniques for colorectal anastomosis. World J Gastroenterol. 2010; 16(13): 1610-1621.
39. Iwanaga TC, Aguiar JL, Martins-Filho ED, Kreimer F, Silva-Filho FL, Albuquerque AV. Analysis of biomechanical parameters in colonic anastomosis. Arq Bras Cir Dig. 2016; 29(2): 90-92.
40. Behfar M, Sarrafzadeh-Rezaei F, Hobbenaghi R, Delirezh N, Dalir-Naghadeh B. Enhanced mechanical properties of rabbit flexor tendons in response to intratendinous injection of adipose derived stromal vascular fraction. Curr Stem Cell Res Ther. 2012; 7(3): 173-178.

Original Article

Proteomics Study of Mesenchymal Stem Cell-Like Cells Obtained from Tumor Microenvironment of Patients with Malignant and Benign Salivary Gland Tumors

Mohammad Reza Haghshenas, Ph.D.[1], Nasrollah Erfani, Ph.D.[1, 2], Soolmaz Khansalar, M.Sc.[1], Bijan Khademi, M.D[3], Mohammad Javad Ashraf, M.D.[4], Mahboobeh Razmkhah, Ph.D.[1*], Abbas Ghaderi, Ph.D.[1, 2*]

1. Shiraz Institute for Cancer Research, School of Medicine, Shiraz University of Medical Sciences, Shiraz, Iran
2. Department of Immunology, School of Medicine, Shiraz University of Medical Sciences, Shiraz, Iran
3. Otolaryngology Research Center, Department of Otolaryngology, Shiraz University of Medical Sciences, Shiraz, Iran
4. Department of Pathology, Khalili Hospital, Shiraz University of Medical Sciences, Shiraz, Iran

**Corresponding Address: P.O.Box: 71345-3119, Shiraz Institute for Cancer Research, School of Medicine, Shiraz University of Medical Sciences, Shiraz, Iran*
Emails: razmkhahm@sums.ac.ir, ghaderia@sums.ac.ir

Received: 24/October/2020, Accepted: 13/February/2021

Abstract

Objective: Salivary gland tumors (SGTs) show some aggressive and peculiar clinicopathological behaviors that might be related to the components of the tumor microenvironment, especially mesenchymal stem cells (MSCs)-associated proteins. However, the role of MSCs-related proteins in SGTs tumorigenesis is poorly understood. This study aimed to isolate and characterize MSCs from malignant and benign tumor tissues and to identify differentially expressed proteins between these two types of MSCs.

Materials and Methods: In this experimental study, MSC-like cells derived from benign (pleomorphic adenoma, n=5) and malignant (mucoepidermoid carcinoma, n=5) tumor tissues were verified by fluorochrome antibodies and flow cytometric analysis. Differentially expressed proteins were identified using two-dimensional polyacrylamide gel electrophoresis (2DE) and Mass spectrometry.

Results: Results showed that isolated cells strongly expressed characteristic MSCs markers such as CD44, CD73, CD90, CD105, and CD166, but they did not express or weakly expressed CD14, CD34, CD45 markers. Furthermore, the expression of CD24 and CD133 was absent or near absent in both isolated cells. Results also discovered overexpression of Annexin A4 (Anxa4), elongation factor 1-delta (EF1-D), FK506 binding protein 9 (FKBP9), cytosolic platelet-activating factor acetylhydrolase type IB subunit beta (PAFAH1B), type II transglutaminase (TG2), and s-formylglutathione hydrolase (FGH) in MSCs isolated from the malignant tissues. Additionally, heat shock protein 70 (Hsp70), as well as keratin, type II cytoskeletal 7 (CK-7), were found to be overexpressed in MSCs derived from the benign ones.

Conclusion: Malignant and benign SGTs probably exhibit a distinct pattern of tissue proteins that are most likely related to the metabolic pathway. However, further studies in a large number of patients are required to determine the applicability of identified proteins as new targets for cancer therapy.

Keywords: Mass Spectrometry, Mesenchymal Stem Cells, Two-Dimensional Polyacrylamide Gel Electrophoresis

Cell Journal(Yakhteh), Vol 24, No 4, April 2022, Pages: 196-203

Citation: **Haghshenas MR, Erfani N, Khansalar S, Khademi B, Ashraf MJ, Razmkhah M, Ghaderi A. Proteomics study of mesenchymal stem cell-like cells obtained from tumor microenvironment of patients with malignant and benign salivary gland tumors. Cell J. 2022; 24(4): 196-203. doi: 10.22074/cellj.2022.7844.**

Introduction

Pleomorphic adenoma (PA) is the most common type of benign parotid gland tumors, characterized by a high recurrence rate following primary surgery. Although classified as a benign tumor, it can display some peculiar behaviours as well as problems in the clinical course due to its tendency to recur and risk of malignant transformation and distant metastases (1).

Mucoepidermoid carcinoma (MEC) is the most frequently diagnosed malignancy in both adults and children. It comprises 34% of malignant salivary gland tumors (SGTs) (2). MECs are with varying potential for aggressive behaviour and are more likely to show neural invasion (3).

The tumor progression and cancer behaviour in different types of cancers, including SGTs, are affected by the components of the tumor microenvironment (TME), particularly mesenchymal stem cells (MSCs) (4, 5). Malignant SGTs are epithelial tumor cells, but they can easily be disseminated to local or distant organs under a process named epithelial-mesenchymal transition (EMT).

MSCs were found to be recruited to salivary gland microenvironment, converted into cancer-associated fibroblasts (CAFs)-like phenotype, and then disband cell-cell connection in SGT cells. The consequences of such conversions and interactions are cancer dissemination (6). There is strong evidence that MSCs play an important role in cancer stem cell survival and can regulate their self-renewal (7, 8). MSC-activated immune responses induce regulatory T cells and regulatory B cells while suppressing proliferation, maturation, and differentiation of T and B lymphocytes (7, 9). In addition to MSCs-based immunomodulation, they

had been described as regulatory players in the metabolic reprogramming of cancer cells (10). It is suggested that MSCs via intracellular/surface proteins or soluble factors contribute to immune suppression and cancer progression.

The proteomic expression of tumor-MSCs is less investigated in comparison to those expressed by tumor cells. Proteomics emerged as a large-scale screening tool for protein discovery. The main methods for proteomics studies are two-dimensional gel electrophoresis (2-DE) and mass spectrometry (MS) (11). MSCs proteomic analysis may provide valuable data that are particularly controlled by MSCs such as proteins involved in immune suppression, cancer metabolism, and cancer development (12, 13).

Therefore, to develop molecular aspects of SGTs carcinogenesis this study aimed to isolate and characterize MSCs from malignant and benign tumor tissues and to identify differentially expressed proteins between these two types of MSCs.

Materials and Methods

Sample collection and MSCs isolation

The study was approved by the local Ethics Committee of Shiraz University of Medical Sciences, Shiraz, Iran (IR.SUMS.REC.1399.675). Written informed consent was obtained from each member before sampling. In this experimental study, MSCs were individually isolated and cultured from tumor tissues derived from patients with PA (n=5) and MEC (n=5) subtypes in a manner named "explants" culture. Briefly, the specimens were washed and minced in very small pieces with a scalpel and distributed into 6-well tissue culture plates and incubated in a 37˚C-5% Co_2 incubator in the presence of Dulbecco's modified Eagle's medium (DMEM), 10% fetal bovine serum (FBS) and 1% penicillin/streptomycin. When the cells reached 60-70% confluency, they were harvested and transferred into a larger culture flask. Crystal violet staining (0.5% crystal violet in methanol) of MSCs isolated from malignant and benign tumor tissues are shown in Figure 1.

Flow cytometry analysis

To verify and compare isolated cells obtained from tumor tissues patients with PA and MEC subtypes, the attached cells (in passages 3 to 4) were harvested by treatment with 1% trypsin-EDTA. After washing, the cells were incubated with CD105, CD24, CD45, CD34 and CD14 antibodies (FITC mouse anti-human), CD44, CD133, and CD166 antibodies (PE mouse anti-human), and CD90 and CD73 antibodies (APC mouse anti-human) at 4˚C for 30 minutes in the dark. The data were collected on BD FACSCalibur flow cytometer and then analyzed by BD CellQuest Pro software package. The respective isotype control antibodies were used in separated tubes as negative controls. The antibodies, the instrument, and the software package were all from BD Biosciences, USA.

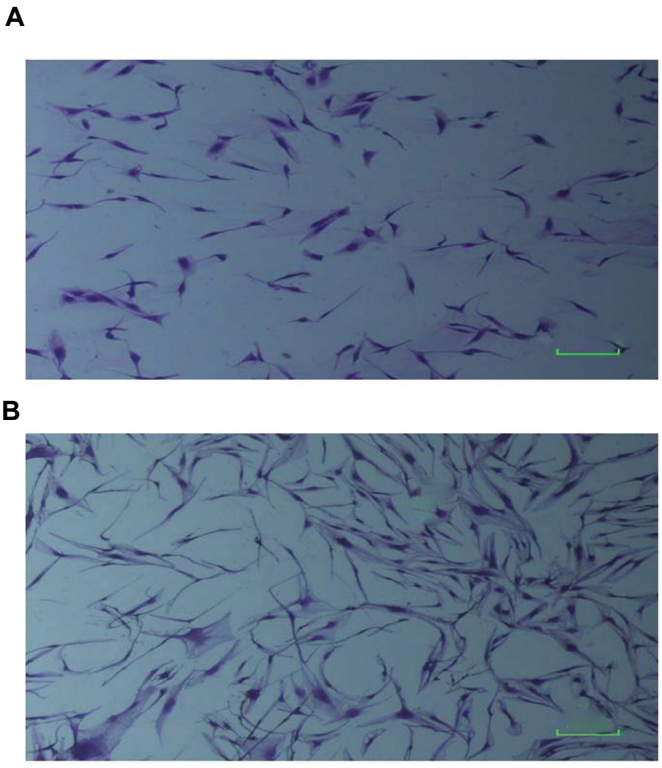

Fig.1: Mesenchymal stem cell (MSC)-like cells isolated from tumor microenvironment of patients with salivary gland tumors. Crystal violet staining of MSC-like cells isolated from **A.** Malignant and **B.** Benign tumor tissues in passage 4. The metric units are 100.00 µm.

Protein extraction, isoelectric focusing, SDS-page electrophoresis, and gel staining

Cell pellets were lysed by a lysis buffer as previously described (12, 13). The protein concentration was calculated by the Bradford assay (14). The first dimension of electrophoresis (or IEF) was done using GE18-cm IPG gel strips (pH=3-10 NL) to separate proteins based on their isoelectric point (pI). 500 µg of each sample was added to rehydration buffer (7 M urea, 2 M thiourea, 2% CHAPS, and 0.002% bromophenol blue), 0.001g of dithiothreitol (DTT), and 0.5 % (1.7 µl) GE immobilized pH gradient (3-10, NL) buffer. The mixture was applied on IPG strips and incubated for 45 minutes at 20˚C. Strips were covered by cover fluid and then actively rehydrated for 16 hours at 50 volt (20ºC). After rehydration, the cover fluid was changed, and strips were focused for 70000 volt-hour at 20ºC. In the second dimension of electrophoresis, proteins were separated based on their molecular weight (MW) by the protean II xi cell system. Before the second dimension, focused strips were equilibrated, reduced, and alkylated in the presence of an equilibration buffer (12, 13). To minimize the variation in analysis, the same parameters were used for each gel, and a control sample was repeatedly run and stained. IPG gel strips were fixed in a fixative solution and coomassie brilliant blue (CBB) G-250 dye solution was used to visualize protein spots on gels.

Gels imaging, spots detection, protein identification, and database analysis

The stained gels were scanned at 300 dpi resolution, and then protein spots were analyzed using the Prodigy SameSpots software package (Nonlinear Dynamics). Differential spots were cut from the gel, and then sent to York University (York, UK) to be identified by Matrix-Assisted Laser Desorption Ionization Tandem Time-of-Flight mass spectrometry (MALDI-TOF-TOF MS). In the present study, MASCOT protein scores ≥62 were considered statistically significant ($P<0.05$). On the other hand, individual ions scores ≥62 indicate identity or extensive homology. PANTHER classification database (http://pantherdb.org), as well as UniProtKB database (https://www.uniprot.org/), were used to analyze the molecular function and biological process of identified proteins.

Statistical analysis

Prodigy SameSpots software package (Version 1.0, Nonlinear Dynamics, UK) automatically calculated normalized volume (% expression), and further statistical analysis was performed by Mann–Whitney U-test and t test (SPSS Inc, Version 11, Chicago IL, USA). $P<0.05$ was considered significant level in all cases.

Results

The clinical and pathological characterization of the patients

Five malignant tumor tissues with MEC tumor types and 5 benign tumor tissues with PA tumor types obtained from patients with SGTs were enrolled in our study. Clinicopathological characterization of each patient with malignant and benign SGTs is shown in Table 1.

Flow cytometric analysis of MSC-like cells

According to the forward (F-) and side (S-) scatter (SC) dot plots, both MSC-like cells isolated from malignant and benign tumor tissues have a similarity in granularity and size (Fig.S1, See Supplementary Online Information at www.celljournal.org). MSCs isolated from malignant and benign tumor tissues strongly expressed the characteristic MSCs markers such as CD44, CD73, CD90, CD105, and CD166, whereas did not express or rarely expressed CD14, CD34, and CD45. The expression of CD24 and CD133 was absent or nearly absent in both isolated cells. Flow cytometric analysis of MSC-like cells is shown in Table 2.

Table 1: Clinicopathological characterization of patients with malignant (MEC) and benign (PA) salivary gland tumors

Cases	Tumor type	Grade/Stage	Tumor location	Age/Gender
M1	MEC	Poorly/III	Parotid	55/Male
M2	MEC	Moderately/I	Parotid	27/Female
M3	MEC	Well/II	Parotid	52/Male
M4	MEC	Poorly/IV	Parotid	57/Male
M5	MEC	Well/IV	Parotid	73/Female
P1	PA	-	Parotid	46/Female
P2	PA	-	Parotid	52/Male
P3	PA	-	Parotid	45/Male
P4	PA	-	Parotid	53/Female
P5	PA	-	Parotid	39/Female

Table 2: Mesenchymal specific markers in MSC-like cells isolated from malignant (MEC) and benign (PA) tumor tissues

MSCs types	CD14	CD34	CD45	CD90	CD73	CD105	CD166	CD44	CD24	CD133
Mucoepidermoid carcinoma (MEC)	1.6 ± 0.27	3.3 ± 0.61	1.4 ± 0.27	92 ± 1.9	94.7 ± 2.7	93.2 ± 4.7	91 ± 2.3	94.2 ± 1.1	1.9 ± 0.33	2.1 ± 0.37
Pleomorphic adenoma (PA)	1.6 ± 0.40	3.5 ± 1.2	2.4 ± 0.57	91.7 ± 0.88	93.5 ± 2.3	97.9 ± 0.48	93 ± 2.4	95.1 ± 097	2.5 ± 0.58	0.84 ± 0.18

Mean ± standard deviation (SD) were calculated using the SPSS program (SPSS Inc, Chicago IL, USA).

Differentially expressed proteins between MSC-like cells isolated from malignant (MEC types) and benign (PA types) tumor tissues

After validation of MSC-like cells with mesenchymal markers, 2-DE and MS analysis were performed. Our results indicated that despite the overall similarity in protein expression pattern, at least 11 different protein spots were differentially, and reproducibility expressed. The location of differential spots on gels were matched to the available proteome map before MS. Of them, 8 spots were identified by a significant score (score ≥62 and P<0.05). The identified proteins were summarized in Table 3. Two spots were identified with scores <62 and one spot did not match the database significantly. Our results indicated that the expression of PAFAH1B, FGH, TG2, FKBP9, Anxa4, and EF1-D significantly elevated among MSC-like cells derived from malignant cases. In comparison, the expression of Hsp70 and CK-7 was significantly higher in MSC-like cells derived from benign cases. The spot details, molecular function, and biological process of identified proteins are presented in Figures 2 and 3, and Table 3.

Table 3: Details of deferential proteins in MSC-like cells derived from malignant and benign tumor tissues

Spot No.	Protein name/Gene name	Accession No.	Calculated pI/ Nominal mass (Mr-KDa)	Score	Matches peptides number/ Sequences number	Coverage %	Molecular function and biological process based on PANTHER classification database and UniProtKB
1	Cytosolic platelet-activating factor acetyl hydrolase type IB subunit beta (PAFAH1*B2)/ PAFAH1B2*	P68402	5.57/25.72	127	2/2	12	Protein modifying enzyme, Ether lipid metabolism, Metabolic pathways
2	S-formylglutathione hydrolase (FGH)/*ESD*	P10768	6.54/31.95	114	1/1	7	Metabolic pathways, Catalytic activity
3	Type II trans glutaminase (TG2)/ *TGM2*	P21980	5.11/78.42	155	3/2	4	Catalytic activity, Cellular process, Metabolic process
4	FK506 binding protein 9 (FKBP9)/ *FKBP9*	O95302	4.91/63.50	348	6/6	10	Calcium ion binding, Protein folding
5	Annexin A4 (Anxa4)/ *ANXA4*	P09525	5.84/36.08	255	4/4	15	NF-kappaB signaling, Epithelial cell differentiation, phospholipase inhibitor activity, Negative regulation of the apoptotic process
6	Keratin, type II cytoskeletal 7 (CK-7)/ *KRT7*	P08729	5.40/51.41	304	5/5	13	Cornification, DNA synthesis
7	Heat shock protein 70 (Hsp70)/ *HSPA9*	P38646	5.87/73.92	442	6/6	11	ATPase activity, Cellular response to unfolded protein
8	Elongation factor 1-delta (EF1-D)/ *EEF1D*	P29692	4.90/31.21	62	1/1	8	Binding, Molecular function regulator, Cellular process, Metabolic process, I-kappaB kinase/NF-kappaB signaling

UniProt accession number. pI; Isoelectric point.

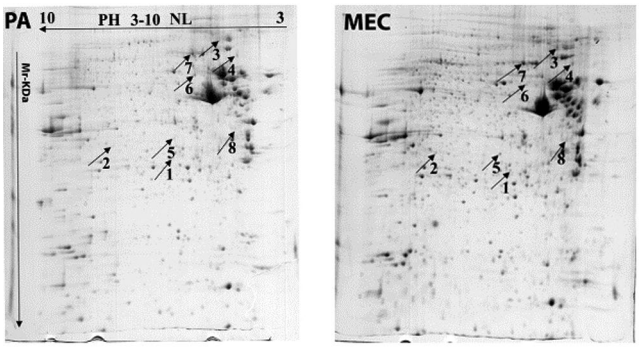

Fig.2: Differential spots on coomassie blue staining gels. Spot numbers are the same as those in Table 3. Left side: Pleomorphic adenoma (PA), Right side: Mucoepidermoid carcinoma (MEC).

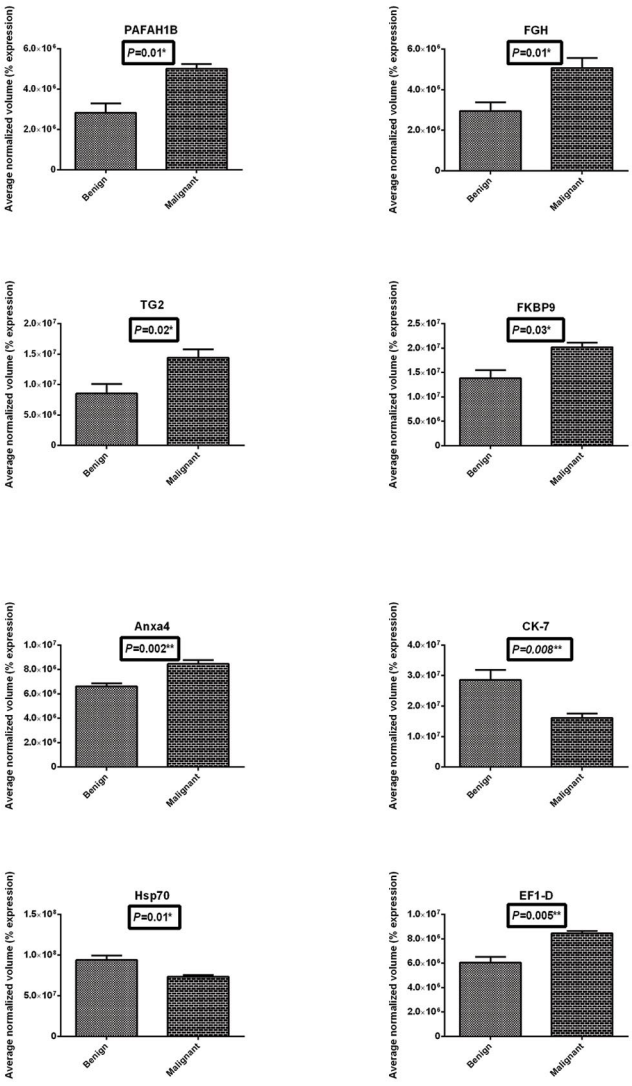

Fig.3: Comparison of average normalized volumes of identified proteins between MSC-like cells isolated from malignant and benign tumor tissues. The expression pattern of PAFAH1B, FGH, TG2, FKBP9, EF1-D, and Anxa4 was found to be significantly elevated in MSC-like cells derived from malignant tissues (MEC tumor type), n=5. The expression of CK-7 and Hsp70 was significantly higher in MSC-like cells derived from benign ones (PA tumor type), n=5. Number represents average normalized volume. Spot numbers are the same as those in Table 3. MEC; Mucoepidermoid carcinoma, PA; Pleomorphic adenoma, *; Difference, and **; Difference are significant at <0.05 and <0.01 levels respectively.

Discussion

In this study, we isolated MSC-like cells from malignant and benign tumor tissues (MEC and PA tumor types), verified them using mesenchymal specific markers, and then investigated the differentially expressed proteins by 2-DE in combination with mass spectrometry. Microscopic images, as well as surface staining of cells derived from both malignant and benign tumor tissues by a panel of fluorochrome antibodies, indicated that morphological features and mesenchymal specific markers of both isolated cells were quite similar to each other and with other known MSCs (12, 13). Since both MSC-like cells were obtained from the same source, parotid tissue, they expressed similar mesenchymal markers (15).

In this regard, both highly expressed CD44, CD73, CD90, CD105, and CD166 markers, and did not express or rarely expressed markers such as CD14, CD34, and CD45. Based on the International Federation of Adipose Therapeutics and Sciences (IFATS) and International Society for Cellular Therapy (ISCT), MSCs characterization are mostly restricted to positive expression of a panel of classical cell surface markers including CD44, CD73 (L-VAP-2), CD90 (Thy-1), and CD105 (Endoglin), and lack of CD14, CD34 and CD45 (leukocyte common antigen) markers (16). CD24 is a receptor that interacts with P-selectin to promote tumor development and metastatic activity (17). CD166 (ALCAM) and CD133 (Prominin-1) could be served as potential cancer stem cell markers (18, 19).

In our study, both benign and malignant MSC-like cells seldom expressed CD24 and CD133, while they were positive for CD166. Furthermore, to determine the molecular pathology behind the malignant and benign tumors, we compared the protein expression pattern between MSC-like cells isolated from malignant tissues (MEC tumor type), and MSC-like cells isolated from benign ones (PA tumor type), and we finally identified differentially expressed proteins. Our results indicated that although MSC-like cells from both tumor tissues expressed similar markers, they exhibited differential expression of proteins. One reason is that MSCs are probably educated by tumor cells and their mediators once they are recruited to the TME (20).

It has been shown that cancer behavior is strongly regulated by the components of the TME through networks of the protein-protein interactions (21). A large number of physiological and pathological processes are strictly controlled by these protein-protein interaction networks, and any changes in the protein expression have a direct influence on cancer behavior and tumor progression (22). Since biological and clinical behaviors of benign and malignant tumors are different, therefore, the protein expression pattern is expected to be dissimilar in these types of cells. In head and neck squamous cell carcinoma, it has been shown that expressed proteins are implicated in various cellular processes including tumor growth, apoptosis, cell death, cell cycle, tumor proliferation,

invasion, migration, metastasis, and response to therapy (23).

Detail characterizations of differentially expressed proteins in cancer patients not only are shedding light on cancer biology, but also are implicated in predicting SGTs aggressiveness, distinguishing malignant SGTs from benign ones, and/or developing new targets for cancer therapy (24, 25). Since benign PA can be misdiagnosed cytologically with ACC or MEC, differentially expressed proteins may serve as complementary markers to discriminate SGTs benign from malignant ones (25).

Database analysis, in our study, indicated that identified proteins were involved in different pathways. Among them, proteins related to metabolic pathways were enriched in proteomic profiles of tumor-MSCs isolated from malignant tumor tissues. Reprogramming of cellular metabolism exhibits an important role in carcinogenesis and metastasis. Cancer cell metabolism may facilitate the deregulated uptake of glucose and essential amino acids as well as the metabolic interactions with TME to sustain cell viability and generate new biomass, situations that are associated with tumor progression (26).

It was recently reported that MSCs, as key regulators of the tumor microenvironment, play an essential role in the metabolic reprogramming of tumor cells in osteosarcoma (10). Consequently, metabolic pathways could be employed as an attractive target for therapeutic policies (27). In our study, the differential expression of proteins was in two forms; proteins overexpressed in MSC-like cells isolated from malignant tissues, and proteins overexpressed in MSC-like cells isolated from benign ones. In this regard, six proteins including PAFAH1B, FGH, TG2, FKBP9, Anxa4, and EF1-D were found to be overexpressed amongst MSC-like cells isolated from malignant tumors. As mentioned, based on the PANTHER classification database and UniProtKB database analysis, the majority of identified proteins in MSC-like cells derived from malignant tissues were found to be involved in metabolic pathways. In this regard, Annexin may be involved in cancer metabolism, at least in part, through phospholipase inhibitor activity.

In breast cancer, PAFAH1B3 has been shown to act as a critical metabolic driver of cancer progression. Overexpression of this enzyme in primary human breast cancer is shown to be related to poor prognosis (28). Thereby, targeting metabolic drivers can be a promising therapeutic strategy in cancer eradiation (29). Another enzyme that was significantly over-expressed in MSC-like cells isolated from malignant tissues was FGH or esterase D (ESD). FGH is mainly implicated in the detoxification of formaldehyde, but little is known regarding its biological function and physiological role. It was reported that this protein might be considered as a predictive marker to determine aggressive lung adenocarcinomas in humans (30).

The other identified protein, TG2, is known as a cancer stem cell survival factor. TG2 also can regulate glucose metabolic reprogramming in a pathway dependent on the nuclear factor (NF)-κB (31). TG2 also is an essential factor in the osteogenesis and chondrogenic differentiation of MSCs (32, 33). Peptidyl-prolylcis-transisomerase (PPIase) families comprise of FK506 binding proteins, cyclophilin, and PIN1. The relation between PPIase families and tumor progression is not clearly defined. However, some evidence showed that FK506 binding proteins and cyclophilin modulate the transformed phenotypes in tumor cells (34). The other PPIase family member, PIN1, plays an essential role in cancer metabolism, cell mobility, and cell proliferation and promotes cancer stem cells (34, 35). EF1D exerts a role in the elongation step of translation and metabolic process and is frequently overexpressed in human tumor cells (36). However, its exact role in the onset and the progression of cancer is not well understood.

In addition to mentioned proteins, AnnexinA4 (Anxa4) was found to be over-expressed in MSC-like cells isolated from malignant tumors. Anxa4 was overexpressed in many types of epithelial cancers including breast, lung, colorectal, gallbladder, gastric, ovarian, renal, prostate, laryngeal, and pancreatic cancers. Anxa4 expression may facilitate the differential diagnosis of major SGTs from thyroid cancer. Anxa4 overexpression may be associated with tumor invasion and cancer development, and may be a potential target for cancer treatment (37).

In contrast to overexpression of the mentioned proteins in MSC-like cells isolated from malignant tumor tissues, CK-7 and Hsp70 were observed to be overexpressed in MSC-like cells isolated from benign tumor tissues. CK-7 can block interferon-dependent interphase and stimulates DNA synthesis in cells. IHC analysis showed that CK-7+/CK-20-pattern is typical in both malignant and benign SGTs (38). The other over-expressed protein, HSPs, is enhanced in response to biological stress. HSPs contribute to cancer development and metastasis and may serve as biomarkers for cancer diagnosis and therapy (39). It was suggested that overexpression of Hsp70 in MSCs was associated with MSCs survival (40).

The exact roles of identified proteins in SGTs and MSCs isolated from SGTs have not been determined to date. The findings may support that MSCs can trigger metabolic dysregulation and tumor growth in malignant SGTs as reported in osteosarcoma (10). However, the current study is an explorative phase of proteomics studies that need to be verified and validated by antibody-based methods such as western blot in larger cohorts of individuals to determine the exact roles of MSCs-derived proteins in cancer progression and cancer therapy.

Conclusion

Our findings show that the cells isolated from malignant and benign tumor tissues similarly express the characteristic MSCs markers. However, malignant and benign SGTs probably exhibit a distinct pattern of tissue proteins that are most likely related to the

metabolic pathway. The identified proteins may exert an important role in the unfavorable behavior of SGTs and more especially in those with malignant type. Our results suggest that MSCs or their components may consider as desirable therapeutic targets in SGTs.

Acknowledgments

This study was supported by a grant from Shiraz University of Medical Sciences [Grant number 99-01-16-22976 (20593)] as well as from Shiraz Institute for Cancer Research (ICR-100-503). The authors wish to thank Dr. Seyed Mohammad Jafari at the Research Consultation Center (RCC) of Shiraz University of Medical Sciences for editing this manuscript. There was no conflict of interest among the authors.

Authors' Contributions

A.Gh., M.R., N.E.; Contributed to the conception and study design. M.R.H.; Contributed to lab experiments, flow cytometric and proteomics analysis, statistical analysis, and data interpretation. S.Kh.; Contributed to proteomics analysis. B.Kh., M.J.A.; Contributed to patient's diagnosis and sample collection. A.Gh., M.R.; Supervised the project. M.R.H.; Drafted the manuscript, and then it was revised by M.R., N.E., S.Kh., B.Kh., M.J.A., A.Gh. All authors read and approved the final manuscript.

References

1. Dulguerov P, Todic J, Pusztaszeri M, Alotaibi NH. Why do parotid pleomorphic adenomas recur? A systematic review of pathological and surgical variables. Front Surg. 2017; 4: 26.
2. Adelstein DJ, Koyfman SA, El-Naggar AK, Hanna EY. Biology and management of salivary gland cancers. Semin Radiat Oncol. 2012; 22(3): 245-253.
3. Lanzel E, Robinson RA, Zimmerman MB, Pourian A, Hellstein JW. The use of immunohistochemistry in detection of perineural invasion in mucoepidermoid carcinoma. Oral Surg Oral Med Oral Pathol Oral Radiol. 2016; 121(6): 636-642.
4. Alame M, Cornillot E, Cacheux V, Tosato G, Four M, De Oliveira L, et al. The molecular landscape and microenvironment of salivary duct carcinoma reveal new therapeutic opportunities. Theranostics. 2020; 10(10): 4383-4394.
5. Baghban R, Roshangar L, Jahanban-Esfahlan R, Seidi K, Ebrahimi-Kalan A, Jaymand M, et al. Tumor microenvironment complexity and therapeutic implications at a glance. Cell Commun Signal. 2020; 18(1): 59.
6. Ma H, Zhang M, Qin J. Probing the role of mesenchymal stem cells in salivary gland cancer on biomimetic microdevices. Integr Biol (Camb). 2012; 4(5): 522-530.
7. Ghaderi A, Abtahi S. Mesenchymal stem cells: miraculous healers or dormant killers? Stem Cell Rev Rep. 2018; 14(5): 722-733.
8. Norozi F, Ahmadzadeh A, Shahrabi S, Vosoughi T, Saki N. Mesenchymal stem cells as a double-edged sword in suppression or progression of solid tumor cells. Tumour Biol. 2016; 37(9): 11679-11689.
9. Razmkhah M, Abtahi S, Ghaderi A. Mesenchymal stem cells, immune cells and tumor cells crosstalk: a sinister triangle in the tumor microenvironment. Curr Stem Cell Res Ther. 2019; 14(1): 43-51.
10. Bonuccelli G, Avnet S, Grisendi G, Salerno M, Granchi D, Dominici M, et al. Role of mesenchymal stem cells in osteosarcoma and metabolic reprogramming of tumor cells. Oncotarget. 2014; 5(17): 7575-7588.
11. Alharbi RA. Proteomics approach and techniques in identification of reliable biomarkers for diseases. Saudi J Biol Sci. 2020; 27(3): 968-974.
12. Saffarian A, Tarokh A, Reza Haghshenas M, Taghipour M, Chenari N, Ghaderi A, et al. Proteomics study of mesenchymal stem cell-like cells isolated from cerebrospinal fluid of patients with meningioma. Curr Proteomics. 2019; 16(4): 282-288.
13. Taghipour M, Omidvar A, Razmkhah M, Ghaderi A, Mojtahedi Z. Comparative proteomic analysis of tumor mesenchymal-like stem cells derived from high grade versus low grade gliomas. Cell J. 2017; 19(2): 250-258.
14. Bradford MM. A rapid and sensitive method for the quantitation of microgram quantities of protein utilizing the principle of protein-dye binding. Anal Biochem. 1976; 72: 248-254.
15. Elahi KC, Klein G, Avci-Adali M, Sievert KD, MacNeil S, Aicher WK. Human mesenchymal stromal cells from different sources diverge in their expression of cell surface proteins and display distinct differentiation patterns. Stem Cells Int. 2016; 2016: 5646384.
16. Bourin P, Bunnell BA, Casteilla L, Dominici M, Katz AJ, March KL, et al. Stromal cells from the adipose tissue-derived stromal vascular fraction and culture expanded adipose tissue-derived stromal/stem cells: a joint statement of the international federation for adipose therapeutics and science (IFATS) and the international society for cellular therapy (ISCT). Cytotherapy. 2013; 15(6): 641-648.
17. Fang X, Zheng P, Tang J, Liu Y. CD24: from A to Z. Cell Mol Immunol. 2010; 7(2): 100-103.
18. Chitteti BR, Kobayashi M, Cheng Y, Zhang H, Poteat BA, Broxmeyer HE, et al. CD166 regulates human and murine hematopoietic stem cells and the hematopoietic niche. Blood. 2014; 124(4): 519-529.
19. Liou GY. CD133 as a regulator of cancer metastasis through the cancer stem cells. Int J Biochem Cell Biol. 2019; 106: 1-7.
20. Sai B, Dai Y, Fan S, Wang F, Wang L, Li Z, et al. Cancer-educated mesenchymal stem cells promote the survival of cancer cells at primary and distant metastatic sites via the expansion of bone marrow-derived-PMN-MDSCs. Cell Death Dis. 2019; 10(12): 941.
21. Korkaya H, Liu S, Wicha MS. Breast cancer stem cells, cytokine networks, and the tumor microenvironment. J Clin Invest. 2011; 121(10): 3804-3809.
22. Boja ES, Rodriguez H. Proteogenomic convergence for understanding cancer pathways and networks. Clin Proteomics. 2014; 11(1): 22.
23. Yarbrough WG, Slebos RJ, Liebler D. Proteomics: clinical applications for head and neck squamous cell carcinoma. Head Neck. 2006; 28(6): 549-558.
24. Donadio E, Giusti L, Seccia V, Ciregia F, da Valle Y, Dallan I, et al. New insight into benign tumours of major salivary glands by proteomic approach. PLoS One. 2013; 8(8): e71874.
25. Seccia V, Navari E, Donadio E, Boldrini C, Ciregia F, Ronci M, et al. Proteomic investigation of malignant major salivary gland tumors. Head Neck Pathol. 2020; 14(2): 362-373.
26. Pavlova NN, Thompson CB. The emerging hallmarks of cancer metabolism. Cell Metab. 2016; 23(1): 27-47.
27. Ngoi NYL, Eu JQ, Hirpara J, Wang L, Lim JSJ, Lee SC, Lim YC, et al. Targeting cell metabolism as cancer therapy. Antioxid Redox Signal. 2020; 32(5): 285-308.
28. Mulvihill MM, Benjamin DI, Ji X, Le Scolan E, Louie SM, Shieh A, et al. Metabolic profiling reveals PAFAH1B3 as a critical driver of breast cancer pathogenicity. Chem Biol. 2014; 21(7): 831-840.
29. DeBerardinis RJ, Chandel NS. Fundamentals of cancer metabolism. Sci Adv. 2016; 2(5): e1600200.
30. Wiedl T, Arni S, Roschitzki B, Grossmann J, Collaud S, Soltermann A, et al. Activity-based proteomics: identification of ABHD11 and ESD activities as potential biomarkers for human lung adenocarcinoma. J Proteomics. 2011; 74(10): 1884-1894.
31. Kumar S, Donti TR, Agnihotri N, Mehta K. Transglutaminase 2 reprogramming of glucose metabolism in mammary epithelial cells via activation of inflammatory signaling pathways. Int J Cancer. 2014; 134(12): 2798-2807.
32. Li B, Tian XB, Hu RY, Xu FB, Zhao JM. Mechanism of BMP and TG2 in mesenchymal stem cell osteogenesis. Eur Rev Med

Pharmacol Sci. 2015; 19(22): 4214-4219.
33. Niger C, Beazley KE, Nurminskaya M. Induction of chondrogenic differentiation in mesenchymal stem cells by TGF-beta cross-linked to collagen-PLLA [poly (L-lactic acid)] scaffold by transglutaminase 2. Biotechnol Lett. 2013; 35(12): 2193-2199.
34. Zhou XZ, Lu KP. The isomerase PIN1 controls numerous cancer-driving pathways and is a unique drug target. Nat Rev Cancer. 2016; 16(7): 463-478.
35. Lu Z, Hunter T. Prolyl isomerase Pin1 in cancer. Cell Res. 2014; 24(9): 1033-1049.
36. Hassan MK, Kumar D, Naik M, Dixit M. The expression profile and prognostic significance of eukaryotic translation elongation factors in different cancers. PLoS One. 2018; 13(1): e0191377.
37. Wei B, Guo C, Liu S, Sun MZ. Annexin A4 and cancer. Clin Chim Acta. 2015; 447: 72-78.
38. Meer S, Altini M. CK7+/CK20- immunoexpression profile is typical of salivary gland neoplasia. Histopathology. 2007; 51(1): 26-32.
39. Elmallah MIY, Cordonnier M, Vautrot V, Chanteloup G, Garrido C, Gobbo J. Membrane-anchored heat-shock protein 70 (Hsp70) in cancer. Cancer Lett. 2020; 469: 134-141.
40. Chang W, Song BW, Lim S, Song H, Shim CY, Cha MJ, et al. Mesenchymal stem cells pretreated with delivered Hph-1-Hsp70 protein are protected from hypoxia-mediated cell death and rescue heart functions from myocardial injury. Stem Cells. 2009; 27(9): 2283-2292.

Original Article

Inhibition of MAT2A-Related Methionine Metabolism Enhances The Efficacy of Cisplatin on Cisplatin-Resistant Cells in Lung Cancer

Xiaoya Zhao, M.D.[1, 2#], Lude Wang, M.D.[1, 2#], Haiping Lin, M.D.[3], Jing Wang, B.Sc.[1, 2], Jianfei Fu, Ph.D.[4], Dan Zhu, Ph.D.[5*], Wenxia Xu, Ph.D.[1, 2*]

1. Central Laboratory, Affiliated Jinhua Hospital, Zhejiang University School of Medicine, Jinhua, Zhejiang Province, China
2. Precision Diagnosis and Treatment Center of Jinhua City, Jinhua, Zhejiang Province, China
3. Department of General Surgery, Affiliated Jinhua Hospital, Zhejiang University School of Medicine, Jinhua, Zhejiang Province, China
4. Department of Medical Oncology, Affiliated Jinhua Hospital, Zhejiang University School of Medicine, Jinhua, Zhejiang Province, China
5. Department of Respiratory, Affiliated Jinhua Hospital, Zhejiang University School of Medicine, Jinhua, Zhejiang Province, China

#These authors contributed equally to this work.

Corresponding Addresses: Department of Respiratory, Affiliated Jinhua Hospital, Zhejiang University School of Medicine, Jinhua, Zhejiang Province, China
Central Laboratory, Affiliated Jinhua Hospital, Zhejiang University School of Medicine, Jinhua, Zhejiang Province, China
Emails: xuwenxia@zju.edu.cn; zhudan4252@sina.com

Received: 23/December/2020, Accepted: 10/May/2021

Abstract

Objective: Tumor drug resistance is a vital obstacle to chemotherapy in lung cancer. Methionine adenosyltransferase 2A has been considered as a potential target for lung cancer treatment because targeting it can disrupt the tumorigenicity of lung tumor-initiating cells. In this study, we primarily observed the role of methionine metabolism in cisplatin-resistant lung cancer cells and the functional mechanism of MAT2A related to cisplatin resistance.

Materials and Methods: In this experimental study, we assessed the half maximal inhibitory concentration (IC_{50}) of cisplatin in different cell lines and cell viability via Cell Counting Kit-8. Western blotting and quantitative real-time polymerase chain reaction (qRT-PCR) was used to determine the expression of relative proteins and genes. Crystal violet staining was used to investigate cell proliferation. Additionally, we explored the transcriptional changes in lung cancer cells via RNA-seq.

Results: We found H460/DDP and PC-9 cells were more resistant to cisplatin than H460, and MAT2A was overexpressed in cisplatin-resistant cells. Interestingly, methionine deficiency enhanced the inhibitory effect of cisplatin on cell activity and the pro-apoptotic effect. Targeting MAT2A not only restrained cell viability and proliferation, but also contributed to sensitivity of H460/DDP to cisplatin. Furthermore, 4283 up-regulated and 5841 down-regulated genes were detected in H460/DDP compared with H460, and 71 signal pathways were significantly enriched. After treating H460/DDP cells with PF9366, 326 genes were up-regulated, 1093 genes were down-regulated, and 13 signaling pathways were significantly enriched. In TNF signaling pathway, CAS7 and CAS8 were decreased in H460/DDP cells, which increased by PF9366 treatment. Finally, the global histone methylation (H3K4me3, H3K9me2, H3K27me3, H3K36me3) was reduced under methionine deficiency conditions, while H3K9me2 and H3K36me3 were decreased specially via PF9366.

Conclusion: Methionine deficiency or MAT2A inhibition may modulate genes expression associated with apoptosis, DNA repair and TNF signaling pathways by regulating histone methylation, thus promoting the sensitivity of lung cancer cells to cisplatin.

Keywords: Cisplatin Resistance, Lung Cancer, Methionine Adenosyltransferase 2A

Cell Journal(Yakhteh), Vol 24, No 4, April 2022, Pages: 204-211

Citation: **Zhao X, Wang L, Lin H, Wang J, Fu J, Zhu D, Xu W. Inhibition of MAT2A-related methionine metabolism enhances the efficacy of cisplatin on cisplatin-resistant cells in lung cancer. Cell J. 2022; 24(4): 204-211. doi: 10.22074/cellj.2022.7907.**

Introduction

Lung cancer is the first malignant tumor with morbidity and mortality in the world (1). The treatment of lung cancer includes surgery, radiotherapy and chemotherapy, as well as targeted therapy. Although targeted therapy is a huge advancement in the field of lung cancer treatment, due to the low gene mutation rate and insufficient understanding of molecular typing of lung cancer, the application range of targeted therapy is limited. Therefore, for most patients with lung cancer, chemotherapy is still the preferred strategy for oncology treatment (2). Platinum-based drugs, such as cisplatin, are commonly used in lung cancer chemotherapy regimens. Cisplatin triggers apoptosis by inducing double-strand break damage mainly through DNA cross-linking (3). Although the use of cisplatin for clinical treatment has been a remarkable success, the drug resistance of tumor cells also hinders the effects of cisplatin, leading to chemotherapy failure (4). The study of drug resistance will remain a continuous and prolonged process.

Tumors are often accompanied by metabolic abnormalities in the process of development, including glucose metabolism, amino acid metabolism, lipid metabolism and other processes (5). The amino acids in the human body are divided into two major categories: essential amino acids and non-essential amino acids. The demand for amino acids in tumor cells is altered, and the demand for non-essential amino acids such as glutamine and serine are much higher than that of normal cells (6,

7). Methionine, an essential amino acid, is necessary for maintaining the demands of cell growth (8) and protein translation (9). Abnormal methionine metabolism has been observed in many tumors such as glioma and lung cancer (10, 11). Methionine adenosyltransferase 2A (MAT2A), a critical enzyme in cell life activity, can catalyze the integration of methionine with adenosine triphosphate (ATP) to methylate bio-macromolecules such as DNA, RNA, proteins and lipids via supplying the biosynthesis of S-adenosylmethionine (SAM), the bio-methylation donor. The methylation of histones can regulate chromatin conformation and transcription in response to changes in environment or physiology (12, 13). H3K4 mono-, di-, or tri-methylation (H3K4me1/2/3) and H3K36me3 are activating marks, promoting gene transcription (14). On the contrary, H3K9 and H3K27 methylation (H3K9me2/3 and H3K27me2/3) are commonly related to gene silencing (14, 15).

MAT2A is highly expressed in various tumors such as liver cancer, gastric cancer, kidney cancer and colon cancer (16-19). Studies have reported that the maintenance of lung cancer stem cells depends on methionine metabolism mainly through increasing MAT2A expression, and targeting MAT2A can impede the initiation of lung cancer cells (20). Therefore, MAT2A is considered to be a potential target for lung cancer treatment. However, the role MAT2A plays in platinum-resistant lung cancer is still unclear.

In this study, we elucidated the regulatory mechanism of methionine availability (methionine deficiency or MAT2A inhibition) in reducing the tolerance of cisplatin-resistant lung cancer cells to cisplatin. Therefore, MAT2A may serve as a new target for targeted interventions in platinum-resistant lung cancer, providing a scientific basis for the development of new strategies to overcome lung cancer resistance.

Materials and Methods

Reagents

This experimental study complies with the requirements of the Regulations on the Ethical Review of Biomedical Research Involving Humans issued by the National Health and Family Planning Commission and the Helsinki Declaration issued by the Joint Congress of the World Medical Associations. The ID number of the Ethical Committee is 2020-205-001. RPMI-1640 medium (31800-105) was purchased from Gibco (Grand Island, New York, USA), and fetal bovine serum (11011-8611) was purchased from Every Green (Hangzhou, China). Trypsin (GNM25200) and penicillin-streptomycin solution (GNM15140) were obtained from Genome (Hangzhou, Zhejiang, China), RPMI-1640 w/o Amino acids and Sodium Phosphate (powder) were bought from US Biological (Salem, MA, USA), arginine, methionine and the other 18 amino acids included in the RPMI-1640 medium, as well as dimethyl sulfoxide (D2650) were bought from Sigma (Louis, MO, USA). TRIzol (15596026) was purchased from Ambion (Carlsbad CA, USA) and Cisplatin and PF9366 were obtained from MedChem Express (Shanghai, China). Radio-immunoprecipitation assay lysis buffer (FD009), BCA Protein Assay Kit (FD2001) as well as enhanced chemiluminescence kit (FD800) were purchased from Fdbio Science (Hangzhou, Zhejiang, China). Rabbit Cleaved PARP (#5625T), rabbit anti-H3 (#4499), rabbit anti-H3K4 me3 (#9751), anti-H3K9 me2 (#4658), anti-H3K27 me3 (#9733) and anti-H3K36 me3 (#4909) were purchased from Cell Signaling Technology (Danvers, MA, USA). Rabbit anti-Tubulin (AF0001) (AA128) was obtained from Beyotime Biotechnology (Shanghai, China) and rabbit anti-MAT2a (ab154343) from Abcam (Cambridge, UK).

Preparation of medium with various concentrations of methionine

Methionine-free RPMI-1640 medium was produced by dissolving RPMI-1640 w/o Amino acids, Sodium Phosphate (powder), sodium bicarbonate, and 19 types of amino acids (excluding methionine), in double-distilled water, which was termed as 0XMet, similar to our previous study (21). We defined the methionine content in the RPMI-1640 complete medium (15 μg/mL) as 1XMet. The 100X Met (1,500 μg/mL) solution was prepared in advance, and subsequently added to methionine-free RPMI-1640 medium to generate 1/8 X Met (1.875 μg/mL), 1/4 X Met (3.75 μg/mL), 1/2 X Met (7.5 μg/mL) and 1 X Met (15 μg/mL), which were used in the following experiments.

Cell culture

We purchased human lung cancer H460 and PC-9 cell lines from the Type Culture Collection of the Chinese Academy of Sciences (Shanghai, China). Cells were cultured in RPMI-1640 medium containing 10% newborn bovine serum (NBS), 100 U/ml penicillin, and 100 μg/ml streptomycin (Thermo Scientific, MA, USA). A humidified incubator with 5% CO_2 was employed to incubate cells and the temperature was set to 37℃. The cisplatin-resistant cell line H460/DDP was generated by persistently subjecting the parental cell line H460 to gradient exposure of cisplatin for about 10 months, through increasing cisplatin concentration from 0.1 μg/ml until the cells acquired resistance to 1 μg/ml. Furthermore, the PC-9 cell line is naturally resistant to cisplatin compared with H460.

Cytotoxicity assay

We plated 8×10^3 cells per well onto 96-well plates and treated cells with various concentrations of drugs for about 24 hours. Then, we analyzed the cell viability through Cell Counting Kit-8 (Beyotime Biotechnology) guided by the manufacturer's instructions. The cellular viability was indicated as mean ± SD from at least three independent experiments.

Western blotting analysis

Cells were lysed in whole-cell lysate buffer [50 mM Tris (pH=7.4), 150 mM NaCl, 1% NP-40] containing 1% protease inhibitor cocktail (100×, MCE, Shanghai, China). Lysates containing 30 μg protein were loaded into 10% or 15% sodium dodecyl sulfate-polyacrylamide gels for electrophoresis (SDS-PAGE) and the separated proteins were transferred to poly vinylidene fluoride (PVDF) membranes (Pall, NY, USA). After blocking with 5% fat-free milk for 1 hour in Tris-buffered saline (TBS), the membranes were incubated with the primary antibody overnight at 4˚C and then with the peroxidase labelled secondary antibody for 1 hour on the next day. Proteins were visualized using an enhanced chemiluminescence kit exposed to immunoblotting membranes, developing and fixing solutions and x-ray films and then quantified with Image J, version 1.52 (NIH, Bethesda, MD, USA).

Quantitative real-time polymerase chain reaction

Trizol reagent was employed to extract total RNA according to the manufacturer's instructions. The concentration and purity of extracted RNA were determined by absorbance assay at 260, 230, and 280 nm wavelengths as well as electrophoresis patterns. Reverse transcription was performed with 1μg of total RNA and Quantscript RT kit (Takara, Osaka, Japan). The mRNA expression level was determined by quantitative real-time polymerase chain reaction (PCR) by Roche lightCycler® 480II qPCR system (Roche, Basel, Switzerland). *GAPDH* was used as an internal control of RNA integrity. The following primers were used:

MAT2A (>NM_005911.6)-

F: 5′-ATGAACGGACAGCTCAACGG-3′
R: 5′-CCAGCAAGAAGGATCATTCCAG-3′

GAPDH (>NM_001256799.3)-

F: 5′-GGAGTCAACGGATTTG GT-3′
R: 5′-GTGATGGGATTTCCATTGAT-3′

The gene expression was calculated by $2^{-\Delta\Delta CT}$. The calculation process is as follows, ΔCT (test)=CT (target, test)-CT (ref, test), ΔCT (calibrator)=CT (target, calibrator)-CT (ref, calibrator), ΔΔCT (calibrator)=ΔCT (test)-ΔCT (calibrator), $2^{-\Delta\Delta CT}$=gene expression.

Crystal violet staining experiment

The density of H460/DDP cells in the logarithmic growth phase was adjusted to 1×10^5 cells per well, the suspension was mixed well and 1 mL was added per well and the cells were incubated in a 24-well plate for 24 hours. The cells were treated with 10 μM of PF9366 and a control group was also established. The original culture solution (control group and PF9366 group) in both wells was discarded every 24 hours, washed with PBS, fixed with a formaldehyde solution for 30 minutes, and then crystal violet staining solution was added for 15 minutes. After the dyeing was finished, the excess crystal violet dye was washed away with phosphate buffer solution (PBS, Beyotime, China) and dried naturally.

RNA-sequencing

TRIzol was used to isolate the total RNA from three independent samples of H460/DDP and H460 cells either without or with 10 μM PF9366 for 24 hours. Illumina TruSeq RNA sample preparation kit (RS-122-2001) and Illumina high-seq 2000 with a read length of 50 bp with pair ends were used to produce and sequence RNA-seq libraries. We mapped RNA-seq reads to the human genome (hg19) through TopHat (22). Next, we just analyzed those reads mapped to unique genomic locations and with <5% mismatches. FPKM (23) was used to test gene transcripts, and DEGSeq (24) was employed to identify genes expressed differentially. The differentially expressed genes were counted and annotated with NCBI, Uniprot, GO and KEGG databases to obtain detailed description information.

Statistical analysis

Data are shown as the mean ± standard deviation. The parametric unpaired Student's t test was used to calculate the statistical significance of the differences between the cell lines by Graph Pad Prism 6.02 for Mac (San Diego, CA, USA). $P<0.05$ indicates a significant difference.

Results

The deficiency of methionine promotes lung cancer cells sensitive to cisplatin

We have established the cisplatin-resistant lung cancer cell (H460/DDP) by the concentration gradient method, as published previously, and conducted relevant research (25). Here, we first reconfirmed the drug resistance of H460/DDP by CCK-8 cytotoxicity assay. The half maximal inhibitory concentration (IC_{50}) value of cisplatin in the parental cell H460 was 0.4384 μg/mL, while the IC_{50} value of the drug-resistant cell H460/DDP was 3.915 μg/mL, and the drug resistance index was 8.93, meanwhile, the IC_{50} value of cisplatin in PC-9 cells was also detected to be 1.755 μg/mL (Fig.1A). Evidence has shown that depleting dietary methionine could lead cisplatin-resistant xenograft tumors to become sensitive to cytotoxic agents (26). To explore the impact of methionine on sensitivity to cisplatin in lung cancer cells, we detected the viability of H460 with the treatment of different concentrations of cisplatin under the medium with or without methionine and H460/DDP with cisplatin under 1 X Met, 1/2 X Met, 1/8 X Met and 0 X Met. We found H460 was more vulnerable to cisplatin under the methionine-deprived medium and the sensitivity of H460/DDP to cisplatin was enhanced under methionine deficiency (Fig.1B, C). When explored further, it was found that the Cleaved-PARP was up-regulated under the treatment of cisplatin accompanied with methionine deficiency in H460, H460/DDP and PC-8 cells (Fig.1D-F), while the Cleaved-PARP was not detected when exposed to methionine-deficient medium only (Fig.1E, F). These results confirm that depleting the methionine could induce sensitivity to cytotoxic agents and apoptosis in cisplatin-resistant lung cancer cells such as H460/DDP and PC-9.

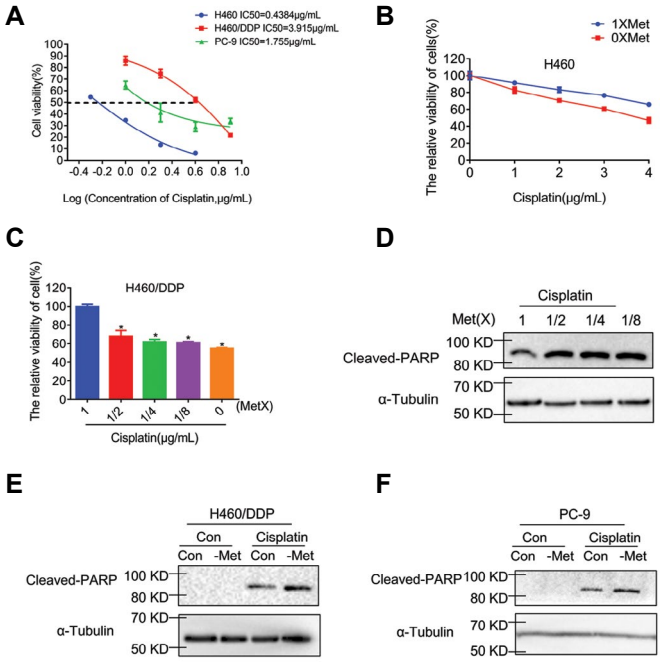

Fig.1: The deficiency of methionine promotes lung cancer cell sensitivity to cisplatin. **A.** The viability of H460, H460/DDP and PC-9 cells with the treatment of various concentrations of cisplatin for 24 hours analyzed by CCK-8 assay. **B.** The activity of H460 cells with different concentrations of cisplatin with or without methionine for 24 hours detected by CCK-8 assay. **C.** The activity of H460/DDP cells with 5 μg/mL cisplatin under various concentrations of methionine for 24 hours analyzed by CCK-8 assay. Error bars show SD (n=3). **D.** Western blotting of Cleaved-PARP in H460 cells with 1 μg/mL cisplatin under different concentrations of methionine. The concentrations of 1 X Met, 1/2 X Met, 1/4 X Met and 1/8 X Met are 15 μg/mL, 7.5 μg/mL, 3.75 μg/mL and 1.875 μg/mL, respectively. The Cleaved-PARP levels were calculated against α-tubulin. **E,** and **F.** Western blotting of *Cleaved-PARP* in H460/DDP cells treated with 5 μg/mL cisplatin and PC-9 cells treated with 2 μg/mL cisplatin cultured in complete medium or medium without methionine. The Cleaved-PARP levels were quantified against α-tubulin. *; P<0.05.

Targeting MAT2A suppresses proliferation and induces apoptosis of cisplatin-resistant lung cancer cells

Methionine adenosyltransferase 2A (MAT2A), an essential enzyme in catalyzing methionine cycle, was located to influence aberrant cell growth and apoptosis via SAM regulation (Fig.2A) and deregulated in several cancer types (27). We found the expression of MAT2A was upregulated in H460/DDP and PC-9 cells compared to H460 (Fig.2B, C). Next, we treated cells with PF-9366, an inhibitor of MAT2A (28). Results showed that the viability of H460/DDP and PC-9 was reduced by PF9366 treatment, which has a positive relationship to the dose (Fig.2D). The proliferation of H460/DDP was significantly inhibited by continuous culture with 10 μM PF9366 (Fig.2E, F). Cleaved-PARP, an apoptosis marker was increased under the joint treatment of cisplatin and PF9366 against to that with cisplatin alone (Fig.2G). These experimental results indicate that MAT2A plays a vital role in the resistance of lung cancer to cisplatin and targeting MAT2A inhibits proliferation and promotes apoptosis of cisplatin-resistant lung cancer cells.

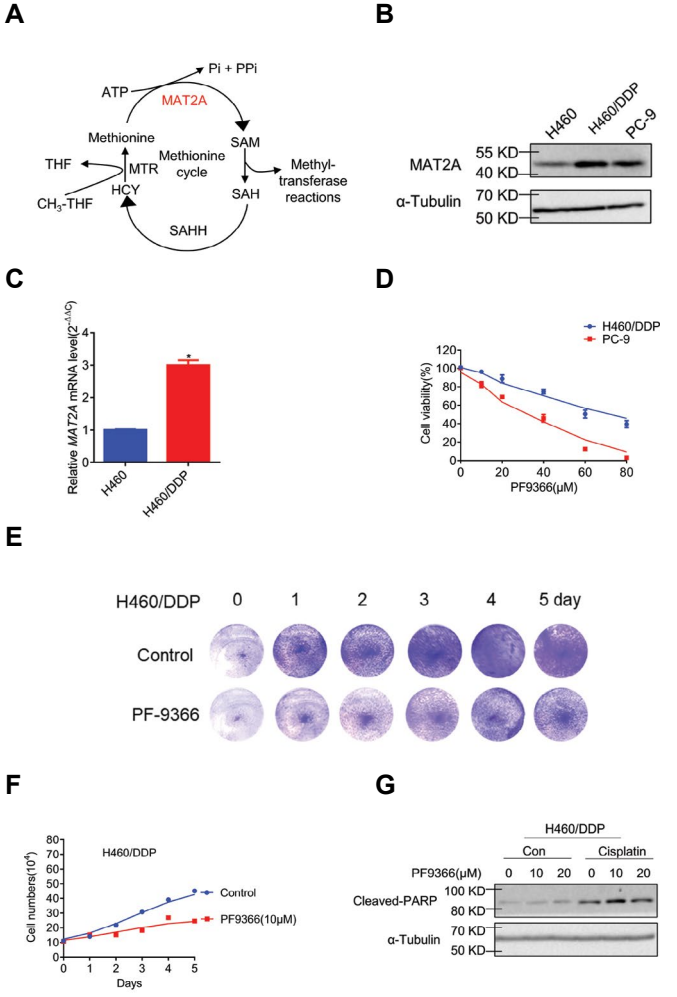

Fig.2: Targeting *MAT2A* inhibits proliferation and enhances sensitivity to cisplatin in lung cancer cells. **A.** The methionine cycle. S-adenosylmethionine synthase, also known as methionine adenosyltransferases (MAT), converts methionine into S-adenosylmethionine (SAM) depending on ATP availability. Subsequently, SAM-dependent methyltransferases transfer the methyl from SAM through the reaction of methylation, producing S-adenosylhomocysteine (SAH), which is then converted into homocysteine (HCY) by S-adenosylhomocysteine hydrolase (SAHH). Methionine synthase (MTR) converts homocysteine back into methionine with a methyl donation from methyl-tetrahydrofolate (CH_3-THF). **B.** Western blotting of *MAT2A* in H460, H460/DDP and PC-9 cells. The *MAT2A* levels were calculated against α-tubulin. **C.** RT-qPCR determined the expression of *MAT2A* mRNA in H460 and H460/DDP cells as indicated. Error bars represent SD (n=3). **D.** The cell viability of H460/DDP and PC-9 cells with different concentrations of PF9366 (0 μM, 10 μM, 20 μM, 40 μM, 60 μM and 80 μM) for 24 hours was analyzed via CCK-8. Error bars show SD (n=3). **E, F.** The proliferation of H460/DDP cells treated with 10 μM PF9366 is shown by crystal violet staining. **G.** Western blotting of *Cleaved-PARP* in H460/DDP cells with 5 μg/mL cisplatin treated with PF9366 (0 μM,10 μM and 20 μM) for 24 hours. The *Cleaved-PARP* levels were quantified against α-tubulin. *; P<0.05.

The transcriptional changes in lung cancer cells after inhibiting MAT2A

Here, we performed RNA-seq of H460 and H460/DDP to gain insight into the mechanism contributing to H460/DDP resistance to cisplatin. Comparative transcriptional expression profiling shown in the heat map (Fig.3A) revealed that there were 10124 gene expression changes in H460/DDP cells compared with H460, involving 4283 up-regulated genes including MAT2A (P=6.61e-08, log2 FC=1.96) and 5841

down-regulated genes including CASP8, CASP7, CASP3, CASP9, CASP2 and CASP10 (Fig.3B, Table S1, See Supplementary Online Information at www.celljournal.org). Seventy one signaling pathways involved in these differential genes were enriched by Kyoto Encyclopedia of Genes and Genomes (KEGG) analysis (Fig.3C, Table S2, See Supplementary Online Information at www.celljournal.org), including TNF signaling pathway and Nucleotide Excision Repair pathways, which was motivated. In order to understand the mechanistic functions of increased MAT2A in cisplatin-resistant cells, we quantified differential genes between H460/DDP and H460/DDP treated with PF9366. We observed 326 up-regulated genes and 1093 down-regulated genes compared with H460/DDP cells (Fig.3D, E). Furthermore, KEGG analysis revealed that 13 signaling pathways were significantly enriched (Fig.3F, Table S3, See Supplementary Online Information at www.celljournal.org). The above 71 signal pathways and 13 signal pathways were analyzed, then 6 common signaling pathways were found, namely, cell adhesion molecules, Fanconi anemia pathway, Ether lipid metabolism, Endocytosis, Endocrine resistance, and TNF signaling pathway (Fig.3G, H). Among them, TNF signaling pathway attracted our attention. The expression levels of major apoptosis genes CASP7 and CASP8 in TNF signaling pathway are significantly downregulated in H460/DDP cells. When treated with PF9366, the expression levels of CASP7 and CASP8 in H460/DDP cells were significantly upregulated (Fig.3I). These observations demonstrate that targeting MAT2A contributes to apoptosis in lung cancer-resistant cells by enhancing the TNF signaling pathway.

Next, we conducted RNA sequencing on H460 cells with PF9366 to assess how MAT2A affects the parent cell H460 (Table S4, See Supplementary Online Information at www.celljournal.org). 1821 expressed mRNAs in H460 cells presented differential expression between control and PF9366 culture conditions (Fig. S1A, See Supplementary Online Information at www.celljournal.org), 1074 down-regulated genes and 747 up-regulated genes were contained (Fig.S1B, See Supplementary Online Information at www.celljournal.org), and cell-cycle regulation and DNA replication pathway were enriched (Fig.S1C, See Supplementary Online Information at www.celljournal.org). Among the genes sensitive to targeting MAT2A we focused on genes with regards to cell apoptosis (Fig.S1B-a, See Supplementary Online Information at www.celljournal.org) and DNA repair (Fig.S1B-b, See Supplementary Online Information at www.celljournal.org), noticing that most of the genes, for example, MAPK8, ATM, BRCA2, TOpBP1, XRCC2, etc., were decreased. These data suggest that inhibiting the activity of MAT2A may impede proliferation via preventing DNA replication and the cell cycle, and accelerate apoptosis through disturbing DNA repair in H460 cells.

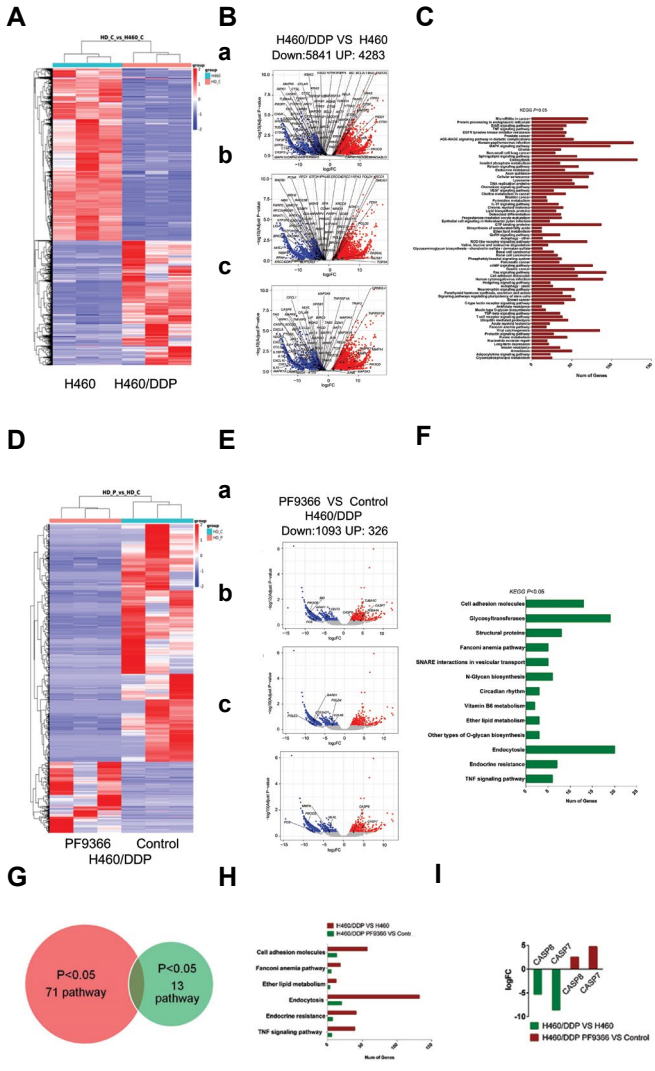

Fig.3: Transcriptional changes in lung cancer cells after inhibiting *MAT2A*. **A, B.** Heatmap and volcano plot displaying global transcriptional changes in H460/DDP cells compared with H460 cells. **B.** Each dot represents a gene, and the red dots represent up-regulated genes (4283), while the blue dots represent down-regulated genes (5841) (adjusted P<0.05) in H460/DDP cells. Differentially expressed genes of apoptosis, DNA repair and *TNF* signaling pathways are showing in a-b, respectively. **C.** KEGG analysis of signaling pathways involved in differentially expressed genes in H460/DDP cells or H460 cells. Each bar graph represents a pathway, and the length of the bar shows differential gene numbers in that pathway. **D, E.** Heatmap and volcano map showing all differentially expressed genes between control and PF9366 (10 μM)-treated H460/DDP cells. **E.** Each dot delegates a gene, and the red dots represent up-regulated genes (326), while the blue dots represent down-regulated genes (1093) (adjusted P<0.05) in H460/DDP cells with the treatment of PF9366. Differentially expressed genes of apoptosis, DNA repair and *TNF* signaling pathways are shown in a-c, respectively. **F.** KEGG analysis of signaling pathways for differentially expressed genes in H460/DDP cells under control and PF9366 (10 μM) treatment. Shown in the bar graph is pathway analysis of differentially expressed genes. Bar length represents the number of genes. **G, H.** Venn diagram showing the overlapping of differential signaling pathways in H460/DDP cells vs H460 (Red), and H460/DDP cells treated with PF9366 vs. control (Green). Bar length represents differentially expressed gene numbers. **I.** The seq-data showing the expression of *CASP7* and *CASP8* in each group as indicated.

Methionine availability maintains histone methylation in lung cancer cells

Methionine availability is predominantly necessary for DNA and RNA methylation (29), as well as histone methylation for regulating gene expression (30, 31), since SAM, generated by consuming methionine and ATP with the

help of MAT2A, is the universal methyl donor for cellular methylation reactions (Fig.4A). We assessed the impact of methionine deficiency on histone methylation in lung cancer cells (H460, H460/DDP, PC-9), and found that H3K4me3, H3K9me2, H3K27me3 and H3K36me3 levels were all reduced (Fig.4B-D). Furthermore, reduced H3K9me2 and H3K36me3 levels and non-significant change H3K4me3 and H3K27me3 levels were shown in H460/DDP and PC-9 cells under PF9366 treatment (Fig.4E, F). These experimental results proove that methionine deficiency or targeting MAT2A affect histone methylation and the latter possesses specificity.

H3K4me3 and H3K36me3 are activating marks involved in gene expression. On the contrary, H3K9me2 and H3K27me3 are related to gene silencing. Combining these different changes of histone methylation with differentially expressed genes, we speculate that methionine deficiency or MAT2A inhibition may modulate genes expression associated with apoptosis, DNA repair and TNF signaling pathways through regulating histone methylation in lung cancer cells.

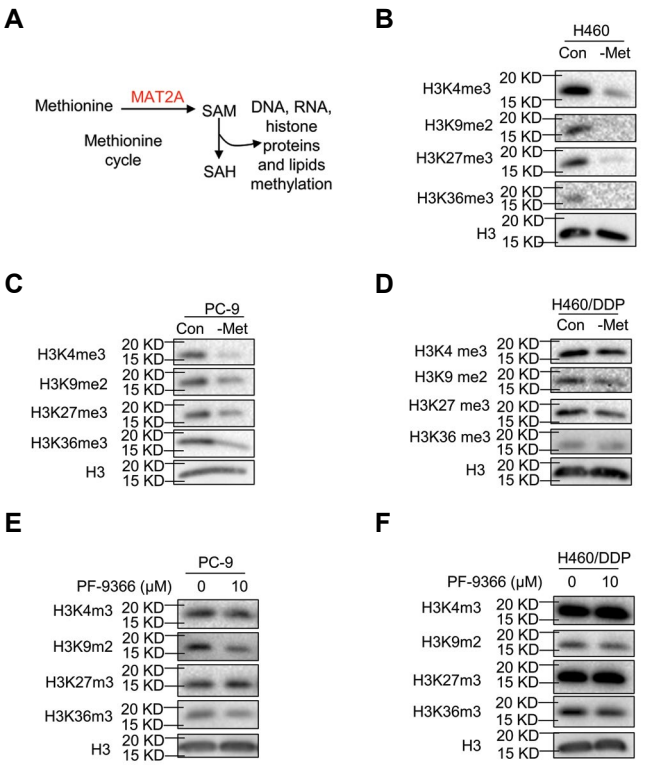

Fig.4: Methionine deficiency or targeting *MAT2A* influences histone methylation in lung cancer cells. **A.** The methionine cycle produces S-adenosylmethionine (SAM), which furnishes the omnipresent methyl group that is used for the methylation of DNA, RNA, histone, proteins and lipids via a large family of SAM-dependent methyltransferases. **B-D.** Western blotting of H3K4me3, H3K9me2, H3K27me3 and H3K36me3 levels in H460, PC-9 and H460/DDP cells under control (Con) and methionine deficiency(-Met) conditions. Total *H3* shown as control. **E** and **F.** Western blotting *of* H3K4me3, H3K9me2, H3K27me3 and H3K36me3 levels in PC-9 and H460/DDP cells with or without PF9366(10 μM) for 24 *hours. Total H3* shown as control.

Discussion

Lung cancer is the malignant tumor with the highest incidence and mortality rate. Chemotherapy is the main strategy for most lung cancer treatments. Platinum plays an important role in lung cancer chemotherapy. However, the resistance of tumor cells to platinum causes failure of chemotherapy. The mechanism of tumor resistance is complex, including enhanced expression of drug efflux protein, enhanced DNA repair ability, inhibition of apoptotic signaling pathways, etc. (32). We performed transcriptome sequencing analysis on lung cancer resistant- (H460/DDP) and -sensitive cells (H460) and enriched the differentially expressed genes. A total of 71 signaling pathways were found to be involved, including resistance-related signaling pathways such as the ErbB signaling pathway, TNF signaling pathway, MAPK signaling pathway, DNA replication proteins and cellular senescence. What's more, differentially expressed genes involved in cell apoptosis (CASP8, CASP7, CASP3, etc..), DNA repair (XRCC5, XRCC6, NHEJ1, etc..) and TNF signaling pathway (CASP8, CASP7, TNFRSF1A, etc..) were shown in figure 3B a-b. These altered pathways and genes suggest that the mechanism by which lung cancer cells are resistant to cisplatin covers multiple aspects and is worthy of further research.

Metabolic reprogramming of tumors, including amino acid metabolism reprogramming, is an important factor leading to tumorigenesis. The amino acids required by the human body include two main types: essential amino acids and non-essential amino acids, of which methionine is an important essential amino acid. Methionine is widely involved in physiological activities such as protein synthesis, amino acid metabolism, and oxidative stress (8). The methionine cycle refers to the action of methionine and ATP under the catalysis of methionine adenosyltransferase to form S-adenosylmethionine (SAM). The methyl group in SAM can be transferred to another substance such as DNA, RNA, protein and lipid, etc. Under the catalysis of methyltransferase, SAM is converted into S-adenosine homocysteine (SAH), from which the removal of adenosine, produces homocysteine (HCY). Integration of homocysteine with the methyl group from N_5-methyltetrahydrofolate can generate methionine. The methionine cycle is essential for the methylation modification of biomacromolecules and is widely involved in DNA replication, transcription, translation, post-translational modifications, etc. (33, 34). Methionine adenosyltransferase (MAT) is a key enzyme in the methionine cycle. There are two types of MAT, including MAT1A and MAT2A in the body (35). MAT1A is expressed only in the liver, while MAT2A is expressed in various organs of the body and participates in the development of plentiful tumors (36). Studies have shown that cultured lung cancer stem cells have a stronger methionine cycle than non-stem cells, as well as methylation processes driven by MAT2A (20). In this study, we explored the inhibitory effect of targeting MAT2A on platinum-resistant lung cancer cells and found that targeting MAT2A can inhibit the proliferation of drug-resistant lung cancer and induce apoptosis. Other studies have also found that targeting MAT2A can inhibit

stem cell proliferation, migration, invasion and drug resistance of tumor cells (36, 37). We have also revealed that inhibition of MAT2A blocked the cell cycle and DNA replication in H460 cells by RNA-seq. These results indicate that MAT2A is a potential target for anti-tumor therapy.

To investigate how targeted MAT2A promotes apoptosis in platinum-resistant lung cancer cells, we performed transcriptome sequencing analysis of cells treated with MAT2A inhibitor PF9366 and combined analysis with previous transcriptome sequencing results of drug-resistant cells. A common enriched signaling pathway, including the TNF signaling pathway was identified. Downstream signaling pathways for TNF activation mainly include caspase family-mediated apoptosis, adaptor protein TRAF-mediated transcription factor NF-κB and activation of JNK protein kinase (38). By sequencing, it was found that the important pro-apoptotic genes CASP7 and CASP8 in the TNF pathway were down-regulated in cisplatin-resistant cells, significantly increased after MAT2A was inhibited. Changes of differential genes associated with apoptosis, DNA repair and TNF signaling pathway were exhibited in our results. These results indicate that cisplatin-resistant cells inhibit the apoptosis process by down-regulating CASP7 and CASP8 genes, while targeting MAT2A reactivates CASP7 and CASP8 to complete the apoptotic process. How CASP7 and CASP8 expression are regulated by MAT2A remains to be further studied.

The lysine methylation modification of histones can remodel the chromatin spatial structure and play an important role in DNA damage repair and transcriptional regulation (39). H3K4 mono-, di-, or tri-methylation (H3K4me1/2/3) and H3K36me3 was a modification that promotes transcription (14, 40), while H3K9 and H3K27 methylation (H3K9me2/3 and H3K27me2/3) restrains gene expression (15, 31). We found a significant decrease in H3K4me3, H3K9me2, H3K27me3, and H3K36me3 levels under methionine deficiency conditions in H460, H460/DDP and PC-9 cells, and a significant reduction of H3K9me2 and H3K36me3 in H460/DDP and PC-9 cells treated with PF9366. We speculate that MAT2A inhibition led to the reduction of H3K9me2 by disturbing the methionine cycle, as a result of which CASP7 and CASP8 were upregulated. The other changed genes involved in cell apoptosis, DNA repair and TNF signaling pathway may also be influenced by the changes of histone methylation level. Subsequent research is needed to further study the dynamic epigenetic regulation mechanism of these genes.

Conclusion

The present study discovered that inhibiting methionine availability enhanced the inhibitory effect of cisplatin on cell activity and the pro-apoptotic effect. Targeting MAT2A can promote sensitivity of cisplatin- resistant lung cancer cells to cisplatin by regulating the expression of apoptosis-related genes. This founding provides a scientific basis for the development of new strategies to overcome lung cancer resistance.

Acknowledgments

This work was supported by Jinhua Science and Technology Research Program (2020-3-046), Doctor Foundation of Jinhua hospital (JY2019-3-001), Jinhua science and Technology Program major projects (2020-3-028), Zhejiang Medical and Health Science and Technology Project (2021KY385). The authors declare no conflict of interest in this work.

Authors' Contributions

All authors participated generally in study conception and design, data acquisition, data analysis and interpretation. X.Z., L.W., J.F., W.X., D.Z.; Contributed to write the manuscript or revise it critically. All authors read and approved the final manuscript.

References

1. Bray F, Ferlay J, Soerjomataram I, Siegel RL, Torre LA, Jemal A. Global cancer statistics 2018: GLOBOCAN estimates of incidence and mortality worldwide for 36 cancers in 185 countries. CA Cancer J Clin. 2018; 68(6): 394-424.
2. Nagasaka M, Gadgeel SM. Role of chemotherapy and targeted therapy in early-stage non-small cell lung cancer. Expert Rev Anticancer Ther. 2018; 18(1): 63-70.
3. Rossi A, Di Maio M. Platinum-based chemotherapy in advanced non-small-cell lung cancer: optimal number of treatment cycles. Expert Rev Anticancer Ther. 2016; 16(6): 653-660.
4. Terlizzi M, Colarusso C, Pinto A, Sorrentino R. Drug resistance in non-small cell lung cancer (NSCLC): Impact of genetic and non-genetic alterations on therapeutic regimen and responsiveness. Pharmacol Ther. 2019; 202: 140-148.
5. Sullivan LB, Gui DY, Vander Heiden MG. Altered metabolite levels in cancer: implications for tumour biology and cancer therapy. Nat Rev Cancer. 2016; 16(11): 680-693.
6. Altman BJ, Stine ZE, Dang CV. From Krebs to clinic: glutamine metabolism to cancer therapy. Nat Rev Cancer. 2016; 16(10): 619-634.
7. Locasale JW. Serine, glycine and one-carbon units: cancer metabolism in full circle. Nat Rev Cancer. 2013; 13(8): 572-583.
8. Sanderson SM, Gao X, Dai Z, Locasale JW. Methionine metabolism in health and cancer: a nexus of diet and precision medicine. Nat Rev Cancer. 2019; 19(11): 625-637.
9. Mazor KM, Dong L, Mao Y, Swanda RV, Qian SB, Stipanuk MH. Effects of single amino acid deficiency on mRNA translation are markedly different for methionine versus leucine. Sci Rep. 2018; 8(1): 8076.
10. Chen K, Liu H, Liu Z, Luo S, Patz EF Jr, Moorman PG, et al. Genetic variants in RUNX3, AMD1 and MSRA in the methionine metabolic pathway and survival in nonsmall cell lung cancer patients. Int J Cancer. 2019; 145(3): 621-631.
11. Wang K, Liu H, Liu J, Wang X, Teng L, Zhang J, et al. IL1RN mediates the suppressive effect of methionine deprivation on glioma proliferation. Cancer Lett. 2019; 454: 146-157.
12. Cyr AR, Domann FE. The redox basis of epigenetic modifications: from mechanisms to functional consequences. Antioxid Redox Signal. 2011; 15(2): 551-589.
13. Mehler MF. Epigenetics and the nervous system. Ann Neurol. 2008; 64(6): 602-617.
14. O'Shea JJ, Lahesmaa R, Vahedi G, Laurence A, Kanno Y. Genomic views of STAT function in CD4+ T helper cell differentiation. Nat Rev Immunol. 2011; 11(4): 239-250.
15. Tripathi SK, Lahesmaa R. Transcriptional and epigenetic regulation of T-helper lineage specification. Immunol Rev. 2014; 261(1): 62-83.
16. Tomasi ML, Ryoo M, Ramani K, Tomasi I, Giordano P, Mato JM, et al. Methionine adenosyltransferase α2 sumoylation positively

regulate Bcl-2 expression in human colon and liver cancer cells. Oncotarget. 2015; 6(35): 37706-37723.
17. Wang L, Shi S, Guo Z, Zhang X, Han S, Yang A, et al. Overexpression of YAP and TAZ is an independent predictor of prognosis in colorectal cancer and related to the proliferation and metastasis of colon cancer cells. PLoS One. 2013; 8(6): e65539.
18. Wang X, Guo X, Yu W, Li C, Gui Y, Cai Z. Expression of methionine adenosyltransferase 2A in renal cell carcinomas and potential mechanism for kidney carcinogenesis. BMC Cancer. 2014; 14: 196.
19. Zhang W, Sviripa V, Chen X, Shi J, Yu T, Hamza A, et al. Fluorinated N,N-dialkylaminostilbenes repress colon cancer by targeting methionine S-adenosyltransferase 2A. ACS Chem Biol. 2013; 8(4): 796-803.
20. Wang Z, Yip LY, Lee JHJ, Wu Z, Chew HY, Chong PKW, et al. Methionine is a metabolic dependency of tumor-initiating cells. Nat Med. 2019; 25(5): 825-837.
21. Zhao X, Fu J, Tang W, Yu L, Xu W. Inhibition of serine metabolism promotes resistance to cisplatin in gastric cancer. Onco Targets Ther. 2020; 13: 4833-4842.
22. Trapnell C, Pachter L, Salzberg SL. TopHat: discovering splice junctions with RNA-Seq. Bioinformatics. 2009; 25(9): 1105-1111.
23. Trapnell C, Williams BA, Pertea G, Mortazavi A, Kwan G, van Baren MJ, et al. Transcript assembly and quantification by RNA-Seq reveals unannotated transcripts and isoform switching during cell differentiation. Nat Biotechnol. 2010; 28(5): 511-515.
24. Wang L, Feng Z, Wang X, Wang X, Zhang X. DEGseq: an R package for identifying differentially expressed genes from RNA-seq data. Bioinformatics. 2010; 26(1): 136-138.
25. Yousafzai NA, Zhou Q, Xu W, Shi Q, Xu J, Feng L, et al. SIRT1 deacetylated and stabilized XRCC1 to promote chemoresistance in lung cancer. Cell Death Dis. 2019; 10(5): 363.
26. Poirson-Bichat F, Gonçalves RA, Miccoli L, Dutrillaux B, Poupon MF. Methionine depletion enhances the antitumoral efficacy of cytotoxic agents in drug-resistant human tumor xenografts. Clin Cancer Res. 2000; 6(2): 643-653.
27. Chen H, Xia M, Lin M, Yang H, Kuhlenkamp J, Li T, et al. Role of methionine adenosyltransferase 2A and S-adenosylmethionine in mitogen-induced growth of human colon cancer cells. Gastroenterology. 2007; 133(1): 207-218.
28. Quinlan CL, Kaiser SE, Bolaños B, Nowlin D, Grantner R, Karlicek-Bryant S, et al. Targeting S-adenosylmethionine biosynthesis with a novel allosteric inhibitor of Mat2A. Nat Chem Biol. 2017; 13(7): 785-792.
29. Sinclair LV, Howden AJ, Brenes A, Spinelli L, Hukelmann JL, Macintyre AN, et al. Antigen receptor control of methionine metabolism in T cells. Elife. 2019; 8: e44210.
30. Dai XJ, Tao JH, Fang X, Xia Y, Li XM, Wang YP, et al. Changes of Treg/Th17 ratio in spleen of acute gouty arthritis rat induced by MSU crystals. Inflammation. 2018; 41(5): 1955-1964.
31. Roy DG, Chen J, Mamane V, Ma EH, Muhire BM, Sheldon RD, et al. Methionine metabolism shapes t helper cell responses through regulation of epigenetic reprogramming. Cell Metab. 2020; 31(2): 250-266.e9.
32. Amable L. Cisplatin resistance and opportunities for precision medicine. Pharmacol Res. 2016; 106: 27-36.
33. Bauerle MR, Schwalm EL, Booker SJ. Mechanistic diversity of radical S-adenosylmethionine (SAM)-dependent methylation. J Biol Chem. 2015; 290(7): 3995-4002.
34. Gut P, Verdin E. The nexus of chromatin regulation and intermediary metabolism. Nature. 2013; 502(7472): 489-498.
35. García-Trevijano ER, Latasa MU, Carretero MV, Berasain C, Mato JM, Avila MA. S-adenosylmethionine regulates MAT1A and MAT2A gene expression in cultured rat hepatocytes: a new role for S-adenosylmethionine in the maintenance of the differentiated status of the liver. FASEB J. 2000; 14(15): 2511-2518.
36. Maldonado LY, Arsene D, Mato JM, Lu SC. Methionine adenosyltransferases in cancers: mechanisms of dysregulation and implications for therapy. Exp Biol Med (Maywood). 2018; 243(2): 107-117.
37. Lu SC, Mato JM. S-Adenosylmethionine in cell growth, apoptosis and liver cancer. J Gastroenterol Hepatol. 2008; 23 Suppl 1: S73-S77.
38. Balkwill F. TNF-alpha in promotion and progression of cancer. Cancer Metastasis Rev. 2006; 25(3): 409-416.
39. Hyun K, Jeon J, Park K, Kim J. Writing, erasing and reading histone lysine methylations. Exp Mol Med. 2017; 49(4): e324.
40. Shen E, Shulha H, Weng Z, Akbarian S. Regulation of histone H3K4 methylation in brain development and disease. Philos Trans R Soc Lond B Biol Sci. 2014; 369(1652): 20130514.

Short Communication

Inhibitory Effect of the HASPIN Inhibitor CHR-6494 on BxPC-3-Luc, A Luciferase-Expressing Pancreatic Cancer Cell Line

Hiromitsu Tanaka, Ph.D.[1]*, Hisayo Nishida-Fukuda, Ph.D.[2], Morimasa Wada, Ph.D.[1], Keizo Tokuhiro, Ph.D.[2], Hiroaki Matsushita, Ph.D.[1], Yukio Ando, M.D., Ph.D.[1]

1. Faculty of Pharmaceutical Sciences, Nagasaki International University, Huis Ten Bosch, Sasebo, Nagasaki, Japan
2. Department of Genome Editing, Institute of Biomedical Science, Kansai Medical University, Shin-machi, Hirakata City, Osaka, Japan

Corresponding Address: Faculty of Pharmaceutical Sciences, Nagasaki International University, Huis Ten Bosch, Sasebo, Nagasaki, Japan
Email: h-tanaka@niu.ac.jp

Received: 29/September/2020, Accepted: 12/January/2021

Abstract

HASPIN acts in chromosome segregation via histone phosphorylation. Recently, HASPIN inhibitors have been shown to suppress growth of various cancer cells. Pancreatic cancer has no symptom in the early stages and may progress before detection. So, the 5-year survival rate is low. Here, we reported that administration of the HASPIN inhibitor, CHR-6494, to mice bearing pancreatic BxPC-3-Luc cancer cells significantly suppressed growth of BxPC-3-Luc cells. CHR-6494 might be a useful agent for treating pancreatic cancer.

Keywords: HASPIN Kinase, Histone H3, Pancreatic Cancer, Protein Kinase

Cell Journal(Yakhteh), Vol 24, No 4, April 2022, Pages: 212-214

Citation: **Tanaka H, Nishida-Fukuda H, Wada M, Tokuhiro K, Matsushita H, Ando Y. Inhibitory effect of the HASPIN inhibitor CHR-6494 on BxPC-3-Luc, a luciferase-expressing pancreatic cancer cell line. Cell J. 2022; 24(4): 212-214. doi: 10.22074/cellj.2022.7796.**

All animal experiments were confirmed by the Guide for the Care and Use of Laboratory Animals and they were approved by the Institutional Committee of Laboratory Animal Experimentation and Research Ethics Committee of Nagasaki International University (Approval number 129).

The mouse histone H3 associated protein kinase *HASPIN* gene, encoding a nuclear-localized Ser/Thr kinase, was cloned from a cDNA library obtained by subtracting W/W^V mutant mouse testis mRNA (1). HASPIN phosphorylates Thr3 of histone H3 in mitotic cells. It is localized on centrosomes and spindles in mitosis, while regulates chromosome and spindle function during mitosis and meiosis (2). It is involved in the phosphorylation of Thr127 of TH2A, a germline-specific H2A variant, in elongating spermatids and early mitotic preimplantation mouse embryos (3). To further clarify its role, *HASPIN* gene-disrupted mice were generated. However, no obvious phenotype was detected in these mice. Light microscopy of the testes obtained from the *HASPIN* null mice showed a few seminiferous tubules, containing no germ cell (4). As part of the KINOME project, a HASPIN kinase inhibitor was isolated. Findings showed that this inhibitor suppresses growth of cancer cells *in vitro* and *in vivo* (5, 6). While HASPIN is essential for proliferation of the cultured cancer cells (5), no abnormality was observed in *HASPIN*-null mice. So function of HASPIN may be counterbalanced by its association with other molecules in normal cells. In addition, it may play important roles in cell division, during proliferation of male germ cells and cancer cells (4-6).

Pancreatic cancer is on the rise globally and it is an important cause of death (7). Pancreatic cancer is painless. So it is generally detected late, in advanced stages. The main treatment is surgery. When invasion and metastases are likely, chemotherapy is also given (8). With few effective therapies, it is crucial to find more effective treatments and to explore the mechanisms involved in improving how to save patients with pancreatic cancer.

Recently, some small molecules have been found to inhibit HASPIN and growth of cancer cells derived from various tissues (5, 9-13). The natural product coumestrol inhibits HASPIN (14). Therefore, we examined whether CHR-6494 suppresses proliferation of pancreatic BxPC-3-Luc cancer cells.

First, a cell viability assay was used to examine whether CHR-6494 (Sigma-Aldrich, Japan) inhibits proliferation of pancreatic BxPC-3-Luc cancer cells (National Institutes of Biomedical Innovation, Health and Nutrition, Japan). Cell viability was assessed using the XTT (sodium 3′-[1-(phenylaminocarbonyl)-3,4-tetrazolium]-bis[4-methoxy6-nitro] benzene sulfonic acid hydrate) assay (Sigma-Aldrich, Japan), according to the manufacturer's protocol (5). CHR-6494 was dissolved at 10 mM in DMSO and stored at -20˚C. This solution was next sequentially diluted in DMSO and equal amounts were added to each well of 96-well plates. A density of 2×10^4 cells per well were seeded and incubated for 24 hours in order to the cell attachment. Then the medium was replaced with new medium containing different drug concentrations (0.01, 0.1, 0.5, 1, 5, 10, 50 and 100 μM), using eight wells for each CHR-6494 concentration, apart from the well with no CHR-6494, as a negative control. The XTT reagent was added 48 hours after drug administration and the absorbance was measured 2 hours later. The half-maximal inhibitory concentration (IC_{50})

was determined using GraphPad Prism (GraphPad, USA). CHR-6494 inhibited cell growth dose-dependently and the IC_{50} was 849.0 nM (Fig.1).

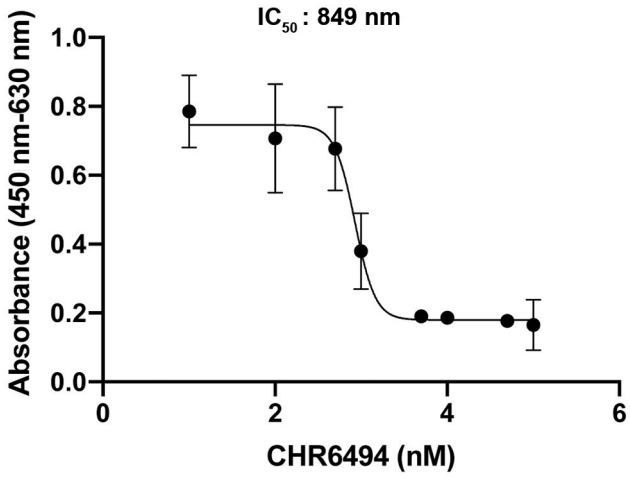

Fig.1: CHR-6494 inhibits proliferation of BxPC-3-Luc cells *in vitro*. Effects of CHR-6494 on the viability of BxPC-3-Luc cells were evaluated using the XTT assay.

Next, 200 µl of BxPC-3-Luc cell suspension, containing 2×10^6 cells, was added into the flanks of 12 nude mice (BALB/cAJcl- nu/nu, CLEA Japan, Japan). They were treated with CHR-6494 or vehicle control. Subsequently, potential effects of intraperitoneal administration of CHR-6494 on tumor size were examined. When the tumor long axis was reached to 130 mm, 2-3 weeks after administration of the BxPC-3-Luc cells, CHR-6494 administration was started. As negative controls, vehicle solution (10% DMSO) and co-solvent (20% 2-hydroxypropyl-b-cyclodextrin; Sigma-Aldrich, Japan) in saline were injected into the peritoneal cavities of six mice (three males and three females). For treatment, 5 µg/µl CHR-6494 in vehicle solution was injected into the peritoneal cavities of six other mice (three males and three females) at 50 mg/kg body weight by adjusting the injection volume. Considering the weight of mice (10-30 g), 100-300 µl solution was injected to each one. The injectable material was stored at -30˚C. Treatments were performed for five cycles consisting of five consecutive injection days and five successive non-treatment days for 4 weeks. The treatments were followed, as previously reported procedures (5). The volume of each tumor was determined by measuring long (L) and short (S) axes with calipers and using the formula L×S2/2. The tumor volume of tumor-bearing mice after 1–4 weeks of CHR-6494 administration was 1.5 ± 0.6, 2.5 ± 0.7, 3.5 ± 0.8 and 3.8 ± 0.9 mm^3, respectively. The tumor size in untreated control mice after 1-4 weeks was 2.0 ± 0.5, 3.0 ± 0.6, 4.0 ± 0.8 and 6.0 ± 1.7 mm^3, respectively (Fig.2). Means were compared between groups using Student's t test; significant differences were determined at the $P<0.05$ level. There was no significant difference in tumor size between the male and female groups. Administration of CHR-6494 for 4 weeks significantly inhibited tumor growth.

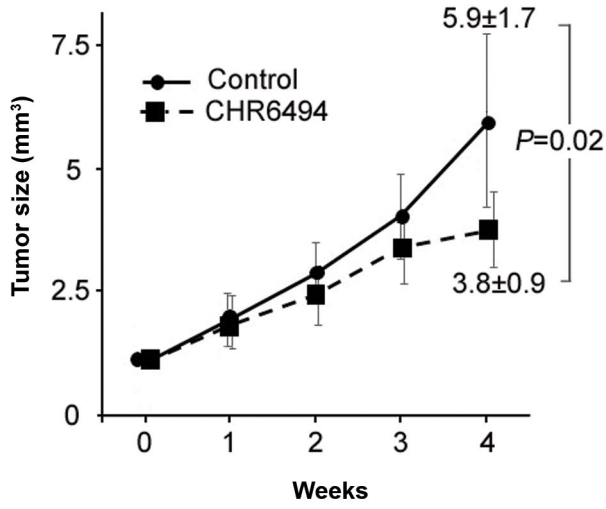

Fig.2: CHR-6494 prevents tumor development in xenograft mice treated with CHR-6494. Tumor size in treated (squares) and not treated (dots) mice with CHR-6494. The vertical axis indicates the average size of tumors in each group. Data are presented as the mean ± SD ($P<0.05$).

BxPC-3-Luc cells contain luciferase reporter gene. Luminescence of the xenograft tumors on nude mice was detected at the Central Institute for Experimental Animals (Kanagawa, Japan) using IVIS (IVIS Lumina XRMS Series III; Perkin Elmer, USA) with D-Lucifer in potassium salt (VivoGlo Luciferin, *in vivo* grade; Promega). The *in vivo* bioluminescence imaging showed no apparent signal of metastasis in the xenograft models (Fig.3).

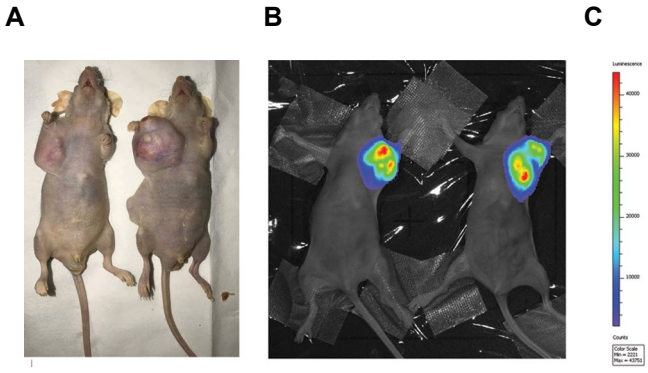

Fig.3: Images of BxPC-3-Luc cell tumors in nude mice. BxPC-3-Luc cell tumors in nude mice in bright images of **A.** Treated and B. Not treated mice with CHR-6494, and luminescence images of **C.** Untreated mice. No BxPC-3-Luc cell metastasis to other organs was observed in nude mice, three weeks after transplantation.

A few chemicals inhibit the kinase activity of HASPIN and suppress cancer cell growth. The HASPIN inhibitor, CHR6494, is more specific for HASPIN kinase activity and suppresses cancer cell growth (5, 9-14). We had established a HASPIN-disrupted mouse line, but contrary to our prediction no abnormality was observed in these mice. Deficiency in HASPIN-specific inhibition did not appear to cause severe abnormalities in normal cell differentiation and proliferation. Nevertheless, HASPIN plays a vital role in cell division via the phosphorylation of histone H3 in cultured cells. H3T3 is phosphorylated by VRK1, dephosphorylated by PP1A. It is also phosphorylated by HASPIN in a cell cycle-dependent manner (15). In HASPIN-null mice, H3T3 is phosphorylated by VRK1, but absence of HASPIN may affect the PP1A phosphatase activity and compensate for the phosphorylation state of H3T3. In dedifferentiated cancer cells, loss of HASPIN kinase activity may be not complemented (5, 6). Since treatment of pancreatic cancer is difficult, effect of CHR-6494 on pancreatic cancer BxPC-3-Luc cells were investigated. We found that CHR-6494 significantly inhibited growth of BxPC-3-Luc cells. In an RNA interference-mediated knockdown experiment, supressing expression of HASPIN, development of pancreatic cancer was suppressed (16); therefore, the HASPIN inhibitor CHR6494 is thought to have no side-effect in humans. These results suggested that, as a potentially useful treatment against pancreatic cancer.

Acknowledgments

We thank Ms. Momoka Esaki for breeding the mice. There is no financial support and conflict of interest in this study.

Authors' Contributions

H.T.; Contributed to the study conception and design, experimental work, data and statistical analyses, data interpretation, and writing the manuscript. H.N.-F.; Contributed to the experimental work and data analyses. M.W., K.T., H.M., Y.A.; Contributed to the materials. All authors read and approved the final manuscript.

References

1. Tanaka H, Yoshimura Y, Nozaki M, Yomogida K, Tsuchida J, Tosaka Y, et al. Identification and characterization of a haploid germ cell-specific nuclear protein kinase (Haspin) in spermatid nuclei and its effects on somatic cells. J Biol Chem. 1999; 274(24): 17049-17057.
2. Dai J, Sultan S, Taylor SS, Higgins JM. The kinase haspin is required for mitotic histone H3 Thr 3 phosphorylation and normal metaphase chromosome alignment. Genes Dev. 2005; 19(4): 472-488.
3. Hada M, Kim J, Inoue E, Fukuda Y, Tanaka H, Watanabe Y, Okada Y. TH2A is phosphorylated at meiotic centromere by Haspin. Chromosoma. 2017; 126(6): 769-780.
4. Shimada M, Goshima T, Matsuo H, Johmura Y, Haruta M, Murata K, et al. Essential role of autoactivation circuitry on Aurora B-mediated H2AX-pS121 in mitosis. Nat Commun. 2016; 7: 12059.
5. Huertas D, Soler M, Moreto J, Villanueva A, Martinez A, Vidal A, et al. Antitumor activity of a small-molecule inhibitor of the histone kinase Haspin. Oncogene. 2012; 31(11):1408-1418.
6. Tanaka H, Wada M, Park J. HASPIN kinase inhibitor CHR-6494 suppresses intestinal polyp development, cachexia, and hypogonadism in Apcmin/+ mice. Eur J Cancer Prev. 2020; 29(6): 481-485.
7. Rahib L, Smith BD, Aizenberg R, Rosenzweig AB, Fleshman JM, Matrisian LM. Projecting cancer incidence and deaths to 2030: The unexpected burden of thyroid, liver, and pancreas cancers in the United States. Cancer Res. 2014; 74: 2913–2921.
8. Brunner M, Wu Z, Krautz C, Pilarsky C, Grützmann R, Weber GF. Current clinical strategies of pancreatic cancer treatment and open molecular questions. Int J Mol Sci. 2019; 20(18): 4543.
9. Maiolica A, de Medina-Redondo M, Schoof EM, Chaikuad A, Villa F, Gatti M, et al. Modulation of the chromatin phosphoproteome by the HASPIN protein kinase. Mol Cell Proteomics. 2014; 13(7): 1724–1740.
10. Amoussou NG, Bigot A, Roussakis C, Robert JH. HASPIN: A promising target for the design of inhibitors as potent anticancer drugs. Drug Discov Today. 2018; 23(2): 409–415.
11. Opoku-Temeng C, Dayal N, Aflaki Sooreshjani M, Sintim HO. 3H-pyrazolo[4,3-f]quinoline HASPIN kinase inhibitors and anticancer properties. Bioorg Chem. 2018; 78: 418–426.
12. Bastea LI, Hollant LMA, Döppler HR, Reid EM, Storz P. Sangivamycin and its derivatives inhibit HASPIN-Histone H3-survivin signaling and induce pancreatic cancer cell death. Sci Rep. 2019; 9(1): 16588.
13. Melms JC, Vallabhaneni S, Mills CE, Yapp C, Chen JY, Morelli E, et al. Inhibition of HASPIN kinase promotes cell-intrinsic and extrinsic antitumor activity. Cancer Res. 2020; 80(4): 798–810.
14. Kim JE, Lee SY, Jang M, Choi HK, Kim JH, Chen H, et al. Coumestrol epigenetically suppresses cancer cell proliferation: Coumestrol is a natural HASPIN kinase inhibitor. Int J Mol Sci. 2017; 18(10): 2228.
15. Moura DS, Campillo-Marcos I, Vázquez-Cedeira M, Lazo PA. VRK1 and AURKB form a complex that cross inhibit their kinase activity and the phosphorylation of histone H3 in the progression of mitosis. Cell Mol Life Sci. 2018; 75(14): 2591–2611.
16. Han X, Kuang T, Ren Y, Lu Z, Liao Q, Chen W. HASPIN knockdown can inhibit progression and development of pancreatic cancer in vitro and vivo. Exp Cell Res. 2019; 385(1): 111605.